

Abstract

HARP, JASON MICHAEL. Investigation of Failed TRISO Fuel Assay Using Gamma-Ray Spectrometry. (Under the direction of Ayman I. Hawari.)

TRISO microsphere fuel is the fundamental fuel unit for Very High Temperature Reactors (VHTR). A single TRISO particle consists of an inner kernel of Uranium Oxycarbide surrounded by layers of pyrolytic carbon and silicon carbide. The silicon carbide serves as the primary barrier to the release of fission products into the core. If the silicon carbide layer fails, fission gas, especially Kr and Xe, will begin to escape the failed particle.

In order to understand the behavior of TRISO fuel under in-core conditions, a series of experiments is being conducted by Idaho National Lab at the Advanced Test Reactor. AGR-1 is the first of these experiments. It will measure fission product release due to failed TRISO particles. Simulations of this experiment have been conducted at North Carolina State University to develop a method for the analysis of the results of the experiment.

The ATR core was simulated using the Monte Carlo code MCNP to calculate the expected neutron energy spectrum for the AGR-1 experimental test train. This spectrum was used to create one-group cross sections for implementation in ORIGEN calculations of the amount of activity produced in the experiment.

Several theoretical models have been developed to describe the phenomenon of gas release. While each model is based on similar physics, different models contain unique features that distinguish them from one another. These Release to Birth (R/B) models are developed and applied to the activity found in the ORIGEN calculations to create expected release activities. The release activity is used to create gamma-ray spectra that are representative of the different R/B models.

Expected R/B due to a model can be calculated for comparison to the experiment with knowledge of the number of failed particles in the spectra. The comparison of measured to predicted R/B ratios gives insight into the physics of release and also helps validate specific models. Direct comparison is possible, but many of the uncertainties associated with direct comparison are nullified through the use of relative indicators.

Each R/B model has a unique set of indicators that reflect the physical processes simulated in the model. Trends in the model indicators can be matched up with trends in indicators derived from the release spectra to validate either an entire model or validate the need to consider certain parameters in the creation of a complete and successful release to birth model.

Gamma spectrometry is a useful tool for the understanding of fission gas release from failed TRISO particles. A better understanding of the processes that influence fission gas release will influence the fuel manufacturing and quality assurance protocols during the continued development of the VHTR. Future work in this area includes experiment in which the conditions can be better controlled to document the effects of temperature and fission rate in the fuel.

Investigation of Failed TRISO Fuel Assay Using Gamma-Ray Spectrometry

by
Jason Michael Harp


A thesis submitted to the Graduate Faculty of
North Carolina State University
in partial fulfillment of the
requirements for the Degree of
Master of Science

NUCLEAR ENGINEERING

Raleigh, North Carolina

2007

APPROVED BY:



Mohamed A. Bourham



Kimberly S. Weems



Ayman I. Hawari
Chair of Advisory Committee

Biography

Jason Michael Harp was born November 17, 1982 in Amarillo, Texas to James Wiley Harp and Rebecca Harp. He was raised in the small West Texas town of Canyon. Canyon is home to West Texas A&M University and is in close proximity to the DOE Pantex site, which would prove influential in his choice to pursue a career in Nuclear Engineering.

After graduating from Canyon High School in May of 2001, Jason began attending Texas A&M University in College Station, TX. In August of 2001 he began class work for his B.S. degree in Nuclear Engineering. During his time as an undergraduate, Jason had the opportunity to intern each summer at a DOE site. He spent two summers at Pantex where he was first introduced to the use of MCNP for modeling nuclear systems. Jason also spent two summers up on the hill at Los Alamos National Laboratory. While at LANL, he worked with the Applied Physics (X) Division Nuclear Data Team on projects that included an investigation of Tritium production in the lithium isotopes and investigation comparing Monte Carlo and deterministic benchmarks for critical assemblies. On May 14, 2005, Jason graduated Magna Cum Laude from Texas A&M University.

In August of 2005, he began his graduate studies at North Carolina State University with Dr. Ayman Hawari. Jason began work on the project that would lead to his thesis. During the summer of 2006 Jason spent time at Idaho National Laboratory learning many of the details associated with the AGR-1 experiment and the operation of the ATR reactor.

After completion of his Master's work, Jason plans to continue at NC State and pursue his Ph.D.

Acknowledgements

I would like to express my most sincere gratitude to Dr. Ayman Hawari for his guidance and support throughout this project. I truly appreciate all the lessons he taught me in the process of completing this work, and I am grateful for the opportunity to work on a high profile project. I look forward to our continued relationship for years to come.

I am also grateful to the Advanced Fuel Cycle Initiative University Fellowship Program for their financial support during my research. Specifically let me thank Cathy Dixon and the rest of her staff for their excellent management of the AFCI Fellowship program.

My thanks go out to the staff members that I worked with at Idaho National Laboratory for helping me better understand the AGR-1 experiment and the Advanced Test Reactor. In particular, I would like to thank Jack Hartwell, Dawn Scates, and Dr. Gray Chang for their help.

Let me also thank Dr. Mohamed Bourham and Dr. Kimberly Weems for agreeing to serve on my thesis committee.

Finally let me thank my parents and the rest of my family for supporting and encouraging me throughout the course of my education.

Table of Contents

	Page
List of Tables	vi
List of Figure	vii
Chapter 1	1
1.1 Introduction.....	1
1.2 VHTR and TRISO Fuel Overview	2
1.3 An Overview of the AGR-1 Experiment	4
1.3.1 The Advanced Test Reactor.....	5
1.3.2 Fission Product Monitoring System.....	7
1.4 Simulation Strategy.....	9
Chapter 2	11
2.1 Creation of Birth Rates	11
2.1.1 ATR MCNP Simulations	12
2.1.2 Choosing the Isotopes of Interest.....	14
2.1.3 Creation of One-Group Neutron Libraries for ORIGEN	15
2.1.4 ORIGEN Simulations	17
2.2 Modeling of Fission Gas Release	19
2.2.1 Introduction.....	19
2.2.2 Development of Booth Model for Short Lived Isotopes	20
2.2.3 The German 2 Model.....	23
2.2.4 The JAERI Revised Model	24
2.2.5 The General Atomics Model.....	27
2.2.6 Comparing the German and JAERI Models	30
2.2.7 Comparing the German and the GA Models	32
2.2.8 General Trends in the R/B ratios	32
2.2.9 Conclusions on Release to Birth Models	35
2.3 Creation of Release Spectra	36
2.3.1 Detector Simulation in MCNP.....	36
2.3.2 MCNP Source Creation	38
2.3.3 Model Applied Spectra	39
2.3.4 Low Resolution Detector Spectra	45
Chapter 3	47
3.1 Interpretation Using Absolute Release Activity	47

3.2	Sources of Uncertainties in Absolute Comparisons.....	49
3.3	Relative Measurement Indicators	50
3.4	Properties of Relative Indicators.....	53
3.4.1	Birth Activity Ratios.....	53
3.4.2	Indicator Trends	55
3.4.3	Trends in Spectra	59
Chapter 4		63
4.1	Conclusions.....	63
4.2	Future Work.....	64
References		66
Appendices		68
Appendix A	Derivation of the Booth Equation.....	69
Appendix B	Simplification of JAERI Model to German Model.....	72
Appendix C	Detector Catalog	77
C.1	Physical Measurements of Detector Properties	77
C.1.1	Spectra Collected from Detectors	78
C.1.2	Detector Properties.....	80
C.2	Simulated Detector Responses to Different Models.....	82
C.2.1	HPGe Detectors	83
C.2.2	High Pressure Xenon Detector.....	88
C.2.3	CZT Detector	92
C.2.4	LaBr ₃ (Ce) Detector	94

List of Tables

	Page
Table 2.1. Nuclides of Interest for Fission Product Release Analysis.....	15
Table 2.2. Availability of Nuclear Data for Different Isotopes of Interest and their Precursors.....	16
Table 2.3. Examples of R/B models that are considered in the current work.....	23
Table 2.4. Model Parameters for (R/B) Correlation	29
Table 2.5. A Comparison of (R/B) values for the German and JAERI Models	30
Table 2.6. GEB Card Fit Parameters for Various Detectors.....	37
Table 3.1. Predicted Indicators using Kr-85m as the reference R/B value.....	52
Table 3.2. Maximum and minimum affect that modifying the expected flux has on Birth Ratios for all isotope pairs of the nuclides of interest excluding Xe-135 and Xe-135m.	55
Table 3.3. Prominent gammas for identification of trends in fission gas release	60
Table B.1 Reduction of the JAERI Failure Term to the German Failure Term	75
Table B.2 Table A.1 in Terms Relative to the German Values	75
Table B.3 Reduction of the Contamination Component of the JAERI Model to the German Term.....	76

List of Figures

	Page
Fig. 1.1. TRISO Fuel Particle Layers and Fuel Element Configurations	3
Fig. 1.2. The Advanced Test Reactor Horizontal View.....	6
Fig. 1.3. Fission Product Monitoring System Detectors with Shield and Liquid Nitrogen Dewar	8
Fig. 2.1. Simulation Process Flowchart	11
Fig. 2.2. Birth Rate Creation Flowchart.....	12
Fig. 2.3. ATR MCNP model with Experimental Capsule	13
Fig. 2.4. Fission Product Inventory for Kr-85m	18
Fig. 2.5. Fission Product Inventories for Different Isotopes at 286 EFPD	19
Fig. 2.6. Reduced Diffusion Coefficient as a function of Temperature for Different Model Components.....	33
Fig. 2.7. Reduced Diffusion Coefficients at 1450 K.....	34
Fig. 2.8. Failure Release to Birth Ratios for various models given expected experimental conditions.....	34
Fig. 2.9. Xe Birth Spectrum vs. Model Applied Spectra	41
Fig. 2.10. Xe Failure Spectra for German, JAERI, General Atomics, and Modified JAERI models	41
Fig. 2.11. Contamination Signal and First TRISO Failure Signal for Xenon according to German Model	43
Fig. 2.12. Contamination Signal and First TRISO Failure Signal for Xenon according to JAERI Model	43
Fig. 2.13. Contamination and First TRISO Failure Signal for Krypton according to the German Model	44
Fig. 2.14. Contamination and First TRISO Failure Signal for Krypton according to the JAERI Model	44
Fig. 2.15. HPXe Birth and Model Applied Spectra for Xe isotopes of interest.....	45
Fig. 2.16. Xe Failed TRISO Particle Spectra for the German, JAERI, and GA models on a LaBr Detector.....	46
Fig. 3.1. Indicator values for failure models as a function of half-life. Given Kr-85m as the reference isotope and AGR-1 experimental conditions	56
Fig. 3.2. Indicators for Contamination models as functions of half-life with Kr-85m as the reference isotope and AGR-1 experimental conditions	57
Fig. 3.3. Simulated spectra demonstrating the doublet formed by Kr-87 2554.8 keV and 2558.1 keV gammas along with the 2548.4 keV gamma from Kr-88.....	61
Fig. 3.4. Normalized plot of Kr-85m 151 keV line and Xe-138 153.86 keV line illustrating model differences	62
Fig. C. 1. HPGe response to Cs-137 sources (Background sources also contribute to this spectrum).....	78

Fig. C. 2. HPXe Response to Cs -137.....	78
Fig. C. 3. CZT Response to Cs-137.....	79
Fig. C. 4. LaBr Response to Cs-137.....	79
Fig. C. 5. Energy versus Resolution of Different Full Energy Peaks for the HPXe.....	80
Fig. C. 6. Energy versus Resolution of Different Full Energy Peaks for the CZT.....	80
Fig. C. 7. Energy versus Resolution of Different Full Energy Peaks for the LaBr.....	81
Fig. C. 8. Combined Energy vs. Resolution response of the 4 detectors.....	81
Fig. C. 9. Effect of applying the German and JAERI Models to Xe Birth Activity Due to Contamination.....	83
Fig. C. 10. Effect of applying the German and JAERI Models to Kr Birth Activity Due to Contamination.....	83
Fig. C. 11. HPGe Response for Different Models Due to the Xe from a Single Failed TRISO Particle.....	84
Fig. C. 12 HPGe Response from the Primary Models Due to the Kr from a Single Failed TRISO Particle.....	84
Fig. C. 13. HPG Response for all Models Due to Xe from a Single Failed Particle.....	85
Fig. C. 14. HPG Response for all Models Due to Kr from a Single Failed Particle.....	85
Fig. C. 15. HPGE response Due to Expected Compact Contamination from Xe.....	86
Fig. C. 16. HPGE response Due to Expected Compact Contamination from Kr.....	86
Fig. C. 17. Contamination and First Failure Spectra for Xe.....	87
Fig. C. 18. Contamination and First Failure Spectra for Kr.....	87
Fig. C. 19. HPXe Response for the Effect of Applying R/B Models to the Birth Activity for Xe.....	88
Fig. C. 20. HPXe Response for the Effect of Applying R/B Models to the Birth Activity for Xe.....	88
Fig. C. 21. HPXe Response Due to Xe for a Single Failed TRISO.....	89
Fig. C. 22. HPXe Response Due to Kr for a Single Failed TRISO.....	89
Fig. C. 23. HPXe Contamination Spectra Due to Xe.....	90
Fig. C. 24. HPXe Contamination Spectra Due to Xe.....	90
Fig. C. 25. HPXe Contamination and First Failure Spectra for Xe.....	91
Fig. C. 26. HPXe Contamination and First Failure Spectra for Kr.....	91
Fig. C. 27. CZT Response to Xe from a Single Failed Particle.....	92
Fig. C. 28. CZT Response to Kr from a Single Failed Particle.....	92
Fig. C. 29. CZT Response to Xe from Contamination.....	93
Fig. C. 30. CZT Response to Kr from Contamination.....	93
Fig. C. 31. LaBr Response to Xe from a Single Failed Particle.....	94
Fig. C. 32. LaBr Response to Kr from a Single Failed Particle.....	94
Fig. C. 33. LaBr Response to Xe from Contamination.....	95
Fig. C. 34. LaBr Response to Kr from Contamination.....	95

Chapter 1

Introduction

1.1 Introduction

The concept of high temperature gas reactor has been under development for nearly 40 years, and there have been many successful gas reactors operated beginning with the DRAGON reactor in the United Kingdom. Several countries have had very active gas reactor programs including the United States, Germany (West Germany), Japan, Russia (USSR), South Africa, and the United Kingdom. In the United States, General Atomics began design of gas reactors in 1957 and began construction of the Peach Bottom Reactor in 1962. Peach Bottom conducted operations from 1967 to 1974, and was followed by the operation of the Fort St. Vrain reactor from 1974 to 1989. Gas reactor looked poised to begin full commercial deployment in 1971 with the sale of 10 units to utilities, but the economic conditions of that decade doomed these projects. Development continued on nuclear fired gas reactors through the 1980s and 1990s which increased both the safety and the potential thermodynamic efficiency of these reactors. In recent years this development lead to the design of the General Atomics Gas Turbine Modular Helium Reactor (GT-MHR) and the similarly designed, but higher temperature Very High Temperature Reactor (VHTR) [1].

The renewed interest in gas cooled nuclear reactors has prompted a new series of tests to examine the TRISO fuel used in these reactors. The Advanced Gas Reactor (AGR) series of experiments at Idaho National Laboratory (INL) will test TRISO fuel under in-core conditions of high neutron flux, high temperature, and high burn-up. An important metric in

these tests is to detect the failure of TRISO fuel to the individual kernel level. Collaboration between INL and North Carolina State University (NCSU) will establish techniques for the use of passive gamma-ray spectrometry in failure detection.

1.2 VHTR and TRISO Fuel Overview

The Very High Temperature Reactor has been selected by the Department of Energy (DOE) Generation IV program as a reactor to aggressively pursue and as the next generation nuclear plant. The VHTR is desirable for its potential to efficiently produce electricity with a thermodynamic efficiency near 50%, and its ability achieve high temperature outlet temperatures that can be used in process heat applications. The process heat applications include the thermo-chemical break down of water to create Hydrogen without producing greenhouse gasses. The reactor is able to reach 50% thermodynamic efficiency by the use of the Brayton Cycle instead of the Rankine Cycle like traditional Light Water Reactors (LWR). The Brayton Cycle uses Helium as a working fluid to drive gas turbines. Helium is heated by flowing down through coolant channels cut in the reactor fuel elements. The heated helium then flows through the power conversion system. Gas turbine efficiency has benefited from years of aerospace industry research, and the invention of nearly frictionless magnetic bearings. Helium also has many advantageous nuclear and chemical properties. Helium will not corrode plant components like water will, and helium will not activate in a neutron field. The graphite fuel elements allow the VHTR to operate at temperatures much higher than Light Water Reactors (LWR). Core outlet temperatures could reach 950°C which is high enough to drive sulfur-iodine thermo-chemical reactions that break water into Oxygen and Hydrogen. The modular nature of the VHTR makes it a viable option for use in a wide variety of other industrial processes that require process heat [2].

Very High Temperature Reactors (VHTR) utilize the TRISO microsphere as the fundamental fuel unit in the core. TRISO stands for TRIsstructural ISOtropic. The TRISO microsphere is composed of a UC_xO_y kernel surrounded by a porous graphite buffer, an inner pyrolytic graphite layer, a silicon carbide (SiC) coating, and an outer pyrolytic graphite layer. These layers can be seen in Fig. 1.1.

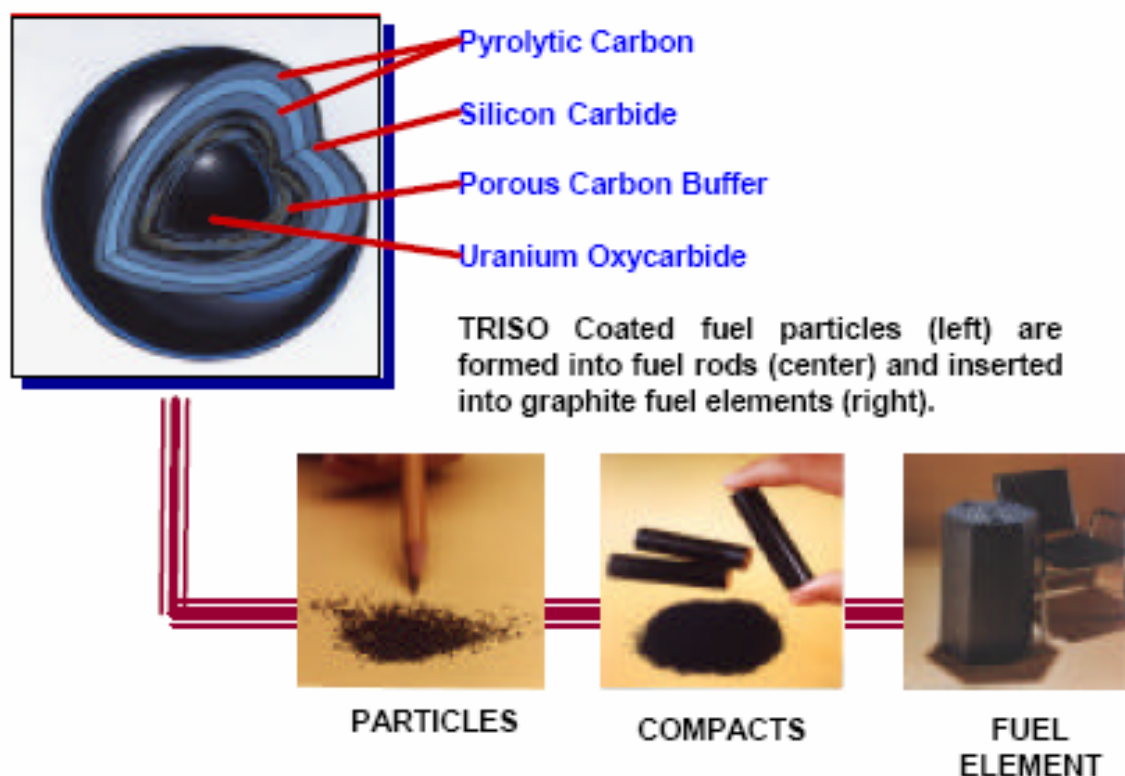


Fig. 1.1. TRISO Fuel Particle Layers and Fuel Element Configurations

A single TRISO particle is approximately 0.8 mm in diameter. The Uranium Oxycarbide (UC_xO_y) kernel is nominally 350 μm in diameter. The buffer layer is nominally 100 μm thick, the inner pyrolytic carbon layer is 40 μm thick, the Silicon Carbide layer is 35 μm thick, and the outer pyrolytic carbon layer is 40 μm thick. The U-235 enrichment is flexible in TRISO fuel and can be fit to the needs of the reactor. Commercial reactors are expected to use 4-10 wt. % enriched kernels mixed with natural uranium kernels to help

mitigate flux peaking. The AGR-1 experiment will use 19.8 wt. % enriched fuel. For the AGR-1 experiment the UC_xO_y kernels were manufactured at BWXT in Lynchburg, VA, and the kernels were coated by Oak Ridge National Lab. Detailed specifications for these TRISO particles are well documented by INL Engineering Design File (EDF) documents [3]. The different particle layers can be thought of as miniature pressure vessels that contain fission fragments during irradiation. The layers also act a containment vessel for radionuclides if the fuel is sent to a geologic repository. The individual TRISO microspheres are combined with a carbonaceous matrix and compacted into cylinders to create fuel compacts. For commercial reactors, these compacts are then loaded into large prismatic fuel elements (see Fig. 1.1). In the AGR-1 experiment the compacts will be loaded into custom made test trains designed for irradiation in the Advanced Test Reactor. At high burn up it is possible for the pressure inside the pyrolytic carbon and SiC layers to reach a critical point where these layers will rupture. In the event of a catastrophic failure of the TRISO layers the matrix material of the compacts and the fuel elements should provide some containment of fission products [4].

1.3 An Overview of the AGR-1 Experiment

The AGR-1 experiment is the first of a series of experiments to test TRISO fuel for the support of the Advanced Gas Reactor Fuel Development and Qualification Program in support of the Next Generation Nuclear Plant. The experiment will be carried out at the Idaho National Lab (INL) Advanced Test Reactor (ATR) facility. The test train consists of a series of capsules cooled by a helium stream that contain TRISO fuel compacts that will be placed in the B-10 position of the ATR core for irradiation. The conditions of the irradiation are meant to closely simulate the high-flux high-radiation-damage environment of a High Temperature Gas Cooled Reactor (HTGR). Some failure of the TRISO fuel particles is

expected. This mechanism of failure will allow for study of the physics of fission gas release. Fission products released from the failed particles will enter into the helium flow stream. The helium lines can then be monitored with radiation detectors.

1.3.1 The Advanced Test Reactor

The ATR originally went online in 1967 with a mission to provide materials and fuel testing support for the US Naval Reactors program. It is located at the Test Reactor Area (TRA) of the INL. Each lobe of the unique serpentine shaped core can be independently controlled to carry out a variety of different irradiation scenarios. The total thermal power of the ATR can reach 250 MW making the ATR the nation's most powerful research reactor, but the power is usually kept below 110 MW. The ATR is surrounded by many different radiation positions located in its beryllium reflector. These irradiation positions are available for use by different government organizations and private companies. Fig. 1.2 contains a horizontal view of the ATR. The fuel is yellow, irradiation positions are represented by purple, the pressurized water loops are in orange, and the gray circles represent the Hafnium coated control drums.

There are three primary types of experiments that are inserted into the irradiation positions of the ATR. The three experiment types are pressurized water test loops, instrumented lead experiments that allow for real time monitoring of temperature and atmosphere control, and simple sealed capsule experiments [5]. The AGR-1 experiment is an example of an instrumented lead experiment. Thermocouples will monitor the experiments temperature and a helium flow loop will help control temperature and carry away fission products for analysis.

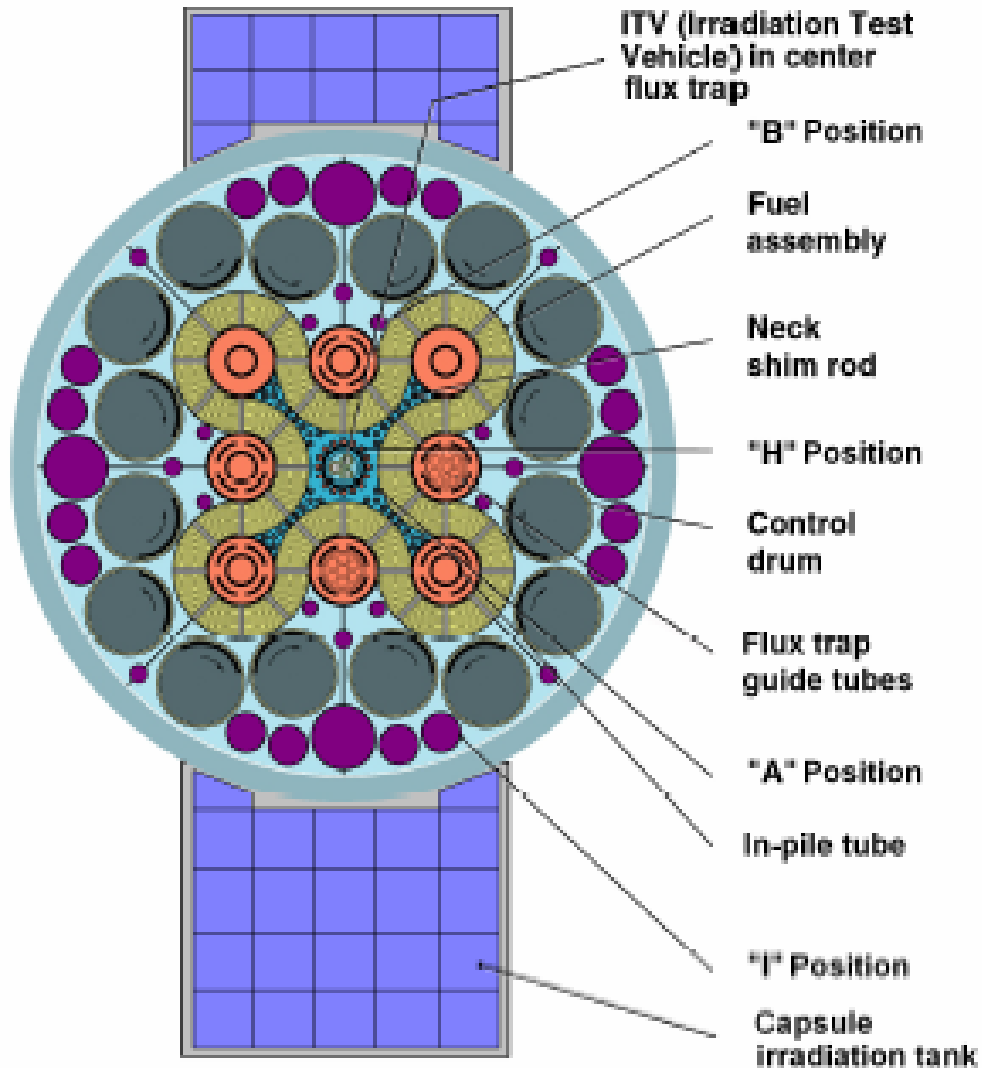


Fig. 1.2 The Advanced Test Reactor Horizontal View

There are some operational challenges in simulating experiments conducted in the ATR. The nominal ATR cycle is 40 days at power with a 7 day outage. In reality the ATR never quite runs the same cycle twice. More recently cycles will typically last 49 to 56 days with 14 day outages. The cycles can also be interrupted by special PALM cycles which increase the power in certain lobes of the ATR. On occasion outages will last for longer periods (i.e. 80 days). During operation of the ATR the neutron energy spectrum can change significantly to suit the needs of the cycle. Because of these variations in core conditions, it is very difficult to accurately simulate the ATR before a cycle is actually concluded.

1.3.2 Fission Product Monitoring System

A system has been developed at INL to monitor the fission products in the helium flow stream of the AGR-1 experimental capsules. All six capsules are independently monitored by a Sodium Iodide (NaI(Tl)) detector for gross counts and a High Purity Germanium (HPGe) detector to generate gamma spectra. The NaI(Tl) detector will record the gross counts for a set counting time interval to produce a counts versus time output. The activity present in the helium will reach a steady state equilibrium level due to Uranium contamination in the graphite matrix. Once a TRISO particle fails, there will be a large spike in the activity detected by the NaI(Tl). This spike will be followed by a shift in the magnitude of the counting continuum. The results from the NPR-1A experiment suggest that there will be other spikes in the gross detector output due to the restructuring of fuel, but these spikes will not be followed by a shift in the magnitude of the counting continuum. The HPGe detectors will be well shielded and will view a 50 cc volume of test loop gas located 5 to 6 inches from the detector face through either a 1.5 inch or 0.75 inch diameter collimator. Gamma Spectra will be collected and analyzed using the INL in house software PCGAP [6].

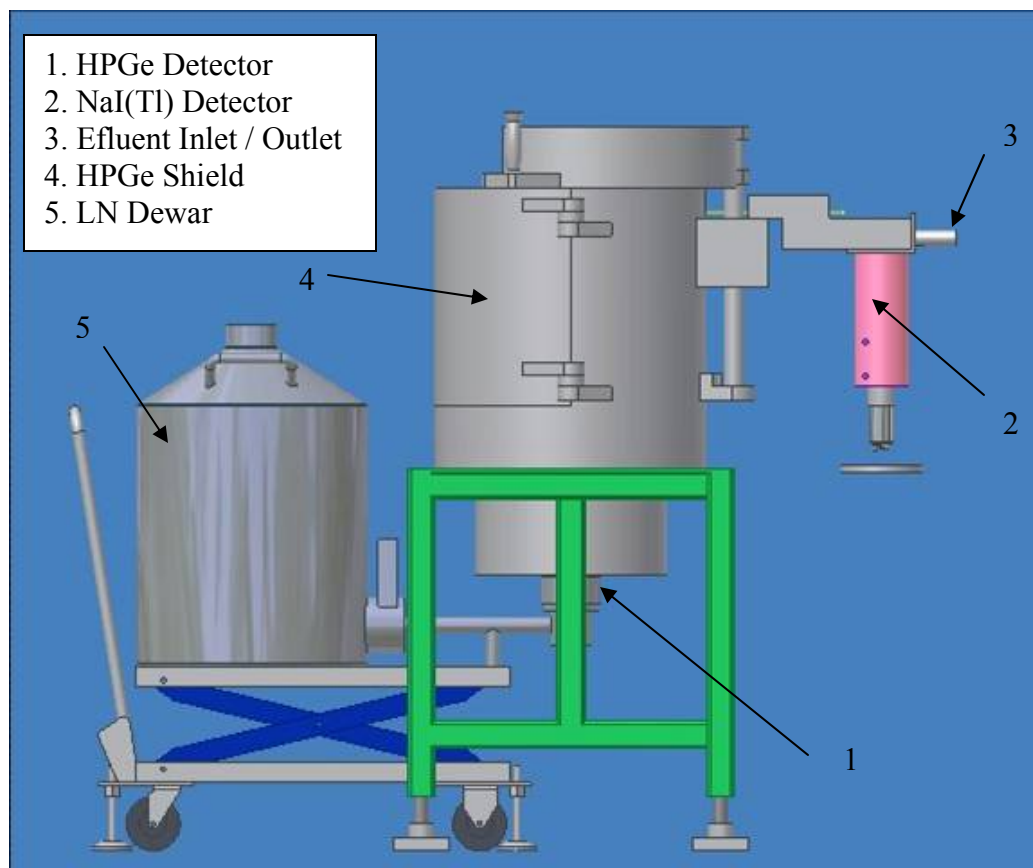


Fig. 1.3 Fission Product Monitoring System Detectors with Shield and Liquid Nitrogen Dewar

There are several impediments to accurate collection of data in the AGR-1 experiment. While most isotopes of Kr and Xe will quickly reach equilibrium concentrations in the effluent stream, long lived isotopes like Xe-133 will not reach equilibrium until a significant part of the nominal irradiation cycle has past. The Xe-133 81 keV gamma would be an ideal gamma to analyze for the experiment, but uncertainties in the actual birth rate may prevent its use in spectral analysis. The cycles of the ATR are governed by the needs of the Navy. Cycles lengths are often extended. From time to time the ATR also performs high power cycles called Powered Axial Locator Mechanism (PALM) cycles that last about 7 days. To do this the Hafnium control drums and shim rods are often set in positions that can cause large swings in the neutron spectrum at the B-10 position. These spectral shifts may have a large effect on the fission rate in the AGR-1 experiment. If a PALM cycle is called

for during the time corresponding to peak fission rate in the experiment (around 300 Effective Full Power Days), the temperature is predicted to go beyond the experimental limits. If a PALM cycle occurs during this time, the natural helium gas will be replaced with He-3, and the flow time will drop from about 150 s from capsule to detector to roughly 30 minutes from capsule to detector. At these travel times there will be a significant drop in the number of short lived isotopes that will be detectable at the detector, but the isotopes with half lives on the order of hours will still be present in the collected spectra. Unfortunately this time also corresponds to the time when failure will be most likely. At the end of the experiment, it may be necessary to increase the temperature of the capsule. For this neon can be injected and used for the flow gas instead of helium. In this case, Ne-23 will be created which has gammas that will contaminate the spectrum. While these complications are troublesome, it is important to remember that the AGR-1 experiment will operate for approximately 3 years. This long time period should provide ample data on fission product release outside of these trouble periods.

1.4 Simulation Strategy

The simulation of the AGR-1 experiment requires several steps. The goal of the simulation is to create a method for analyzing the gamma-ray spectra collected by the FPMS. The analysis method is developed by creating simulated gamma-ray spectra based on experimental conditions and assumed fission fragment Release to Birth ratio (R/B) models. The first step in the simulation is to estimate the inventory of different isotopes of Krypton and Xenon fission fragments that are prevalent in the collected gamma spectra. In the steady state these inventories are equivalent to the birth rate of the isotopes of interest. Several different (R/B) models have been developed throughout the years. These models can be

applied to the birth rates to calculate fission fragment release rates at the fuel. The release rates are then corrected for travel time to the detectors and used in detector models to create simulated gamma spectra. The simulated spectra for a specific model can be compared to the experimental results to help identify which (R/B) model accurately describes the true nature of fission gas release from the TRISO fuel.

Chapter 2

Simulation Approach

Simulation of fuel testing experiments including the AGR-1 experiment at INL requires many calculation steps. These steps are best illustrated by the flowchart seen in Fig. 2.1. Birth Calculations are primarily performed using a depletion code. In this work, ORIGEN 2.2 was used[7]. The release models are taken from the literature and convert the birth rates to release rates. The release rates are then used to create a source that is used in a detector simulation that creates model dependent spectra. The spectra can then be analyzed and compared to the results of the AGR-1 experiment. This would enable the identification of trends in the gamma spectrum. These trends may be indicative of the predicted behavior of a given model or combination of release models.

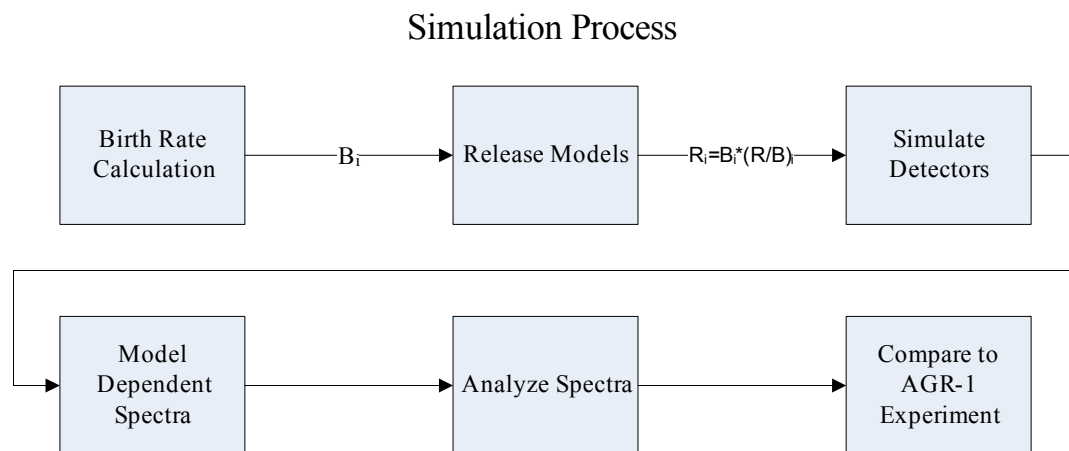


Fig. 2.1. Simulation Process Flowchart

2.1 Creation of Birth Rates

In order to create birth rates for the simulation it is necessary to pull together several different input streams and combine them with many different programs. This process is

illustrated in Fig. 2.2. The irradiation conditions of the AGR-1 experiment are used to create the ATR model in MCNP-5 version 1.40 (Section 2.1.1) [8]. These conditions along with the nuclear data libraries are fed into NJOY-99 to create special problem dependent ACE libraries for use in creating special one group ORIGEN libraries (Section 2.1.3) [9]. ORIGEN is then run to finally calculate the predicted birth rates (Section 2.1.4).

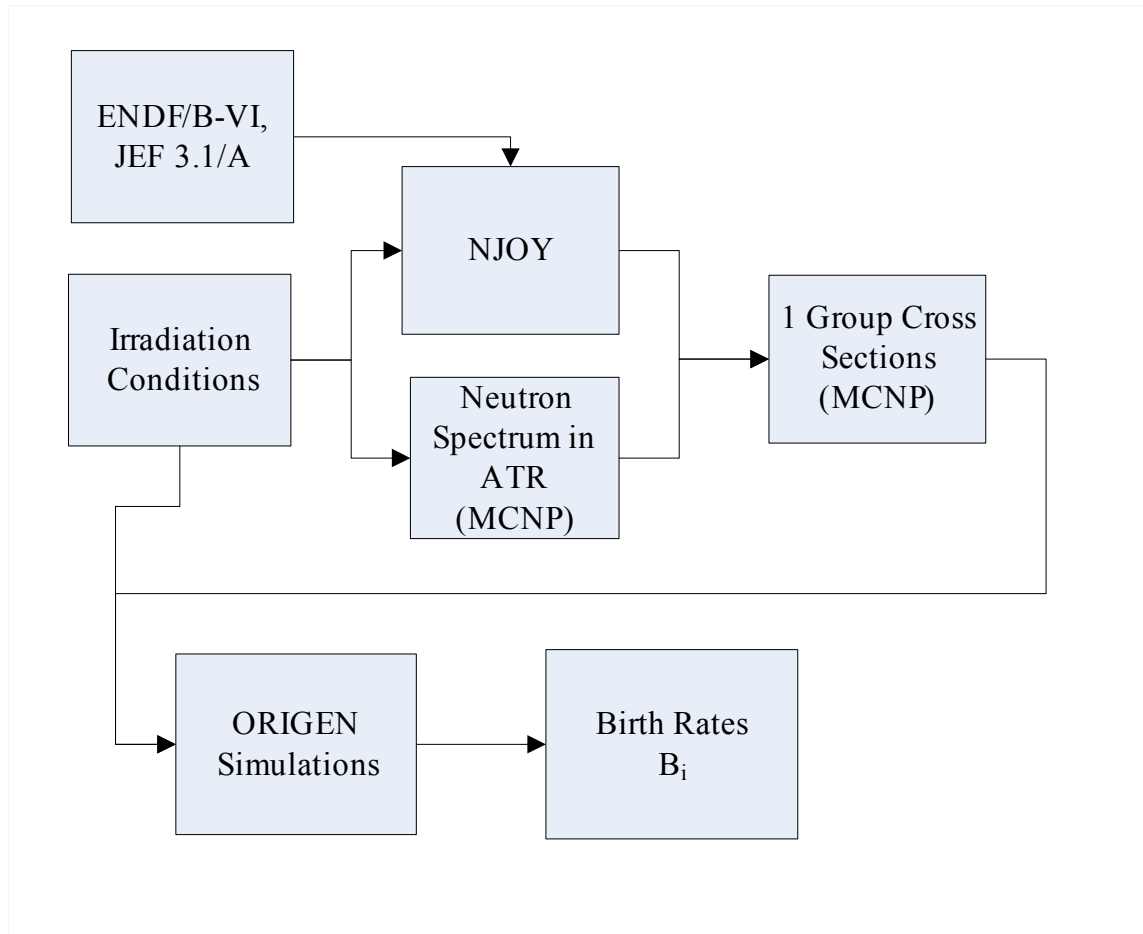


Fig. 2.2. Birth Rate Creation Flowchart

2.1.1 ATR MCNP Simulations

At NCSU an MCNP model of the Advanced Test Reactor (ATR) was created. The model incorporates the serpentine fuel elements, the nine pressurized water loops and the beryllium reflector around the core. The test capsule is simulated at the B-10 position along

with the two closest hafnium control drums. The hafnium can be rotated to change the thermal neutron spectrum in the B-10 position of the model. Part of the model is shown in Fig. 2.3. This model was used to estimate the neutron spectrum in the experimental capsule.

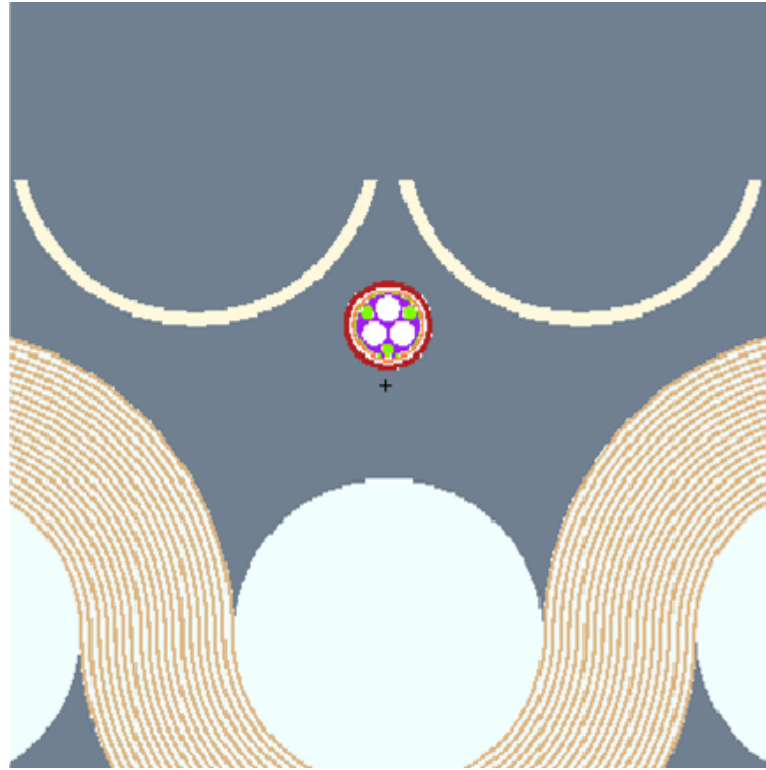


Fig. 2.3. ATR MCNP model with Experimental Capsule

MCNP k-code calculations were used along with “F4” tallies of the fuel capsules to determine the neutron energy spectrum. The position of the hafnium would affect the strength of the thermal neutron portion of the spectrum. By rotating the right drum 51 degrees positive and the left drum 51 degrees negative from the positions seen in Fig. 2.3, a thermal hump was acquired that closely matched a neutron spectrum provided by INL. The resulting 51 degree rotated spectrum could then be used to create one group cross sections for use in ORIGEN libraries.

2.1.2 Choosing the Isotopes of Interest

When a TRISO particle fails, all the fission products associated with Uranium fission will be released. Most of these products are reactive and will be contained by the carbon buffer. However since Krypton and Xenon are chemically inert they will be released into the helium effluent in the experiment. The various different release models are applicable to any isotope of Krypton and Xenon, but only certain isotopes are useful for analysis. The isotope must have a short enough half life that its inventory quickly reaches equilibrium in the fuel, but the nuclide must also not be so short lived that it all decays during transport between the capsule and the detector. For the AGR-1 experiment a half-life of less than 10 hours and greater than 30 seconds seems to be the optimum window. Nuclides of Kr that fit this window are Kr-85m, Kr-87, Kr-88, Kr-89, and Kr-90 and for Xe the nuclides include Xe-135, Xe-135m, Xe-137, Xe-138, and Xe-139. Some exceptions to the optimum window were also analyzed. These nuclides include Kr-85, Kr-91, Xe-131m, and Xe-133. Kr-85 has a 10.76 year half life at this large of a half life it does not fit the assumptions of the release to birth models. Simulations show that it may be hard to get statistically significant peaks from the short lived Kr-91 given the travel time of the AGR-1 experiment. Xe-131m does not reach equilibrium in the fuel quickly with its 11.9 day half life. It also only produces one very faint gamma compared to the other Xe isotopes. Xe-133 would be a very useful isotope to measure. Unfortunately with its 5.2 day half life it does not reach equilibrium until halfway through the expected ATR irradiation cycle. For spectra collected near the end of an ATR operating cycle the 81 keV gamma of Xe-133 should be a useful metric because of its high yield and the high relative activity of Xe-133. Table 2.1 displays the “nuclides of interest” referred to in this thesis and their half lives.

Table 2.1. Nuclides of Interest for Fission Product Release Analysis

Nuclide	Half Life	Nuclide	Half Life
Kr-85m	4.48 h	Xe-131m	11.9 d
Kr-87	1.27 h	Xe-133	5.243 d
Kr-88	2.84 h	Xe-135	9.10 h
Kr-89	3.15 m	Xe-135m	15.3 m
Kr-90	32.3 s	Xe-137	3.82 m
Kr-91	8.6 s	Xe-138	14.1 m
		Xe-139	39.7 s

2.1.3 Creation of One-Group Neutron Libraries for ORIGEN

Neutron cross sections for a specific isotope and nuclear reaction vary widely across the neutron energy range that is present in a nuclear fission reactor. Monte Carlo transport codes like MCNP use continuous energy neutron cross section libraries that contain hundreds to thousands of data points. Depletion calculations are performed using neutron energy spectrum averaged cross sections. Specifically, ORIGEN uses one energy group cross sections for each nuclear reaction that it tracks. One group cross sections are problem dependent and can be calculated by taking the weighted average of the cross section over the entire energy range as seen in Equation (2.1).

Since MCNP uses continuous energy neutron cross sections, it was used to perform the averaging or folding of the continuous energy cross sections into one-group cross sections. In MCNP a void sphere was placed around an isotropic neutron source whose spectrum was derived from the ATR core simulations. The cross sections are created by dividing an “F4” tally of the sphere modified with a tally multiplier card over a non-modified “F4” tally. This process is equivalent to the averaging technique shown in Equation (2.1).

$$\sigma_{1-group} = \frac{\int \sigma(E)\phi(E)dE}{\int \phi(E)dE} \quad (2.1)$$

Initial ORIGEN simulations were run with only the standard MCNP data set. In the final calculations, NJOY was used to create additional continuous energy libraries that are not packaged with MCNP and to broaden the raw ENDF format libraries to the 1450 K temperature of the experiment. Most of the fission product nuclides of interest and their precursors do not have evaluated nuclear data, but the JEF 3.1/A library contains several fission product isotopes such as Xe-133, I-133 and Xe-135. I-135 and the actinides are available in the ENDF VI library [10], [11]. Table 2.2 displays the availability of nuclear data for different isotopes of interest and their precursors. An 'X' indicates the existence of data, while an 'XX' indicates the use of the data to create special MCNP libraries in NJOY. Since ORIGEN only uses a specific set of reactions for fission product nuclides and actinide nuclides, only these reactions were calculated in MCNP. For actinides these reactions are (n,γ) , $(n,2n)$, $(n,3n)$, and $(n,\text{fission})$. For fission products these reactions are (n,γ) , $(n,2n)$, (n,α) , (n,p) .

Table 2.2. Availability of Nuclear Data for Different Isotopes of Interest and their Precursors

Nuclide	MCNP	ENDF - 6	JEF 3.1/A
KR 85		X	XX
XE131M			XX
I 131		X	XX
Te 131m			XX
XE133		X	XX
I 133			XX
XE135	X	X	XX
I 135		XX	
U 235	X	XX	
U 238	X	XX	
Pu 239	X	XX	
Pu 240	X	XX	
Pu 241	X	XX	

2.1.4 ORIGEN Simulations

The ORIGEN code is used to calculate the birth rate or activity of the fission products of interest contained in a TRISO particle under irradiation. ORIGEN 2.2 solves the production/destruction Bateman equation by employing the matrix exponential method to solve the large system of first order differential equations. Version 2.2 retains the ability for users to easily specify any input fuel stream and create user specified cross section libraries.

ORIGEN irradiates either in constant flux or constant power steps. Constant flux steps were chosen to simulate the AGR-1 experiment. Initially simulations were run under the assumption that the flux in the experiment would be dominated by neutrons from outside the experimental capsule. Unfortunately irradiation conditions change significantly during the life of the AGR-1 experiment. These changes require periodic updates to the flux and cross sections used in the ORIGEN simulation. Boron in the experimental capsule acts as a burnable poison. This causes the fission rate to peak around 300 Effective Full Power Days (EFPD) of the experiment. The peaking of the fission rate also corresponds to a peaking of the fission product inventories as seen in Fig. 2.4 for Kr-85m. The boron is used to reduce the fission rate in the fuel. This reduction is necessary in order to keep the temperature of the experiment below the experimental limit of less than 1400°C [12]. To accurately simulate this process a Monte Carlo neutron transport code is coupled with an isotopic depletion code to estimate the fission product inventories. At INL these coupled calculations were performed with their MCWO (Monte Carlo With ORIGEN) code [13]. MCWO uses a UNIX script to link MCNP and ORIGEN. These calculations did not use the updated one group cross sections that were created at NCSU. In order to find the fission product inventories that result from the new cross sections, ORIGEN was run using the constant flux from the MCWO inputs, and Uranium cross sections derived from the change in Uranium inventory

between subsequent MCWO inputs. This allowed for both the benchmarking of the INL predicted fission product inventories and demonstrated the importance of knowing the cross sections of the fission products. There was a large discrepancy between the INL predicted Xe-135 inventory and the NCSU inventory. An analytical solution for the Xe-135 inventory was calculated that confirmed the NCSU numbers. The difference in the two inventory values is thought to stem from a difference in Xe-135 and I-135 cross sections. The inventories for the isotopes of interest are shown in Fig. 2.5.

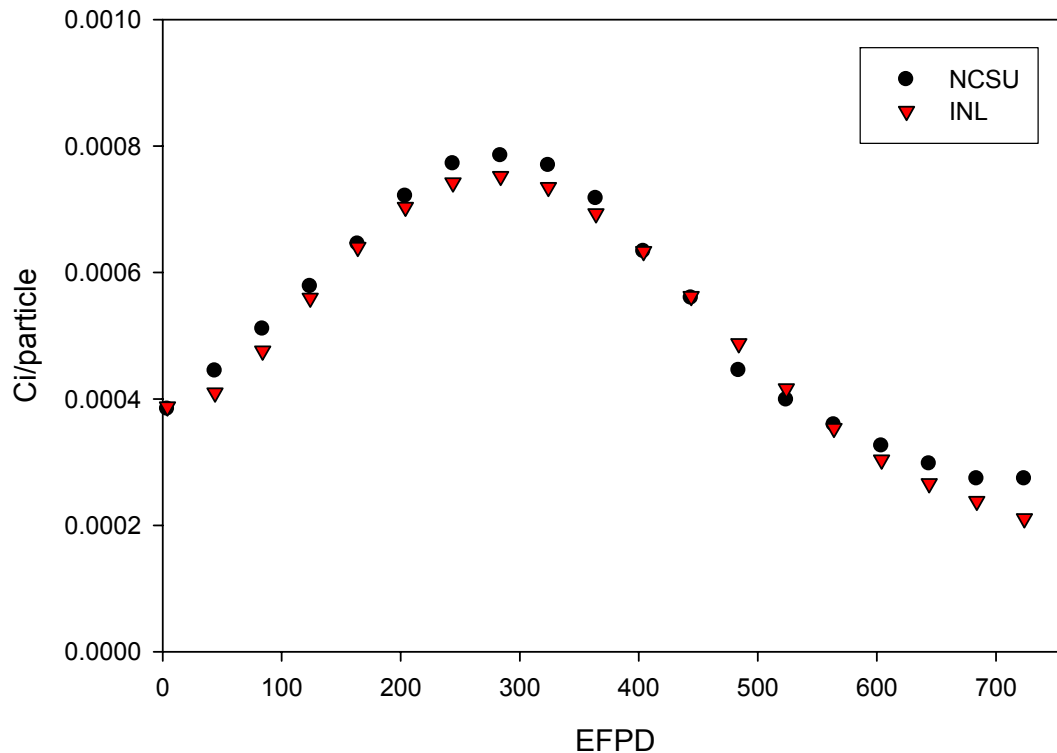


Fig. 2.4. Fission Product Inventory for Kr-85m

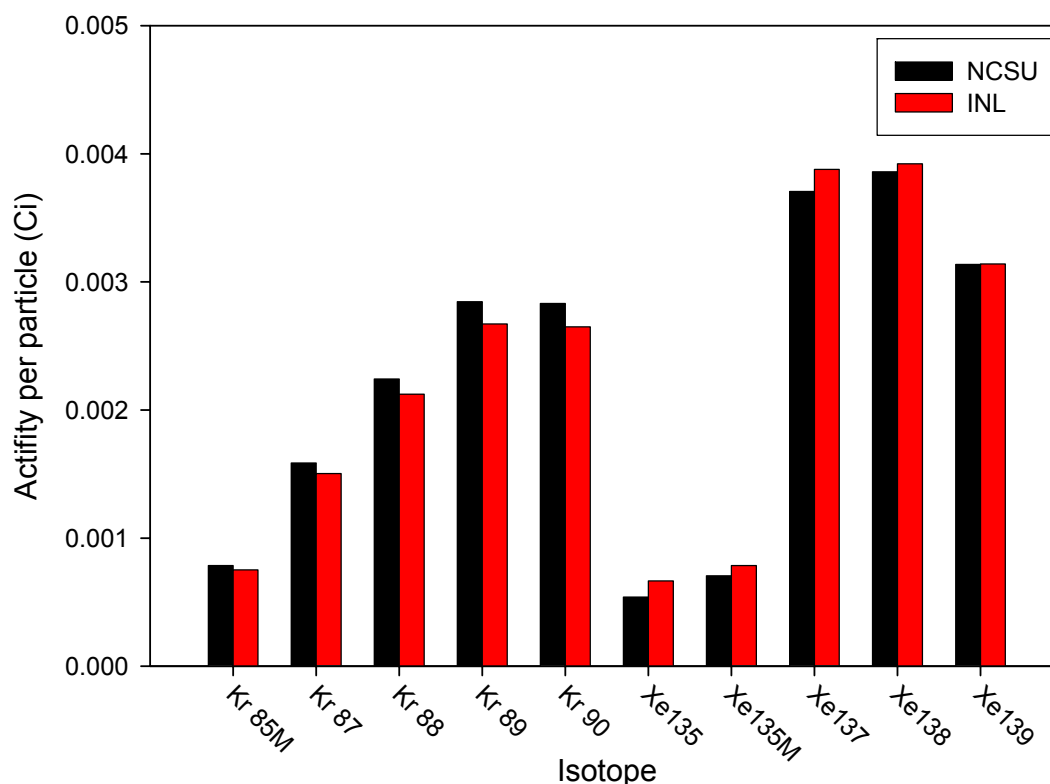


Fig. 2.5. Fission Product Inventories for Different Isotopes at 286 EFPD

2.2 Modeling of Fission Gas Release

2.2.1 Introduction

Fission gas is released from the fuel when gas migrates through the crystal structure of the fuel into the free volume between fuel grains then through the graphite matrix and into the effluent stream. A distinction is made between long lived fission products for which fractional releases are measured and short lived fission products for which release to birth ratios are measured. Fractional releases for long lived isotopes like Krypton 85 must be time dependent to account for the build up of the fission fragments with burn up. Shorter lived isotopes of Krypton and Xenon quickly reach equilibrium levels in the fuel. Since release to birth ratios apply to short lived isotopes, steady state models are used. Release to birth ratios

are of particular interest for catastrophic through coating failure of TRISO particles. These events along with contamination in the fuel compact matrix are the majority contributors to the activity of the effluent stream of a high temperature gas cooled reactor. Current models for release to birth (R/B) ratios are generally based on the Booth equivalent sphere model for release which is based on the diffusion equation. R/B models include terms for coating failure, heavy metal contamination in the fuel compact matrix, and the direct recoil of fission fragments. The details of these models as well as their underlying physics will be discussed.

2.2.2 Development of Booth Model for Short Lived Isotopes

The half lives of the Krypton and Xenon isotopes of interest are sufficiently short that they quickly reach steady state levels under reactor conditions in the fuel kernels. For these isotopes (R/B) ratios apply. Most (R/B) models use the Booth equivalent sphere model to predict (R/B). The Booth model is applicable to diffusion release by the kernel and contamination in the fuel matrix [14], [15]. The general form of the Booth model can be derived from the steady state diffusion equation

$$0 = y\dot{F} + D \frac{1}{r^2} \frac{d}{dr} \left(r^2 \frac{dC}{dr} \right) - \lambda C, \quad (2.2)$$

where y is the fission yield of a nuclide, \dot{F} is the fission rate, D is the diffusion coefficient, C is the concentration of the nuclide, and λ is the decay constant of an isotope. This equation can be solved for the relative release (R/B) at the outer radius of the sphere 'a' [16].

$$\left(\frac{R}{B} \right) = \frac{3D}{\lambda a^2} \left[\left(\sqrt{\frac{\lambda a^2}{D}} \right) \coth \left(\sqrt{\frac{\lambda a^2}{D}} \right) - 1 \right] \quad (2.3)$$

Equation (2.3) in various different forms is the basic equation used for calculating the diffusion component of (R/B) ratios. For a detailed derivation see Appendix A.

For the diffusion coefficient, models often use a reduced diffusion coefficient ($D'=D/a^2$) derived from experiments. Fundamentally the reduced diffusion coefficient is expected to be dependent on the temperature and the porosity of the fuel. As the reduced diffusion coefficient is increased diffusion is enhanced and the (R/B) fraction approaches 1. With a higher reduced diffusion coefficient, the isotope is less likely to decay before leaving the equivalent sphere. Every different R/B model derives its relation for the reduced diffusion coefficient from experimental results of in-pile or post irradiation annealing experiments. Experimental data is empirically fit to produce the temperature dependent coefficients. Different models contain many other terms in the calculation of the coefficients. For instance they may depend on the element of interest (Kr or Xe), or the relationship may be a true diffusion coefficient that is dependent on the equivalent radius. The equivalent radius term 'a' in D' is the spherical radius for TRISO particles. In other materials if 'a' is necessary, it is estimated as the equivalent crystal radius of the average crystal size in the medium. If a model contains terms for contamination in the fuel matrix, the reduced diffusion coefficient relationship for failure release will be different from the relationship for contamination release [16].

At low temperatures the fuel tends to release more gas than can be expected by diffusion alone. Experimental data suggests that there is a temperature independent but geometry dependent process enhancing fission gas release at lower temperatures. This temperature independent process contributes to the majority of release until diffusion becomes important at around 900 K. Direct recoil of atoms by decay has been suggested to explain this observation [17]. Recoiling atoms travel in near straight lines through the fuel structure with path lengths typically on the order of 10 μm . A recoiling atom may also

collide with another atom creating a primary knock-on atom. Knock-on atoms can have more collisions to create secondary and higher order knock-on atoms. Often these two types of atoms come to rest inside the fuel material, but if the recoil event occurs near the surface the atom may be ejected. Ejected knock-on atoms are referred to as knockout atoms [16]. The (R/B) value for recoil is on the order of 0.01 to 0.03. This value may seem small but recoil coupled with diffusion in the fuel matrix accounts for 20, 60 or even 98 % of the total (R/B) ratio for some very short lived isotopes in certain models.

The specific details for different models are widely varied. Some models include correction factors for burnup, while other models include recoil terms. The general equation for the total (R/B) ratio of isotope *i* can be written as the sum of the (R/B)'s attributed to failed particles multiplied by the fraction of failed TRISO particles and the (R/B)'s attributed to contamination in the fuel matrix multiplied by a contamination fraction. The contamination fraction is equal to the number of failed TRISO particles that would be equal to the mass of Uranium contamination divided by the total number of TRISO particles. (R/B)'s for failure or contamination may be a combination of contributions from different release mechanisms like diffusion or recoil [18], [19].

$$\left(\frac{R}{B}\right)_i = f_{TRISO\ failure} \left(\frac{R}{B}\right)_{i, fail} + f_{contamination} \left(\frac{R}{B}\right)_{i, contamination} \quad (2.4)$$

Equation (2.4) is representative of the German 2 and JAERI models. These models show an improvement over earlier models with the inclusion of a contamination term. In earlier fuel types, the major contribution to activity in the coolant was expected to be due to failed TRISO particles, but with improvements in the manufacture of TRISO particles the activity contribution from heavy metal contamination in the fuel matrix is now significant [14]. This earlier approach is seen in other failure models like the GA Model that is

applicable for failed particles but does not include a contamination term. Table 2.3 shows the form of the master formula for different (R/B) models.

Table 2.3. Examples of R/B models that are considered in the current work.

Model [17]	Simplified German Approach, German II, PARFUME
Master formula	$\left(\frac{R}{B}\right)_i = f_{\text{fail}} \left(\frac{R}{B}\right)_{i,\text{fail}} + f_{\text{Contamination}} \left(\frac{R}{B}\right)_{i,\text{contamination}}$
Model [14], [19]	Japanese revised, JAERI revised
Master formula	$\left(\frac{R}{B}\right) = \left(\left(\left(\frac{R}{B}\right)_{k,r} \times \left(\frac{R}{B}\right)_{m,d} \right) + \left(\left(\frac{R}{B}\right)_{k,d} \times \left(\frac{R}{B}\right)_{m,ad} \right) \right) f_k + \left(\left(\frac{R}{B}\right)_{m,r} + \left(\frac{R}{B}\right)_{m,d} \right) f_c$
Model [20]	General Atomics 1994
Master formula	$\left(\frac{R}{B}\right) = f_{\text{rec}} \{ \eta_{\text{rec}} + (1 - \eta_{\text{rec}}) f_{\text{sm}} \} + (1 - f_{\text{rec}}) \{ (R/B)_K + [1 - (R/B)_K] (R/B)_{DR} \}$

2.2.3 The German 2 Model

The Simplified German model or German 2 model is directly based on the Booth equivalent sphere diffusion model. The General equation for this model is shown in Table 2.3. Both $(R/B)_{\text{fail}}$ and $(R/B)_{\text{contamination}}$ are directly calculated by equations of the form of Equation (2.3). In this model, the reduced diffusion coefficients for contamination are a function of temperature and element. The correlations are shown in Equation (2.5) for Kr and Equation (2.6) for Xe. The reduced diffusion coefficients for failure are dependent on kernel diameter and temperature with one empirical fit for temperatures below 1173 K and another fit for temperatures above 1173 K this fit is shown in Equation (2.7). Notice that there are not separate Kr and Xe correlations for failure. This model was chosen for incorporation into INL's PARFUME code because of its close agreement with the NPR-1A

experiment [18]. German R/B values for the expected experimental conditions can be found in Table 2.5.

$$D' = 3.0 \times 10^{-5} \exp \left[\frac{-1.06 \times 10^5}{(8.314)T} \right] \text{ for Kr} \quad (2.5)$$

$$D' = 1.7 \times 10^{-7} \exp \left[\frac{-7.86 \times 10^4}{(8.314)T} \right] \text{ for Xe} \quad (2.6)$$

$$D' = \left(\frac{500}{d} \right)^2 10^{\left[-7.97 - \left(\frac{1920}{T} \right) \right]} \text{ for } T < 1173 \text{ K} \quad (2.7)$$

$$D' = \left(\frac{500}{d} \right)^2 10^{\left[-2.60 - \left(\frac{8220}{T} \right) \right]} \text{ for } T > 1173 \text{ K}$$

2.2.4 The JAERI Revised Model

The Japanese Atomic Energy Research Institute (JAERI) has also developed a (R/B) model based on the Booth equations. Like the German 2 model there are (R/B) terms for failure and contamination, but the JAERI model also includes effects from the recoil of the fission gas. This model also uses a Burnup correction factor and considers the diffusion of the Krypton and Xenon precursor isotopes. Equation (2.8) is the master equation for the JAERI model.

$$\left(\frac{R}{B} \right) = \left(\left(\frac{R}{B} \right)_{k,r} \times \left(\frac{R}{B} \right)_{m,d} \right) + \left(\left(\frac{R}{B} \right)_{k,d} \times \left(\frac{R}{B} \right)_{m,ad} \right) f_k + \left(\left(\frac{R}{B} \right)_{m,r} + \left(\frac{R}{B} \right)_{m,d} \right) f_c \quad (2.8)$$

$\left(\frac{R}{B} \right)$: Fractional release of fission gases from fuel compact

$\left(\frac{R}{B} \right)_{k,r}$: Recoil release fraction from kernel

$\left(\frac{R}{B} \right)_{m,d}$: Fractional release from fuel compact matrix

$\left(\frac{R}{B} \right)_{k,d}$: Fractional release from kernel by diffusion

$\left(\frac{R}{B} \right)_{m,ad}$: Fractional release by grain boundary diffusion

- f_k : Fraction of through-coatings failed particle
 $\left(\frac{R}{B}\right)_{m,r}$: Recoil release fraction from fuel compact matrix
 f_c : Uranium contamination fraction in fuel compact matrix

Equations (2.9) through (2.12) are used to calculate the kernel diffusion term. This set of equations is quite different from the German 2 model and diffusion coefficients. However, it can be shown that the $f_{k,d}$ term will reduce to the form of Equation (2.3) given certain physical assumptions discussed in Section 2.2.6. The subscript 1 terms apply to precursors and the subscript 2 terms apply to the target isotope.

$$\left(\frac{R}{B}\right)_{k,d} = 3 \left(\frac{1}{\Gamma_1} \left(\frac{\coth \sqrt{\mu_1}}{\sqrt{\mu_1}} - \frac{1}{\mu_1} \right) + \frac{1}{\Gamma_2} \left(\frac{\coth \sqrt{\mu_2}}{\sqrt{\mu_2}} - \frac{1}{\mu_2} \right) \right) f_{BU} \quad (2.9)$$

$$\Gamma_1 = 1 - \frac{\mu_1}{\mu_2}, \quad \Gamma_2 = 1 - \frac{\mu_2}{\mu_1}, \quad \mu_i = \frac{\lambda_i}{D_i} \quad (2.10)$$

$$D'_{Kr} = D'_{Xe} = 55 \exp\left(-\frac{38,000}{T}\right) \quad (2.11)$$

$$D'_{1=Br} = 200 D'_{2=Kr}, \quad D'_{1=I} = D'_{2=Xe} \quad (2.12)$$

$$f_{Bu} = 1 + 0.2 Bu \quad (2.13)$$

In the above equations, the decay constants are in units of s^{-1} , the temperature T is in Kelvin, and the Burnup Bu for f_{Bu} is in terms of Fraction Initial Metal Atom (FIMA). Since the recoil terms are functions of geometry not temperature, this model is dominated by recoil release at lower temperatures. Recoil from the kernel is calculated by

$$\left(\frac{R}{B}\right)_{k,r} = \left(\frac{3}{4}\right) \left(\frac{R}{a}\right) - \left(\frac{1}{16}\right) \left(\frac{R}{a}\right)^3, \quad (2.14)$$

where R is the average recoil distance assumed to be 10 μm , and a is the kernel diameter. The matrix diffusion fractional release term $f_{m,d}$ has two components: the fractional release by in-grain diffusion $f_{m,gd}$ and fractional release by grain boundary diffusion $f_{m,ad}$.

$$\left(\frac{R}{B}\right)_{m,d} = \alpha \times f_{m,gd} + (1-\alpha) f_{m,ad} \quad (2.15)$$

The α term is the fraction of fission product generated in-grain. For this work a conservative estimate of all the fission products being generated at the grain boundary was made ($\alpha=0$). This assumption leads to contamination R/B values similar to the German model values. In general the matrix diffusion terms are found by the following equation.

$$\left(\frac{R}{B}\right)_{m,*d} = 3\sqrt{\frac{D'_*}{\lambda}} \left[\coth\left(\frac{\lambda}{D'_*}\right) - \sqrt{\frac{D'_*}{\lambda}} \right] \quad (2.16)$$

Where the reduced diffusion coefficients for in-grain (gd) and grain boundary (ad) are found by the following relationships.

$$D'_{gd} = 7.32 \times 10^{-10} \exp\left(-\frac{3.62 \times 10^4}{T}\right) \quad (2.17)$$

$$D'_{ad} = 4.5 \times 10^{-4} \exp\left(-\frac{1.8 \times 10^4}{T}\right) \quad (2.18)$$

In the above equations, 'T' temperature is in Kelvin. The recoil from heavy metal contamination is given by the following equation

$$\left(\frac{R}{B}\right)_{m,r} = \frac{R(3(r_i + r_o) - 2R)}{6(r_o^2 - r_i^2)}, \quad (2.19)$$

where R is the average recoil distance (10 μm), r_i is the inner radius of the fuel compact, and r_o is the outer radius of the fuel compact. While the inner radius is unnecessary for the AGR-

1 experiment, it is necessary for the JAERI experiments since they use annular fuel compacts.

Work is still ongoing on this model. More improvements are expected to be made by JAERI to this model so that it better fits observed experimental data collected from the Japanese High Temperature Engineering Test Reactor [19]. Calculated JAERI R/B values that correspond to the AGR-1 experimental conditions can be found in Table 2.5.

2.2.5 The General Atomics Model

General Atomics developed but never published in the open literature its own release to birth model. This model was developed in response to the need for a model that reflected the behavior of recent TRISO fuel tests. The GA model consists of components for low temperature release from recoil and knock-out and high temperature release from diffusion and thermal re-solution. Graphite matrix contamination is not considered for this model. There are only terms for fission gas release from failed particles. All of the empirical parameters are based on the HFR-B1 test. The model is in good agreement with these experimental results without the use of any ad hoc fitting terms. The number of adjustable parameters in this model, and its adherence to the fission product release theory outlined in Reference [16] make it an attractive model for consideration [20].

The R/B expression for this model is given by

$$\left(\frac{R}{B}\right) = \left[f_{rec} \{ \eta_{rec} + (1 - \eta_{rec}) f_{sm} \} + (1 - f_{rec}) \left\{ \left(\frac{R}{B}\right)_K + \left[1 - \left(\frac{R}{B}\right)_K \right] \left(\frac{R}{B}\right)_{DR} \right\} \right] f_{gas} \quad (2.20)$$

$\left(\frac{R}{B}\right)$: Fractional release of fission gases from fuel compact

f_{rec} : Fraction of fission gas inventory released by direct recoil from the kernel

η_{rec} : Fraction of recoiled atoms that do not embed in surrounding materials

f_{sm} : Fraction of fission-gas inventory in surrounding materials from embedded recoils that is released by diffusion

- $\left(\frac{R}{B}\right)_K$: Fraction of fission gas inventory release by knockout from the kernel
 $\left(\frac{R}{B}\right)_{DR}$: Fraction of fission-gas inventory released from the kernel by diffusion and bubble re-resolution mechanisms
 f_{gas} : Factor to account for decay during the transport of the fission gas

The f_{gas} term is not included in the calculation of R/B ratios for purposes of comparison with other R/B models. The f_{gas} term is applied when calculating the activity at the detector, and a similar term is applied to all models when calculating predicted spectra.

This model can also be approximated by the following equation for high temperatures.

$$\left(\frac{R}{B}\right) \cong \left[f_{rec} \eta_{rec} + (1 - f_{rec}) \left(\frac{R}{B}\right)_{DR} \right] f_{gas} \quad (2.21)$$

This approximation is possible due to diffusion dominating the fission gas release at higher temperatures. A complete formulation of the GA model follows.

$$f_{rec} = \frac{1}{4} a_g \mu_{ff} \quad (2.22)$$

- a_g = ratio of surface area to volume $3/r_k$ (r_k radius of kernel)
 μ_{ff} = fission fragment range (10 microns)

$$\left(\frac{R}{B}\right)_K = \left(\frac{\alpha_U \mu_{ff}}{4N_U} \right) a_t \left(\frac{\dot{F}}{\lambda} \right) \quad (2.23)$$

- a_U = knock-out ejection yield of uranium
 N_U = number density of uranium atoms in the kernel
 a_t = ratio of total kernel surface area to kernel volume
 \dot{F} = kernel fission-rate density
 λ = radioactive decay constant
 r_k = kernel radius

$$\left(\frac{R}{B}\right)_D = 3(\Gamma G)^{0.5} \left\{ \coth \left[(\Gamma G)^{-0.5} \right] - (\Gamma G)^{0.5} \right\} \quad (2.24)$$

$$\Gamma = \frac{D'}{\lambda} = \frac{D}{r_k^2 \lambda} \quad (2.25)$$

$$G = \frac{\lambda + b_F + b_T}{\lambda + b_F + g + b_T g / \lambda} \quad (2.26)$$

$$\left(\frac{R}{B}\right)_R = H \left[1 - \left(\frac{R}{B}\right)_D \right] \quad (2.27)$$

$$H = \frac{g b_T / \lambda}{\lambda + b_F + b_T + g + g b_T / \lambda} \quad (2.28)$$

$$\left(\frac{R}{B}\right)_{DR} = \left(\frac{R}{B}\right)_D + \left(\frac{R}{B}\right)_R = \left(\frac{R}{B}\right)_D + H \left[1 - \left(\frac{R}{B}\right)_D \right] \quad (2.29)$$

Functional Model Parameters

$$D' = A_o \exp(-T_A / T) \quad (2.30)$$

$$b_T = A_{o,T} \exp(-T_{A,T} / T) \quad (2.31)$$

T is temperature in Kelvin.

$$g = c_1 \dot{F} \quad (2.32)$$

$$b_F = c_2 \dot{F} \quad (2.33)$$

\dot{F} is the fission rate.

Table 2.4. Model Parameters for (R/B) Correlation

Parameter	Definition	Value	Units
f_{rec}	recoil fraction	$7.5/r_k$, where r_k is kernel radius in μm	dimensionless
η_{rec}	fraction of recoiled atoms that do not embed in surrounding material	0.0156	dimensionless
A_o	pre-exponential for kernel diffusion coefficient	$2.047 * 10^{-5}$ (Kr) $3.133 * 10^{-6}$ (Xe)	s-1
T_A	activation temperature for kernel diffusion coefficient	12722	K
c_1	trapping frequency constant	$2.09 * 10^{-4}$	10-14 cm ³ /fission
c_2	fission-induced re-solution frequency constant	$1.976 * 10^{-5}$	10-14 cm ³ /fission
$A_{o,T}$	pre-exponential for thermal re-solution frequency	$3.988 * 10^{13}$	s-1
$T_{A,T}$	activation temperature for thermal re-solution frequency	65000	K

2.2.6 Comparing the German and JAERI Models

The physics behind the German and JAERI models are similar. However, while the German model strictly adheres to the simple steady state formulation of the Booth model, the JAERI model includes the effects of precursor nuclides, burnup, and recoil. To further complicate the comparison of these two models, the different reduced diffusion coefficients are based on different experiments and have different empirical fits. Table 2.5 shows a comparison between (R/B) values for the German model and the JAERI model for both fuel failure and heavy metal contamination. Immediately it is clear that the German model produces much higher release fractions for fuel failure than the JAERI model. This has important implications for the ability to detect the first TRISO failure above the noise signal from the contamination. The contamination release fraction also differs between the two models, but these models only differ at most by a factor of five for Xe-139.

Table 2.5. A Comparison of (R/B) values for the German and JAERI Models

Isotope	Half Life	(R/B) _{fG}	(R/B) _{fJ}	(R/B) _{tG}	(R/B) _{tJ}	(R/B) _{fG} / (R/B) _{fJ}	(R/B) _{tG} / (R/B) _{tJ}
Kr-85	10.76 yrs	9.876E-01	6.668E-01	9.710E-01	9.325E-01	1.481	1.041
Kr-85m	4.48 h	4.678E-02	6.666E-04	3.038E-02	2.008E-02	70.173	1.513
Kr-87	1.27 h	2.511E-02	2.963E-04	1.627E-02	1.111E-02	84.738	1.464
Kr-88	2.84 h	3.737E-02	4.333E-04	2.424E-02	1.617E-02	86.241	1.499
Kr-89	3.15 m	5.137E-03	4.894E-05	3.319E-03	2.908E-03	104.966	1.141
Kr-90	32.32 s	2.126E-03	1.961E-05	1.374E-03	1.678E-03	108.456	0.819
Kr-91	8.57 s	1.095E-03	9.855E-06	7.074E-04	1.257E-03	111.148	0.563
Xe-131M	11.9 d	3.315E-01	1.426E-02	5.647E-02	1.477E-01	23.240	0.382
Xe-133	5.243 d	2.308E-01	6.235E-03	3.773E-02	1.001E-01	37.008	0.377
Xe-135	9.10 h	6.622E-02	9.694E-04	1.024E-02	2.820E-02	68.306	0.363
Xe-135M	15.3 m	1.130E-02	1.398E-04	1.719E-03	5.430E-03	80.829	0.317
Xe-137	3.82 m	5.656E-03	5.162E-05	8.594E-04	3.120E-03	109.574	0.275
Xe-138	14.1 m	1.085E-02	1.023E-04	1.651E-03	5.246E-03	106.043	0.315
Xe-139	39.7 s	2.356E-03	2.097E-05	3.577E-04	1.772E-03	112.381	0.202

* G - German, J - Japanese, f - failure, t - contamination

The drastic difference between the German and JAERI failure models can be better understood by breaking apart the different features of the JAERI model and simplifying it

until it is equivalent to the German model. By removing components of the JAERI model it is possible to identify which component is the source of the large difference between the two models. The failure component of the JAERI model is shown in Equation (2.34). The first step in equilibrating the German and JAERI model is to drop the $f_{m,d}$ terms. This term represents the fractional fission gas loss to decay during diffusion through the graphite matrix in the fuel compact. For the experimental conditions assumed in this work, this is a significant loss. The majority of the difference between the failure terms of the two models stems from the inclusion of the matrix diffusion term in the JAERI model. Recoil contributes some of the difference between the two models but not to the same degree as matrix diffusion.

If the recoil ($f_{k,r}$) term is set to zero and it is assumed that diffusion through the matrix can be ignored ($f_{m,d}=f_{m,ad}=1$), then Equation (2.34) reduces to Equation (2.9), $f_{k,d}$.

$$\left(\frac{R}{B}\right)_{fail} = \left(f_{k,r} \times f_{m,d}\right) + \left(f_{k,d} \times f_{m,ad}\right) \quad (2.34)$$

The $f_{k,d}$ term includes precursor (Γ_1, Γ_2) and burnup (f_{Bu}) effects. If these terms are ignored Equation (2.9) can be rewritten as Equation (2.35) which is equivalent to Equation (2.3) ($D^*=D/a^2$). With German reduced diffusion coefficients, Equation (2.35) will produce the same results as the German model.

$$f_{k,d} = 3 \left(\frac{\coth \sqrt{\mu_2}}{\sqrt{\mu_2}} - \frac{1}{\mu_2} \right) = \frac{3D_2'}{\lambda_2} \left[\left(\sqrt{\frac{\lambda_2}{D_2'}} \right) \coth \left(\sqrt{\frac{\lambda_2}{D_2'}} \right) - 1 \right] \quad (2.35)$$

The same type of simplification can be applied to the contamination part of the JAERI model to produce German equivalent (R/B) ratios with the JAERI model. See Appendix B for a step by step numerical demonstration of this process of reducing the JAERI model to the German model.

2.2.7 Comparing the German and the GA Models

The General Atomics model for failure is much closer to the German model than the JAERI model. Many of the extra features of the GA model do not make significant contributions to the final R/B value. At high temperatures where recoil is insignificant the GA model readily reduces to the German Model. Without recoil the GA model can be approximated as $(R/B)_{DR}$ given by Equation (2.29). Two terms that set the GA model apart from the German model are G the diffusion trapping parameter and H the thermal re-resolution parameter. For isotopes with $T_{1/2} < 10$ hours which includes most of the isotopes on interest, the H term approaches 0, and the G term approaches 1. Under these conditions the formulation of the GA model is of the same form as the German model (Equation (2.3)). The majority of the difference between the German and the GA models is due to the difference in the reduced diffusion coefficient of the two models at the experimental temperature. One significant difference between the two models occurs in the way reduced diffusion coefficients are calculated. The German model only uses a single relationship for Kr and Xe, while the GA model uses two different relationships for the two elements. This distinction proves to be important when differentiating between different models.

2.2.8 General Trends in the R/B ratios

All the models are generally based on the Booth equation which gives all the models the same form as Equation (2.3). If you consider the German Model to be the base model, it is possible to maneuver each model towards the same form and values as the German Model by removing or adding model components.

The reduced diffusion component can be used to compare the expected magnitude of fission product release due to a certain model. The diffusion component of the release is the

largest contributor to the signal at the experimental temperatures, and the magnitude of the reduced diffusion coefficient is proportional to this form of release. In general fission product release magnitude will follow coefficient magnitude. Deviations from this trend indicate the presences of influential non-diffusion mechanisms. The reduced diffusion coefficients have been graphed in Fig. 2.6 to illustrate the temperature dependence of these values between the different models. Fig. 2.7 shows the coefficient value for each model at the peak expected temperature of the experiment. The influence of reduced diffusion coefficient on the magnitude of the R/B ratio for a model is further illustrated by comparing the trend in D' for failed particles shown in Fig. 2.7 to the calculated failed particle R/B Ratios for each model and isotope in Fig. 2.8.

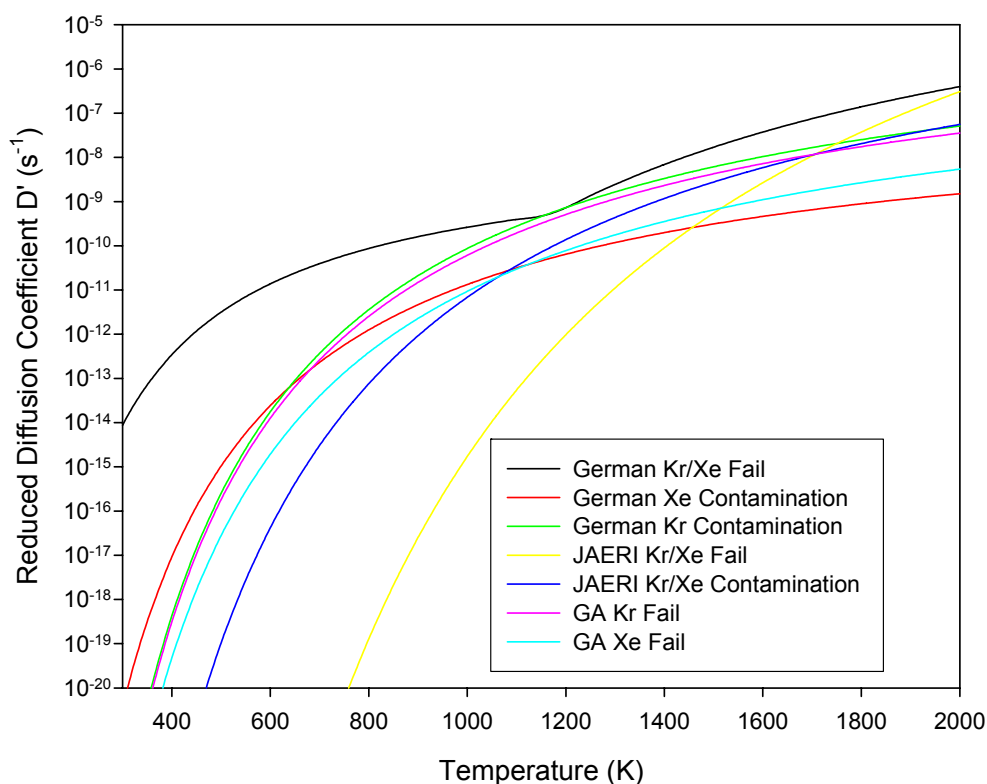


Fig. 2.6. Reduced Diffusion Coefficient as a function of Temperature for Different Model Components

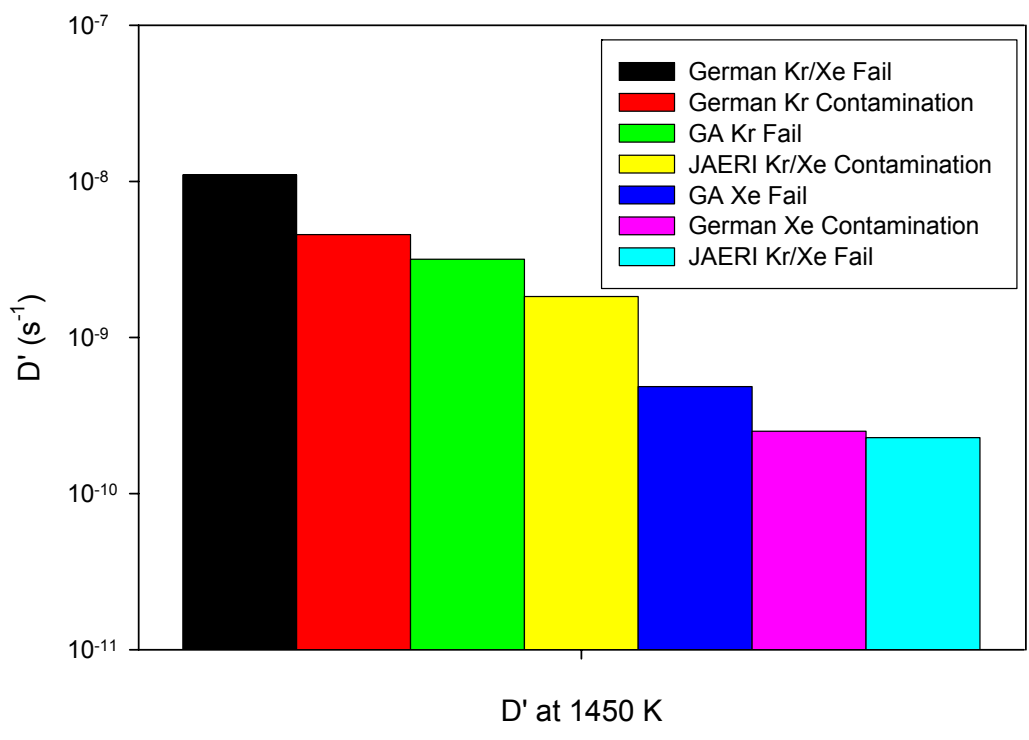


Fig. 2.7. Reduced Diffusion Coefficients at 1450 K

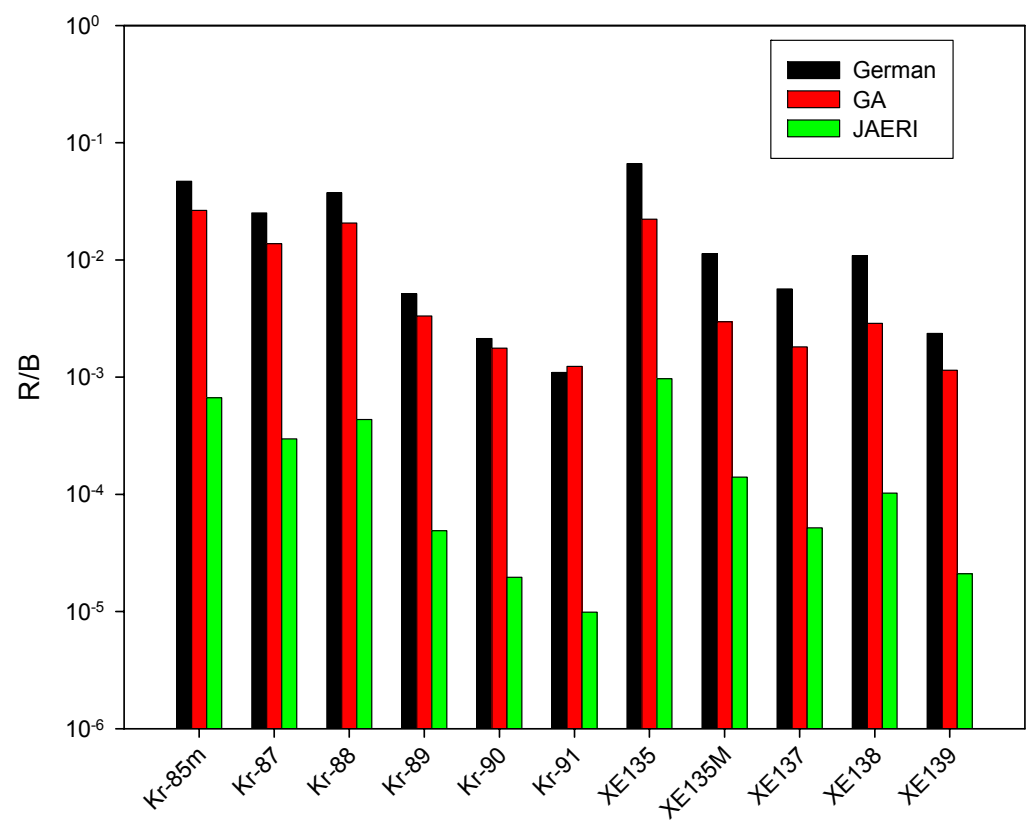


Fig. 2.8. Failure Release to Birth Ratios for various models given expected experimental conditions

Many different modifications to the models have been performed to fill in the gaps between the models and in order to better understand the effects different model parameters have on fission gas release. Each model contains some parameters that are based on specific experimental results. If the AGR-1 experiment does not perform as expected by any model as written it may be necessary to create hybrid models in order to accurately predict the release spectra. For example it may be necessary to consider model features like recoil, but the fission products may diffuse with the German diffusion coefficients.

An important model modification for understanding the properties of the R/B models has been dubbed the Modified JAERI model. In this modification the source of the largest discrepancy between the two models, the matrix diffusion term, is ignored ($f_{m,d}=1.0$). The results of this model are graphed along side other model dependent spectra in Appendix C. This modified model is similar in magnitude to the German and the GA model. One consequence of ignoring matrix diffusion is that the recoil term especially for short lived isotopes becomes a significant contributor to the release activity. Construction of this modification demonstrated two important points: the source of the major differences between the German and the JAERI models and the significance of recoil release for short lived nuclides.

2.2.9 Conclusions on Release to Birth Models

Different groups have created steady state (R/B) ratio models for short lived fission gasses that produce quite different results. The differences in these models come about from the use of different diffusion constants, and the use of extra correction parameters like precursor and burnup effects. Since these models are based on the same physics it is possible

to explain the source of these differences. The implications of which model most accurately describes future experiments are important for determining the success or failure of these experiments. Under the German model, the detection of the first TRISO failure should be quite easy, but under the JAERI model, first failure detection becomes much harder. The stark magnitude differences in these models may also allow for low resolution detectors to be used.

2.3 Creation of Release Spectra

The final step in simulation of the AGR experiment is the creation of model dependent spectra. These spectra help visually demonstrate the effects of different models and their components. These results can be used to precondition the spectral analysis approach used in the experiment through the identification of preferred peaks that are well defined and free from interference from other peaks. Simulation of the spectra is also useful for investigating the possible use of low resolution room temperature detectors [21].

2.3.1 Detector Simulation in MCNP

The Monte Carlo simulations that take place in MCNP do not directly simulate the actual physics of radiation detectors. When a photon interacts with the active volume of a detector it produces an electron which then produces a random number of secondary electrons as the charge is collected in the electric field. The collected charge is proportional to the energy deposited by the incoming photon. For full photon energy absorption events, the random production of secondary electrons produces full energy peaks with normal distributions about the incident photon energy in the gamma ray spectra.

MCNP uses the F8 Tally to simulate detector responses. This tally works very differently from other tallies in MCNP. It monitors the incoming and outgoing energy of a

particle track. A score is then added to the energy bin of the tally that contains the difference in these energies. This produces simulated spectra with discrete full energy peaks and sharp Compton edges. The fix for this problem is to apply a Gaussian Energy Broadening operation to the tally by way of the GEB card. This card normally distributes the score in each bin based on the energy versus full width half max relationship of the detector being simulated. MCNP uses the relationship shown in Equation (2.36) to relate energy (E) to full width half max (FWHM). The coefficients a, b, and c are found by fitting the equation to experimental measurements of energy vs. FWHM for the detector under investigation. Table 2.6 contains the values for a, b, and c that are used to simulate the different detectors. More detailed figures showing the experimental data and fits used to acquire the GEB parameters can be found in Appendix C.

$$FWHM = a + b\sqrt{E + cE^2} \quad (2.36)$$

Table 2.6. GEB Card Fit Parameters for Various Detectors

Detector	a	b	c
HPGe	1.9211E-06	1.6446E-03	-3.0480E-05
HPXe	2.0000E-03	1.5200E-02	6.6500E-01
LaBr	-2.7036E-03	2.7064E-02	-9.5661E-02
CZT	1.0210E-02	1.8280E-03	3.7310E+00

The correction to the F8 tally that the GEB card adds allows for satisfactory simulation of High Purity Germanium (HPGe), High Pressure Xenon (HPXe), Cadmium Zinc Telluride (CZT), and Lanthanum Bromide LaBr₃(Ce) detectors. In the observed HPXe detectors there was severe low energy tailing, possibly caused by wall effects, for gammas with full energy peaks above 1 MeV. This tailing violates the Gaussian shaped peak requirement for good MCNP detector simulation. An additional problem is also present with HPXe detectors. The Xenon K-shell X-ray often escapes from the active volume. This

creates a sister peak to each full energy peak, and these sister peaks do not follow the same energy vs. FWHM trend that the full energy peaks do.

After the parameters for the GEB card have been identified for the detector to be simulated, a corresponding MCNP geometry can be created. The geometry does not need to be too complex, but the active volume of the detector should be well modeled.

2.3.2 MCNP Source Creation

MCNP sources are created by combining the fission product inventories from ORIGEN with the release to birth ratios from the failure models. The gamma energies for the simulations are derived from the ENDF/B-VI decay data [11]. All the gammas for Kr-85, Kr-85m, Kr-87 through Kr-91 were incorporated into the MCNP simulations of the Krypton source. Likewise all the gammas for Xe-131m, Xe-133, Xe-135, Xe-135m, Xe-137, Xe-138, and Xe-139 were used to create the Xenon source for the MCNP simulations. The separate Kr, Xe source method assumes the use of an isotopic separation system that has been developed at North Carolina State University [22]. This system works much like a mass spectrometer. It ionizes incoming gas and uses a magnetic field to send either Kr or Xe towards the detector.

Birth rates are inferred from fission product inventories by the following assumption. The short lived fission products reach an equilibrium activity in the fuel. Since the activity is in a steady state it can also be considered the birth rate for that isotope once the TRISO particles have failed and any trapped activity is released. The results of the NPR-1A experiment performed at INL support this assumption. In the NPR-1A experiment there was only one fuel capsule and the irradiation conditions were more extreme than in the AGR-1 experiment. NPR-1A did use a helium gas loop similar to AGR-1. Gross counts of the flow

gas were recorded for this experiment. From these counts versus time figures it is clear that when a TRISO particle fails an initial burst of activity will be seen in the gross counts followed by a shift in the base count rate of the flow gas. The shift in the gross counts indicates that TRISO failure results in a continuous steady state release of activity into the flow gas that is measurable by the gamma spectrometers [23].

Expected Krypton and Xenon gamma spectra are calculated by combining birth rates from ORIGEN, a (R/B) model, the yield of a specific gamma (Γ_k), and a decay correction for isotope travel from the capsule to the detector. The release rate for isotope i , release model j , and gamma k is calculated by Equation (2.37).

$$R_{i,j,k} = B_i \left(\frac{R}{B} \right)_{i,j} \Gamma_k e^{-\lambda_i t_{travel}} \quad (2.37)$$

These release rates are combined and normalized to 1 for use as the probability distribution function of an MCNP source (SP card). The MCNP source along with a given MCNP detector geometry is used to create expected gamma spectra based on a specific release model j .

2.3.3 Model Applied Spectra

Several different detectors were considered in the simulations. High Purity Germanium (HPGE) detectors with their superb resolution are well suited for analyzing the complex spectra resulting from the fission gas release. Peak areas from the resulting HPGe spectra can easily be resolved to estimate the activity present in the detection volume. Specific model details that manifest themselves in only a select few isotope activities will be detectable in the high resolution spectrum that would otherwise be lost in the spectrum from a lower resolution detector. The coarse model effects are also readily detectable in the high resolution spectra.

Monte Carlo tallies are usually reported in a per source particle unit. In order to compare different models, it is necessary to multiply the tally by a (R/B) model dependent source particle factor. The number of source particles by which to normalize the spectra changes throughout the course of the experiment. Without knowing the exact counting conditions and irradiation conditions, it is not possible to convert the MCNP spectra into true counts spectra.

For purposes of demonstrating the effects of the different R/B models the MCNP spectra have been normalized by the source strength of the release activity due to a particular model. . The source particle factor for a model is calculated by summing the number of gammas that are expected at the detector from each isotope as shown in Equation (2.38) for model 'i' given the different isotopes 'j' contributing to the source.

$$F_i = \sum_j \left(\frac{\gamma' s}{decay} \right)_j \left(\frac{R}{B} \right)_{i,j} B_j e^{-\lambda_j t_{travel}} \quad (2.38)$$

For the spectra shown in this work the birth activities are taken at the end of a typical ATR cycle approximately 300 EFPD into the experiment. The magnitude of the birth activities will change throughout the experiment, but activities relative to each other will remain fairly constant for most isotopes of interest.

MCNP simulations of High Purity Germanium (HPGe) detectors are highlighted in the following section. The effect the R/B ratios on the spectra seen at the detector is best seen by graphing spectra that would correspond to the birth activities versus the spectra for an applied model. This can be seen in Fig. 2.9 which shows the birth spectra for the Xe isotopes of interest and the corresponding Xe contamination spectra for the German and JAERI models.

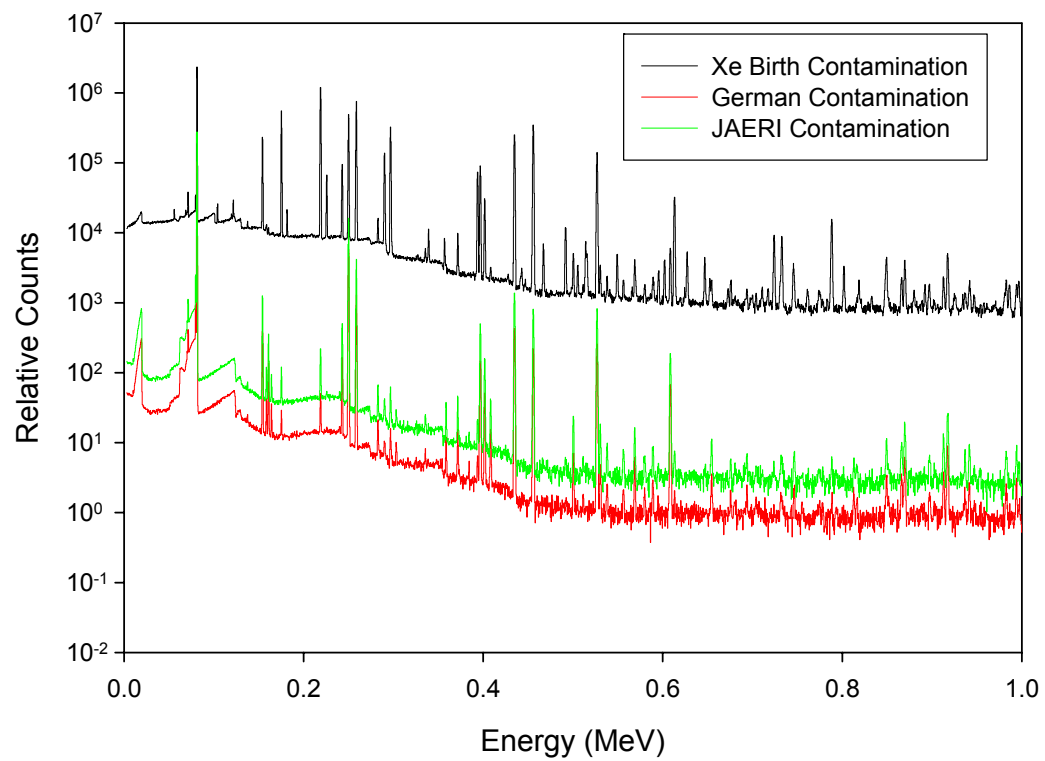


Fig. 2.9. Xe Birth Spectrum vs. Model Applied Spectra

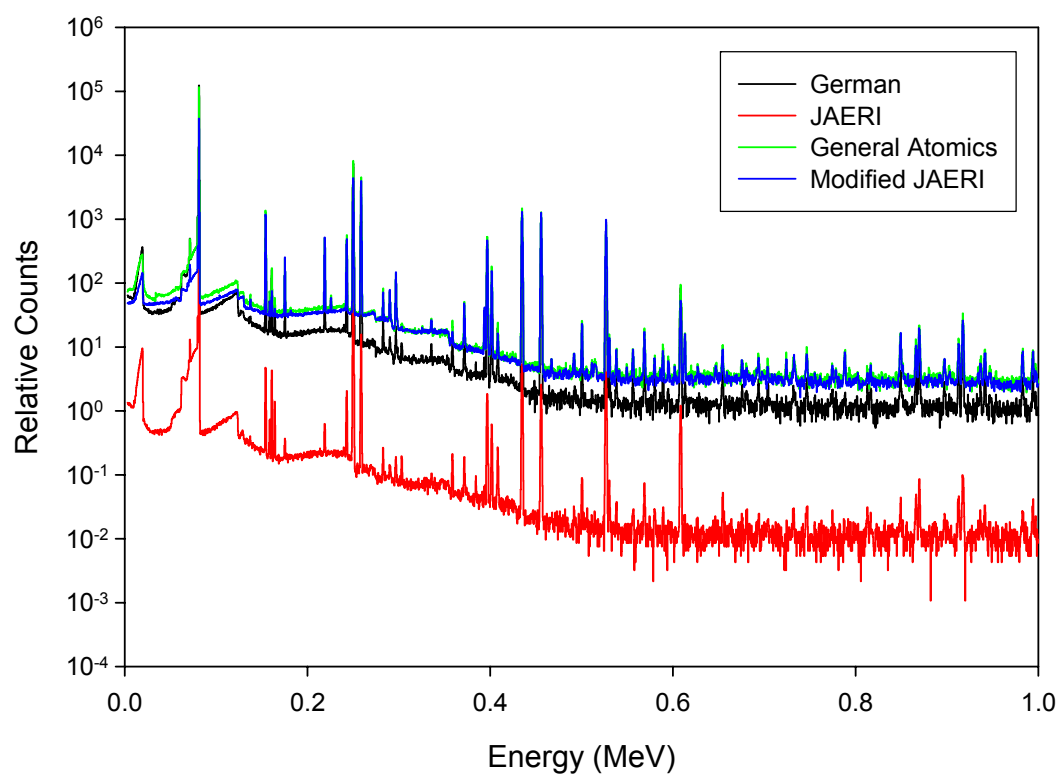


Fig. 2.10. Xe Failure Spectra for German, JAERI, General Atomics, and Modified JAERI models

The plot in Fig. 2.10 illustrates the signal strength difference for failure between the different models for the Xe isotopes. Most of the magnitude difference between the German and JAERI model can be attributed to the JAERI model's use of an additional matrix diffusion mechanism discussed in Section 2.2.6. If the $f_{m,d}$ term is set to 1.0 the "Modified JAERI" model is created. The magnitude of this model is very similar to the German and GA models. Notice also that many of the full energy peaks in each spectrum have different relative intensities when compared between the models. This is caused by model properties that create an enhancement in the release of shorter lived isotopes due to recoil in the kernel.

The ability to detect a single particle failure is considered very important. For this reason the contaminated plus one particle failure spectrum has also been graphed. The large German signal strength allows for the first TRISO failure to be easily seen above the contamination signal as demonstrated in Fig. 2.11 for Xe and Fig. 2.13 for Kr which show the response for the Xe and Kr isotopes. This is in sharp contrast to the JAERI contamination and contamination plus 1 spectra seen in Fig. 2.12 for Xe and Fig. 2.14 for Kr. The small magnitude of the JAERI failure signal makes the first TRISO failure signal almost indistinguishable from the contamination signal in the JAERI model. The full set of simulated spectra for Xe and Kr isotopes of interest, and all the detector types can be seen in Appendix C.

Not all (R/B) models have a contamination component. For these models contamination can be considered to act under either the German or JAERI model, failure would be governed by the other model. Since the GA (R/B) model for failure closely resembles the German model in magnitude, the first failure signal should be distinguishable

from the contamination signal if either contamination model was used. This is also true for the Modified JAERI Model.

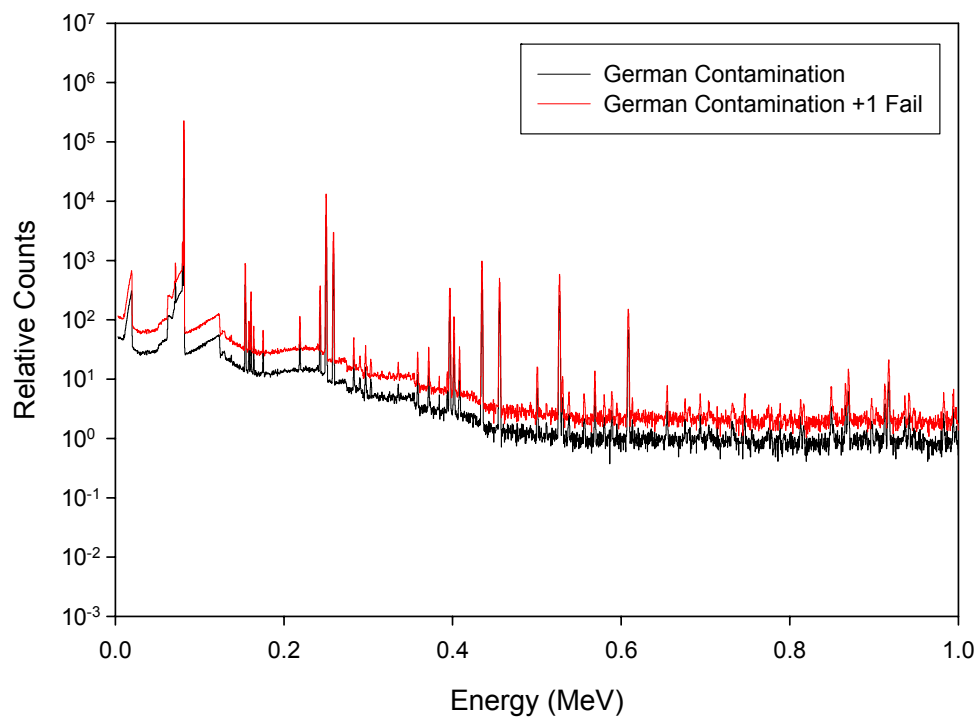


Fig. 2.11. Contamination Signal and First TRISO Failure Signal for Xenon according to German Model

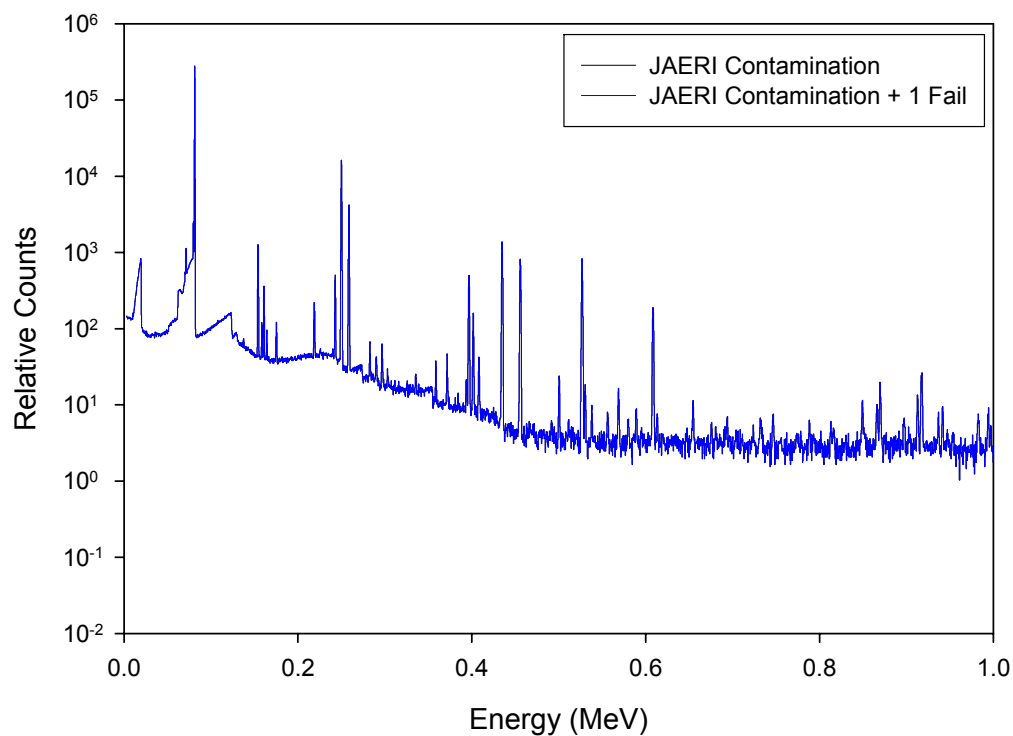


Fig. 2.12. Contamination Signal and First TRISO Failure Signal for Xenon according to JAERI Model

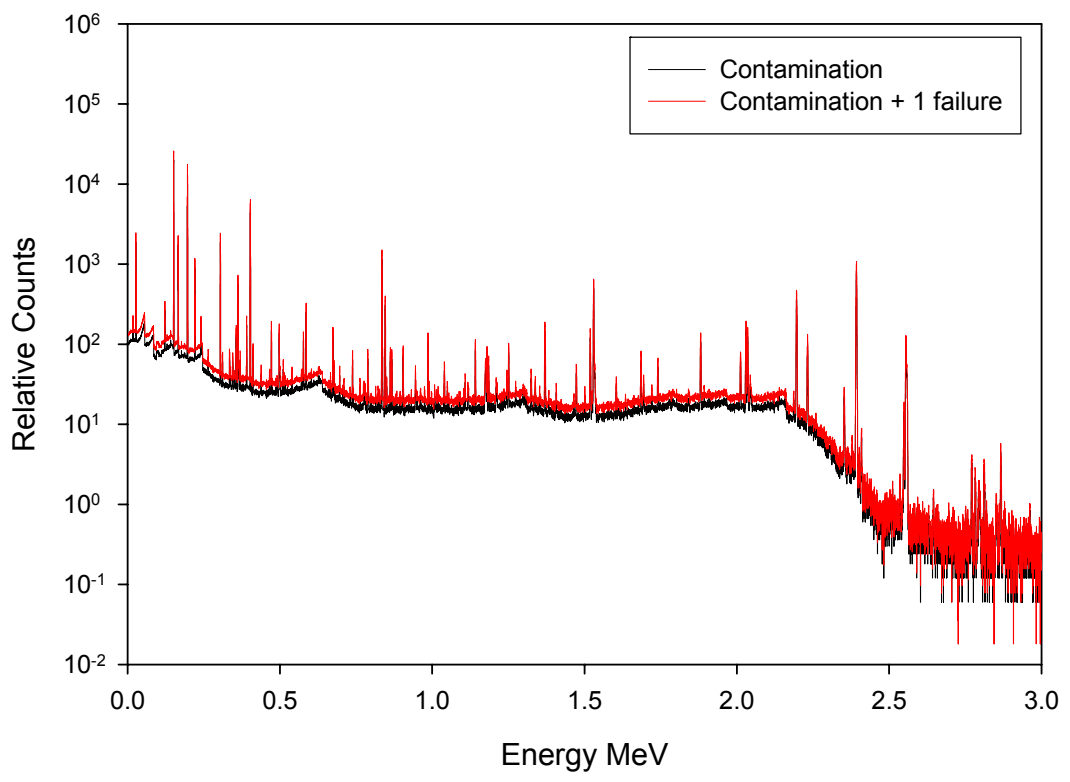


Fig. 2.13. Contamination and First TRISO Failure Signal for Krypton according to the German Model

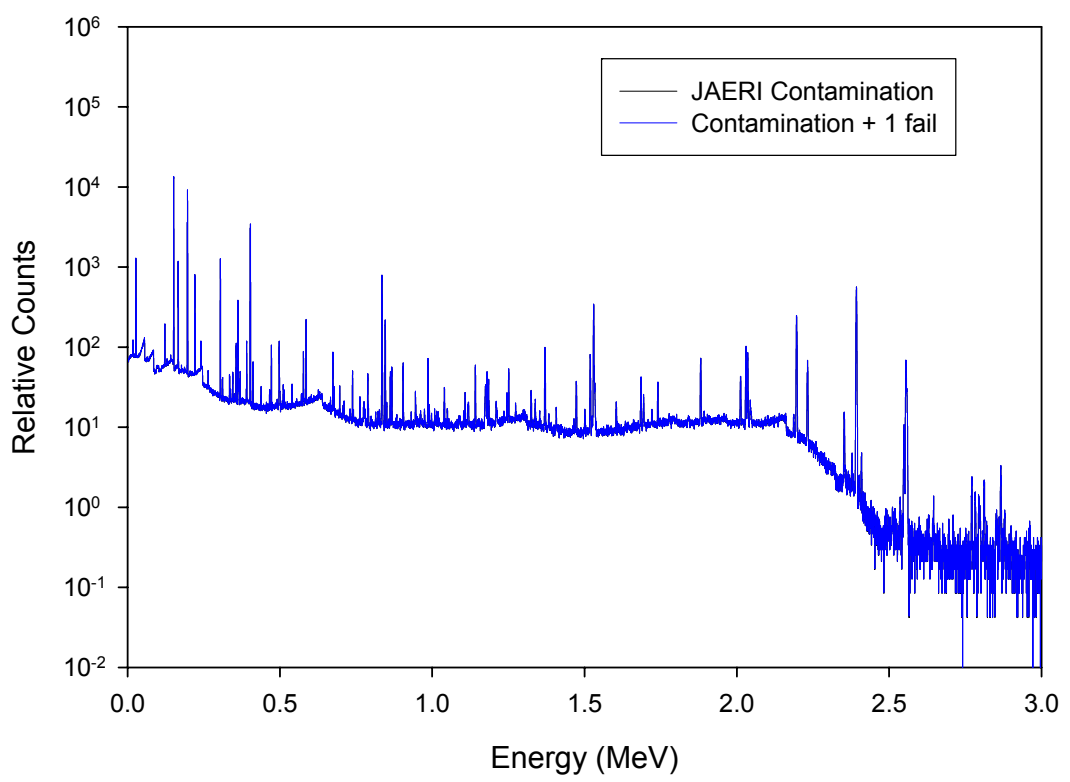


Fig. 2.14. Contamination and First TRISO Failure Signal for Krypton according to the JAERI Model

2.3.4 Low Resolution Detector Spectra

Lower resolution detectors have also been simulated. These detector types include High Pressure Xenon (HPXe) ion chambers, Cerium Zinc Telluride (CZT) semi-conductors, and Lanthanum Bromide (LaBr or LaBr₃(Ce)) scintillators. The trends observed in the high resolution HPGe spectra can also be seen in the simulations of lower resolution detectors. Instead of using specific peaks, areas of the resulting spectra that correspond to several characteristic peaks could prove useful in benchmarking the release models. While low resolution detectors may not be able to identify differences in the fine details of the release models, the coarse effects conveyed by different models are still present in the spectra of low resolution detectors. A good example of coarse effects is the large release activity difference between the German and JAERI models that is easily identifiable in low resolution spectra. The general trends present in Fig. 2.9 and Fig. 2.10 for HPGe detectors are mirrored in Fig. 2.15 for a HPXe detector and Fig. 2.16 for a LaBr detector.

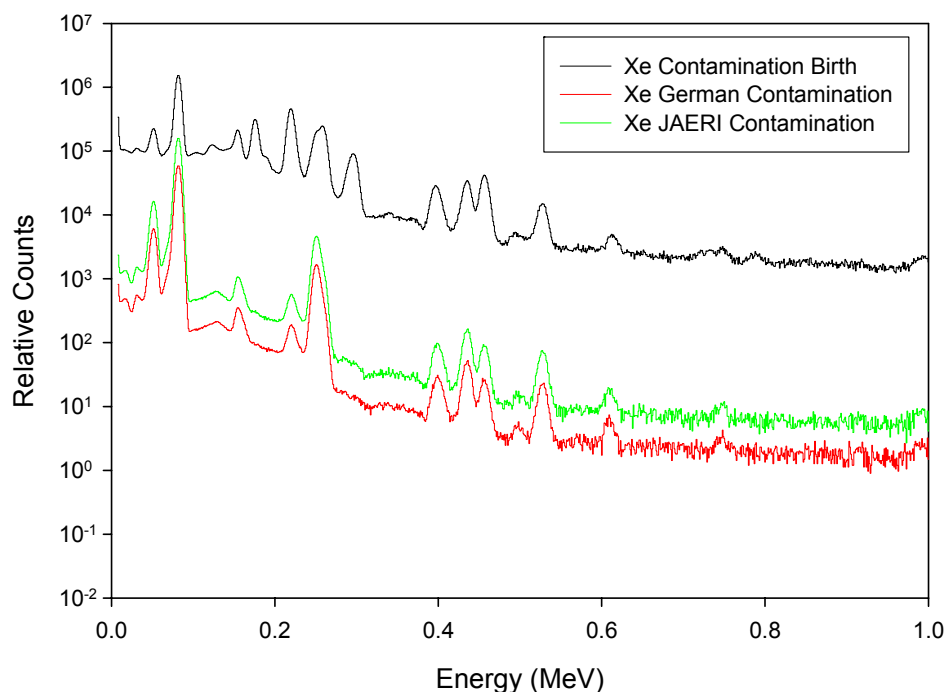


Fig. 2.15. HPXe Birth and Model Applied Spectra for Xe isotopes of interest

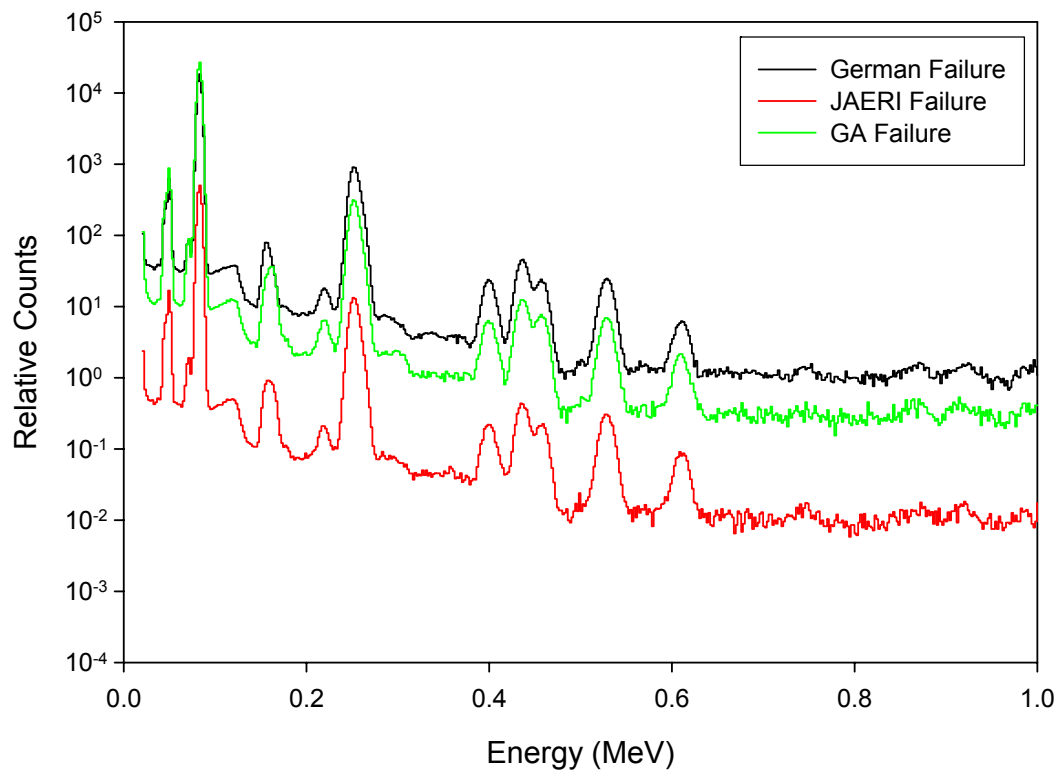


Fig. 2.16. Xe Failed TRISO Particle Spectra for the German, JAERI, and GA models on a LaBr Detector

Chapter 3

Interpretation of Simulations

3.1 Interpretation Using Absolute Release Activity

One approach to benchmarking the R/B models would be to directly compare the release activities as derived from the gamma-ray spectra measured in the experiment with those predicted from the ORIGEN and MCNP simulations. Ideally, these two activities should correspond if the model used to create the simulated spectra does in fact represent reality.

Simulated release activities are found by combining the birth activities calculated in ORIGEN and the R/B ratios calculated for a certain model as seen in Equation (3.1) for isotope i and release model j (e.g., German Model). The terms in Equation (3.1) are heavily dependent on experimental conditions. The R/B ratios are dependent on the temperature in the experimental capsule. Changes in the flux and isotopic composition of the fuel and the test capsule assembly directly impact the birth activities.

$$R_{i,j} = \left(\frac{R}{B}\right)_{i,j}^{contamination} B_i^{contamination} + \left(\frac{R}{B}\right)_{i,j}^{failure} B_i^{failure} \quad (3.1)$$

The experimental gamma ray spectrum can be analyzed to find the experimental release activity. The actual signal that is counted at the detector is not the release activity, but it is instead a collection of several parameters that are used to back calculate the release activity as seen in Equation (3.2). These parameters include:

- $PA_{E\gamma,i}$ The measured peak area of a specific gamma of energy 'E' for a specific isotope 'i'
- $Y_{E\gamma}$ The yield of a specific gamma of energy 'E' for a specific isotope

$\varepsilon_{E\gamma}$	The detector efficiency at energy 'E'
$e^{-\lambda_i t_{trav}}$	The probability isotope 'i' not decaying while traveling to the detect
V	The volume of sweep gas the detector views
\dot{V}	The volumetric flow rate of the sweep gas
Δt	The counting time of the collected spectrum

The general equation for release activity at the test capsule ' $R_{i,E,\gamma}$ ' is then:

$$R_{i,E,\gamma} = \frac{PA_{E\gamma}}{Y_{E\gamma} \varepsilon_{E\gamma} e^{-\lambda_i t_{trav}}} \frac{V}{\dot{V} \Delta t} \quad (3.2)$$

Many of the terms in Equation (3.2) can be estimated or measured like the volume of the detection chamber, the detectors efficiency, the decay constant of the isotope, and yields of gamma-rays which are tabulated in the nuclear data. The travel time from the test capsule to the detector is an important parameter for short lived isotopes. If this value is not well known, activities measured from short lived isotopes may be unreliable. The volumetric flow rate should remain constant, but it will be changed to different levels at different times during the course of AGR-1.

Absolute measurements are well suited for some applications. The large difference between the release expected according to the German model versus the JAERI model is clear even using absolute measurements. The detection of the next failed particle will be calculated using absolute measurements, but a gross count NaI(Tl) detector will be used not the HPGe spectrum. Relative measurements are bracketed between pure contamination values and pure failure values. Once enough particles have failed the next failed particle will not manifest itself in a detectable change in relative measurements, but the change will be perceivable in absolute measurements.

3.2 Sources of Uncertainties in Absolute Comparisons

There are several sources of uncertainty from both computational and experimental sources that may exclude the use of absolute measurements as benchmarks for R/B ratio models.

Simulation of the AGR experiment requires the utilization of several different codes all of which add uncertainty to the predicted release activities. Temperature is the most important input for R/B calculation that is dependent on experimental conditions. The R/B ratios should be well known as long as the experimental thermocouples faithfully report the temperature in the test capsules. However the AGR-1 experiment is expected to run for three years and it is entirely possible that the thermocouples could fail in that time period. The other component to predicted release activities is the birth rate of the different isotopes. Flux in the test capsule, the current number density of U-235, and the U-235 fission cross section are directly proportional to the Birth rate of fission products in the fuel. These conditions will change slowly but continuously throughout the course of the experiment. Also, the experimental capsule contains burnable poisons that regulate the thermal flux. The spectral shift that occurs over the course of the experiment affects the effective one group cross section for U-235 fission. Any uncertainty in the calculation of flux in the experimental capsule or in the burn up calculations that determines U-235 number density will be directly reflected as uncertainties in the predicted activity. ORIGEN calculations are currently based on the ideal ATR cycle. Even once these simulations are corrected for the as run ATR conditions the accuracy of ORIGEN calculations are limited.

Uncertainties in the calculation of release activities from the experimental spectra are also a concern. Uncertainty associated with the net peak area can come from two sources.

Interference from other peaks close in energy to the peak of interest and the statistical uncertainty that is inherent in calculating gamma peak areas contribute to uncertainty. Another component of uncertainty is the absolute efficiency obtained from calibration of the detector. Uncertainty in the branching ratio and decay constant also contribute to the overall uncertainty. In general the uncertainty in absolute efficiency of an HPGe detector is on the order of 2 – 3 %, and the uncertainty in the branching ratio for a gamma is on the order of 1 – 2 %. In addition to all these common uncertainty sources in gamma spectroscopy calculations, the travel time of the gas from the test capsule to the detector volume and the volumetric flow rate of the gas will have an impact on the accurate reporting of the release activities especially for the short lived ($T_{1/2} < 1$ min) isotopes of interest.

3.3 Relative Measurement Indicators

The uncertainties associated with direct activity measurement from the gamma spectrum may be too large to distinguish between the different R/B models. For this reason a set of relative measurement indicators has been developed. Several different approaches to creating relative measurement indicators can be taken. Indicators could be derived from the predicted peak areas of the simulated spectra that were generated for each model in Section 2.3.3. This is however probably a poor choice because this approach relies on simulating physical equipment (detectors, shields) whose characteristics are not fully known. A better approach would use relative indicators constructed from the ratios of release activities calculated from the combination of ORIGEN birth rates and model dependent R/B ratios. An alternative approach would be to divide the release activities by the total birth activities found from ORIGEN to form total R/B ratios. This approach is especially advantageous when there is little to no heavy metal contamination contributing to the experimental spectra

or when release from only failure can be effectively isolated from the collected spectra. Indicators of this form could be compared to the ratio of measured release activities (as found by Equation (3.2)) divided by the same total birth activities.

$$I_{i,j} = \frac{R_i}{R_j} \left(\frac{B_j}{B_i} \right) \quad (3.3)$$

An experimental indicator ‘ I_{ij} ’ of this form is illustrated by Equation (3.3). The release activities (R_{ij}) for test isotope i and reference isotope j are found from Equation (3.2), and the birth ratio of isotope j to isotope i is derived from ORIGEN calculations. Individually, total birth activities from ORIGEN have a high uncertainty, but birth activity ratios are fairly resilient to changes in experimental conditions as shown in Section 3.4.1.

The total R/B ratio system of theoretical indicators combines the birth rates from ORIGEN with the R/B values from a selected model. Equation (3.4) shows the formulation for the relative indicator $I_{i,j}^k$ determined by i the test isotope, j the reference isotope, and model k where n is the number of failed particles in the system.

$$I_{ij}^k = \frac{\left(R_{i,tramp}^k + nR_{i,fail}^k \right) / B_{i,tot}}{\left(R_{j,tramp}^k + nR_{j,fail}^k \right) / B_{j,tot}} = \frac{\left(\left(\frac{R}{B} \right)_{i,tramp}^k B_{i,tramp} + n \left(\frac{R}{B} \right)_{i,fail}^k B_{i,fail} \right) / B_{i,tot}}{\left(\left(\frac{R}{B} \right)_{j,tramp}^k B_{j,tramp} + n \left(\frac{R}{B} \right)_{j,fail}^k B_{j,fail} \right) / B_{j,tot}} \quad (3.4)$$

As the number of failed particles increases the indicator value transitions between being dominated by the components attributed to the contamination in the compact to domination by the failed particle component. The transition is useful in bracketing an expected range of indicator values for a given model that is independent of the number of particles that have failed. The birth activity associated with heavy metal contamination is expected to be around to 10^{-4} of the loaded heavy metal. This is equivalent to about 5.14 TRISO particles per experimental capsule containing 12 compacts each. If the signal is solely due to failure,

Equation (3.4) simplifies to the ratio of two R/B values for different isotopes. This is advantageous because it allows many of the unique properties in the R/B models to become readily apparent. Table 3.1 displays indicators that use Kr-85m as the reference isotope.

Table 3.1. Predicted Indicators using Kr-85m as the reference R/B value

Failure only Values		Ratio of R/B relative to Kr-85m			% difference from German Model	
Isotope	Half Life	German	JAERI	GA	JAERI	GA
Kr-85m	4.48 h	1	1	1	0.00%	0.00%
Kr-87	1.27 h	0.5368	0.4445	0.5204	-17.19%	-3.05%
Kr-88	2.84 h	0.7988	0.65	0.7793	-18.63%	-2.44%
Kr-89	3.15 m	0.1098	0.0734	0.1257	-33.15%	14.50%
Kr-90	32.3 s	0.0455	0.0294	0.0669	-35.30%	47.11%
XE135	9.10 h	1.4155	1.4542	0.8424	2.73%	-40.49%
XE135M	15.3 m	0.2415	0.2097	0.1123	-13.18%	-53.51%
XE137	3.82 m	0.1209	0.0774	0.0687	-35.96%	-43.21%
XE138	14.1 m	0.2319	0.1534	0.1088	-33.83%	-53.09%
XE139	39.7 s	0.0504	0.0315	0.0433	-37.56%	-13.94%

Contamination		Ratio of R/B relative to Kr-85m			% difference from German Model	
Isotope	Half Life	German	JAERI	GA	JAERI	GA
Kr-85m	4.48 h	1	1	--	0.00%	--
Kr-87	1.27 h	0.5354	0.5532	--	3.13%	--
Kr-88	2.84 h	0.7979	0.8054	--	0.79%	--
Kr-89	3.15 m	0.1093	0.1448	--	31.97%	--
Kr-90	32.3 s	0.0452	0.0835	--	83.79%	--
XE135	9.10 h	0.3371	1.4043	--	139.83%	--
XE135M	15.3 m	0.0566	0.2704	--	172.15%	--
XE137	3.82 m	0.0283	0.1554	--	212.03%	--
XE138	14.1 m	0.0543	0.2612	--	173.50%	--
XE139	39.7 s	0.0118	0.0882	--	325.01%	--

Contamination plus 1 Failure		Ratio of R/B relative to Kr-85m			% difference from German Model	
Isotope	Half Life	German	JAERI	GA*	JAERI	GA
Kr-85m	4.48 h	1	1	1	0.00%	0.00%
Kr-87	1.27 h	0.5357	0.5525	0.5332	3.13%	-0.46%
Kr-88	2.84 h	0.7981	0.8044	0.7952	0.79%	-0.36%
Kr-89	3.15 m	0.1094	0.1443	0.1116	31.97%	2.06%
Kr-90	32.3 s	0.0453	0.0832	0.0483	83.79%	6.79%
XE135	9.10 h	0.5857	1.4046	0.4102	139.83%	-29.97%
XE135M	15.3 m	0.0992	0.2700	0.0646	172.15%	-34.85%
XE137	3.82 m	0.0496	0.1549	0.0341	212.03%	-31.25%
XE138	14.1 m	0.0953	0.2605	0.0622	173.50%	-34.70%
XE139	39.7 s	0.0207	0.0879	0.0163	325.01%	-20.96%

* Uses German Contamination R/B values

3.4 Properties of Relative Indicators

3.4.1 Birth Activity Ratios

A major source of uncertainty in a direct comparison test would come from the birth activity calculations. The birth activities are normally found in ORIGEN, but it is also possible to solve for these values analytically to help demonstrate the effectiveness of using relative indicators. Flux in the test capsule and the current number density of U-235 are directly proportional to the Birth rate of fission products in the fuel. These conditions will change often throughout the course of the experiment. However, it can be shown from the analytic solution of the production/destruction equations that the ratio birth rates between two different nuclides are fairly resilient to changes in experimental conditions.

It is possible to eliminate both the flux and the U-235 number density information from the birth activity ratios. The analytic solution for a given nuclide is a linear combination of exponential whose constants are a combination of decay constants, fission yields, cross sections and fluxes as shown in Equation (3.5). Each constant is proportional to the terms shown in Equation (3.6). The numerator of all these constants contains a flux and a Uranium 235 number density term. When two different Birth activities are divided as shown in Equation (3.7) flux and number density terms will cancel each other out.

$$B_i = C_1 e^{-\sigma_i \phi t} + C_2 e^{-\sigma_i \phi t} + C_3 e^{-(\lambda_{pre,i} + \sigma_{\gamma,pre,i} \phi) t} + C_4 e^{-(\lambda_i + \sigma_{\gamma,i} \phi) t} \quad (3.5)$$

$$C_* \propto \frac{\sigma_{f,U235} \phi N_{U235}}{\lambda_i + \sigma_{i,\gamma} \phi - \sigma_{f,U235} \phi} \quad (3.6)$$

$$\frac{B_i}{B_j} = \frac{C_1 e^{-\sigma_i \phi t} + C_2 e^{-\sigma_i \phi t} + C_3 e^{-(\lambda_{pre,i} + \sigma_{\gamma,pre,i} \phi) t} + C_4 e^{-(\lambda_i + \sigma_{\gamma,i} \phi) t}}{C_1 e^{-\sigma_j \phi t} + C_2 e^{-\sigma_j \phi t} + C_3 e^{-(\lambda_{pre,j} + \sigma_{\gamma,pre,j} \phi) t} + C_4 e^{-(\lambda_j + \sigma_{\gamma,j} \phi) t}} \propto \frac{\frac{\sigma_{f,U235} \phi N_{U235}}{\lambda_i + \sigma_{i,\gamma} \phi - \sigma_{f,U235} \phi}}{\frac{\sigma_{f,U235} \phi N_{U235}}{\lambda_j + \sigma_{j,\gamma} \phi - \sigma_{f,U235} \phi}} \quad (3.7)$$

The denominator of the constants also contains flux terms but under the proper conditions the flux dependence is insignificant or nonexistent. If the half life of the isotope of interest and its precursors are short lived (less than a few hours) or the nuclide of interest and its precursors do not have a significant cross section, the decay constant will dominate the denominator.

When the decay constant dominates the denominator birth activity ratios, the only terms that contain flux are exponentials. These terms will either be dominated by decay constants or can be shown to be insignificant for most of the isotopes of interest. The end result is a ratio can be characterized almost entirely by constant nuclear data values like decay constant, fission yield, and branching ratio.

A good example of the decay constant suppressing the flux terms in the birth rate equation is Kr-85m. It has a half life of 4.48 hours and no capture cross section. When the decay constant of Kr-85m is added to the maximum expected flux and U-235 microscopic cross section combination, the difference between the decay constant value and the decay constant and flux term value is less than 0.2%. This signifies that the total denominator of Equation (3.6) can be estimated as just the decay constant. This simplification holds for most nuclides of interest as they are even shorter lived (larger decay constants). It does not hold for Xe-135 which has a longer half-life and a large capture cross section, or Xe-135m whose precursor I-135 is long lived and has a significant capture cross section.

Analytic solutions to the birth rates and their respective ratios show that a 500% greater than expected flux will only perturb the birth ratios by at most 10% for birth ratios excluding Xe-135 and Xe-135m. A 500% greater than expected flux produces an unacceptable, but not incredibly large 75% maximum percent change in the Xe-135 ratios. If

the true flux is smaller than the predicted flux, the uncertainty in Birth ratios is much smaller. Most of the Kr and Xe isotopes of interest do not have a known cross section in the evaluated nuclear data, but if the nuclides of interest or their precursors actually have a cross section it would have to be very large ($>1000b$) before they begin to have an impact on the calculations. Table 3.2 contains the maximum and minimum effect that changing the flux has on the birth ratios of all isotopes excluding ratios containing Xe-135 or Xe-135m.

Table 3.2 Maximum and minimum affect that modifying the expected flux has on Birth Ratios for all isotope pairs of the nuclides of interest excluding Xe-135 and Xe-135m at 125 EFPD.

Flux Multiplier	% Difference	
	Maximum Effect	Minimum Effect
0.01	1.2633	0.0566
0.10	1.1556	0.0518
0.13	1.1254	0.0505
0.25	0.9730	0.0437
0.50	0.6599	0.0297
0.75	0.3357	0.0152
1.00	0.0000	0.0000
1.25	0.3486	0.0158
2.00	1.4846	0.0669
4.00	5.2859	0.2361
8.00	17.6104	0.7639
10.00	27.1166	1.1504

3.4.2 Indicator Trends

By understanding the physics of a given R/B model, it is possible to observe several key trends in Table 3.1. For example, the German model uses a single expression to describe the diffusion coefficients of Kr and Xe for failure. In this case, half-life becomes the important factor in the R/B value. There is a clear trend for the ratios to decrease as half-life decreases. This trend results in straight line half-life versus indicator relationship in a loglog plot. However, in the GA model this trend is not observed. The GA model uses different relationships for Kr and Xe to determine the diffusion coefficients. This results in the R/B

values for the GA model decreasing with half life at one rate for the Xe isotopes and a different rate for the Kr isotopes. This trend is illustrated by Fig. 3.1.

The JAERI model also appears to follow the same trend as the German model, which is expected since the JAERI model also only uses a single diffusion coefficient relationship like the German model. However, deviations from this trend are observed when examining the data for Xe-135m ($T_{1/2} = 15.3$ min) and Xe-138 ($T_{1/2} = 14.1$ min). This is attributed to the JAERI model considering the half-life of the precursor for a given isotope. Consequently, the long lived precursor of Xe-135m increases its R/B when compared to a nuclide with similar half life like Xe-138. The indicators for the JAERI model also demonstrate a nonlinear response on a loglog plot of half-life versus indicator (Fig. 3.1). This nonlinearity is caused by recoil enhancing the release of the shorter lived nuclides. A recoil induced non-linear response in the GA model can also be observed in Fig. 3.1.

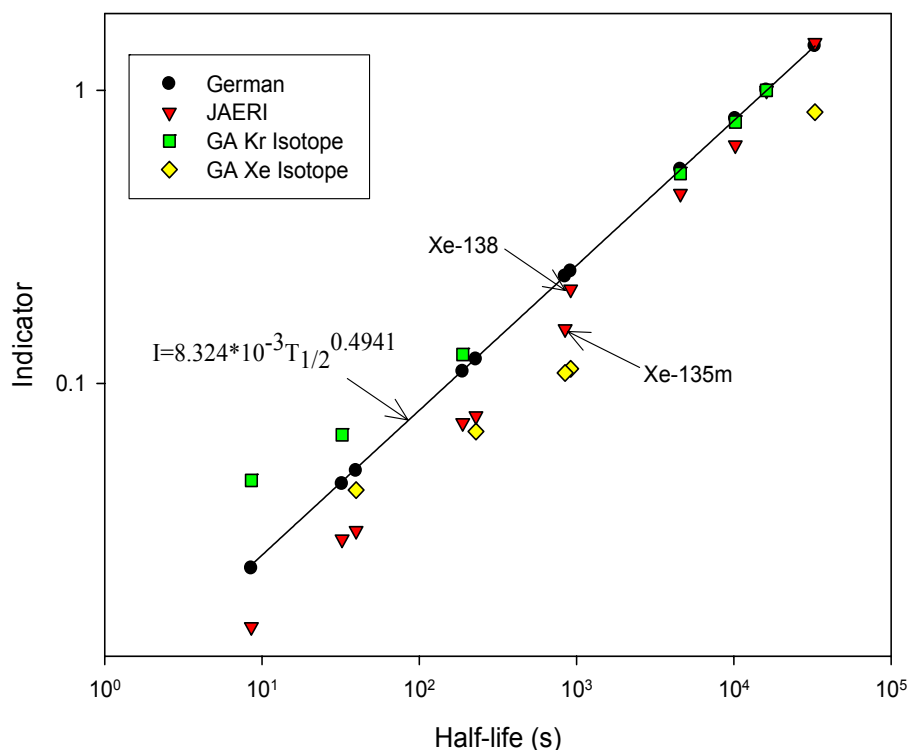


Fig. 3.1. Indicator values for failure models as a function of half-life. Given Kr-85m as the reference isotope and AGR-1 experimental conditions

Similar trends can be observed by studying the indicators created from heavy metal contamination. Notice in Table 3.1 the similarity between the indicator values of Xe-135m and Xe-138 for contamination in the JAERI model. Indicator values that were over 25% different for the failure R/B indicators are less than 4% different in the contamination R/B indicators. The JAERI model does not use a precursor term for the contamination R/B term hence the indicator terms are quite similar. In general the JAERI indicator values for contamination follow a single half life trend for Kr and Xe, but the short lived isotopes deviate from this trend due to recoil. The German model follows two separate half life trends for Kr and Xe much like the GA model does for failure. For contamination the German model uses two different element dependent correlations to calculate reduced diffusion coefficients for contamination release. These trends can be seen in Fig. 3.2.

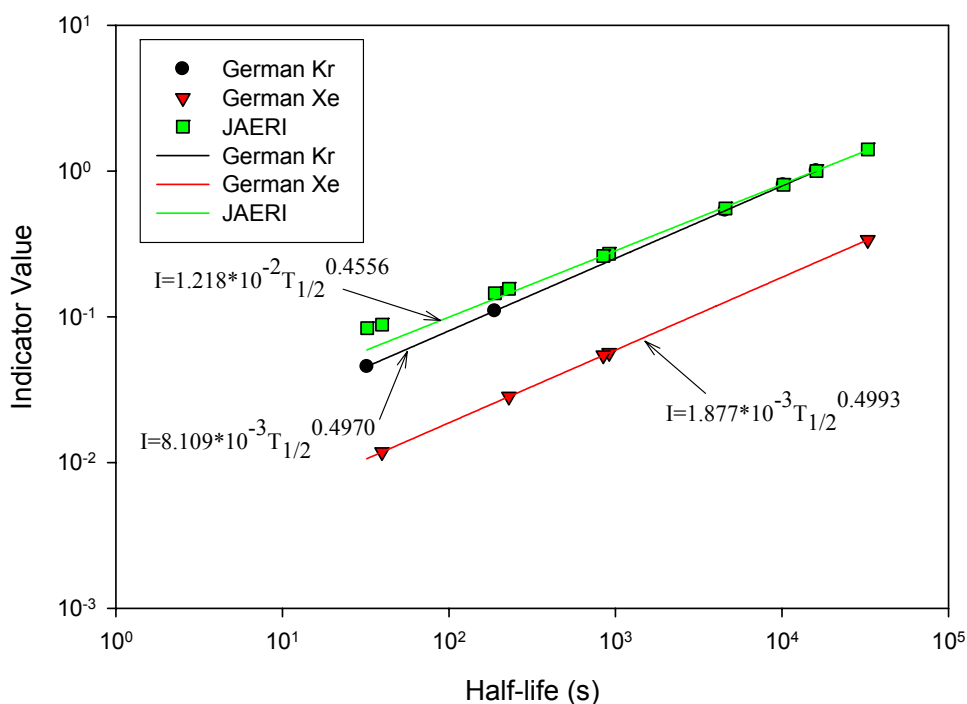


Fig. 3.2. Indicators for Contamination models as functions of half-life with Kr-85m as the reference isotope and AGR-1 experimental conditions

Another trend can be observed by examining the relationship between the Kr German failure and contamination indicators and the Kr JAERI failure and contamination indicators in Table 3.1. The two sets of German indicators are almost identical while the two sets of JAERI indicators are not. This shows evidence of a secondary effect in the Japanese model beyond the decay constant and the temperature dependent reduced diffusion coefficient. The absence of a secondary release mechanism in the German model allows for the German indicators $I_{i,j}^{German}$ to be estimated as shown by Equation (3.8) for both failure and contamination. Since the diffusion coefficients for failure are not element dependent, the German indicators for failure simplify further to the square root of the ratio of the decay constants. This approximation is not valid for the JAERI model. The additional terms present in the JAERI model like recoil and precursor effects prevent the use of this approximation.

$$I_{i,j}^{German} \approx \sqrt{\frac{D'_i}{D'_j}} \sqrt{\frac{\lambda_j}{\lambda_i}} \quad (3.8)$$

The similarity between the GA model and the German model would suggest that its trends could also be approximated by Equation (3.8). The longer lived isotopes of Kr would seem to support this conclusion, but the shorter lived isotopes do not follow this approximation. The recoil terms in the GA model are responsible for this deviation from the approximation. This shows up in the short lived isotopes because recoil tends to contribute more to the total release activity of shorter lived isotopes. For more evidence of recoil having a large effect on enhanced release of short lived nuclide consider also the results of the Modified JAERI model discussed in Section 2.3.3.

Equation (3.8) also helps explain the form of the correlations seen in Fig. 3.1 and Fig. 3.2. In the figures, the half-life of the test isotope is roughly proportional to the square root of the half life. This trend corresponds to the indicators inverse square root proportionality to decay constant shown in Equation (3.8).

Combined contamination and failure indicators will fall between the pure contamination and pure failure values. Another implication of Equation (3.8) is that only cross elemental indicators are useful for distinguishing additional TRISO failures in the German model. Since the indicators for Kr isotopes referenced to another Kr isotope are roughly the same (as in Table 3.1), each additional failed TRISO particle will not change the indicator derived from the collected spectra. The indicators for Xe isotopes referenced to Kr isotopes have distinct values for failure and contamination and will change as more TRISO particles fail. As the number of failed particles increases during the course of the experiment it will be increasingly hard to distinguish the next failed TRISO. As a result, the indicators with large differences between the pure contamination value and the pure failure value will be the most able to detect the next TRISO failure.

By combining the accuracy of relative R/B indicators with such observed trends for the various models, analysis of the experimental data (i.e., the gamma-ray spectra of released fission gases) can be extended to understanding, differentiating and validating the various models for fission gas release [24].

3.4.3 Trends in Spectra

In the previous section the theoretical trends in the models and their effects were discussed. The same trends that are present in the R/B models are also built into the simulated spectra. Examination of these virtual spectra allows for the identification of key

spectrum features (e.g. full energy gamma-ray peaks) for observing trends in the fission gas release before the experiment is even conducted.

Theory suggests a set of Kr and Xe isotopes that would be useful to observe. Inspection of the simulated spectra reveals that only some of these isotopes are viable candidates for detection given the travel time involved in the experiment. Kr-90 and Kr-91 have half lives that are too short to observe in the spectrum. The following table contains a list of isotopes and their corresponding gamma-rays that are high yield and free of interference.

Table 3.3. Prominent gammas for identification of trends in fission gas release

Isotope	1 st Choice Gamma (keV)	2 nd Choice Gamma (keV)	3 rd Choice Gamma (keV)
Kr85m	304.47	151.00	N/A
Kr87	402.58	845.44	1740.50
Kr88	196.30	2195.80	2392.10
Kr89	904.27	585.80	220.90
Kr-90	N/A	N/A	N/A
Kr91	N/A	N/A	N/A
Xe-135	249.79	608.15	N/A
Xe-135m	526.56	N/A	N/A
Xe-137	455.49	N/A	N/A
Xe-138	258.41	1768.30	434.56
Xe-139	218.59	174.97	296.53

The order of the gammas in Table 3.3 does not necessarily follow the gamma yields. The 304.47 gamma of Kr-85m is located in a much cleaner portion of the spectrum than the 151.0 keV which is in close proximity to the 153.86 keV Xe-138 peak. A more extreme example is present in Kr-87. The second (2554.8 keV) and fourth highest (2558.10 keV) yield gammas form a doublet with one another, and the fifth gamma (2011.9 keV) is also in a doublet. Another example of a difficult to use gamma-ray is the Xe-133 81 keV line. Aside

from the problems associated with Xe-133 reaching steady state concentrations, the 79.62 keV gamma from Xe-133 contaminates the 81 keV peak.

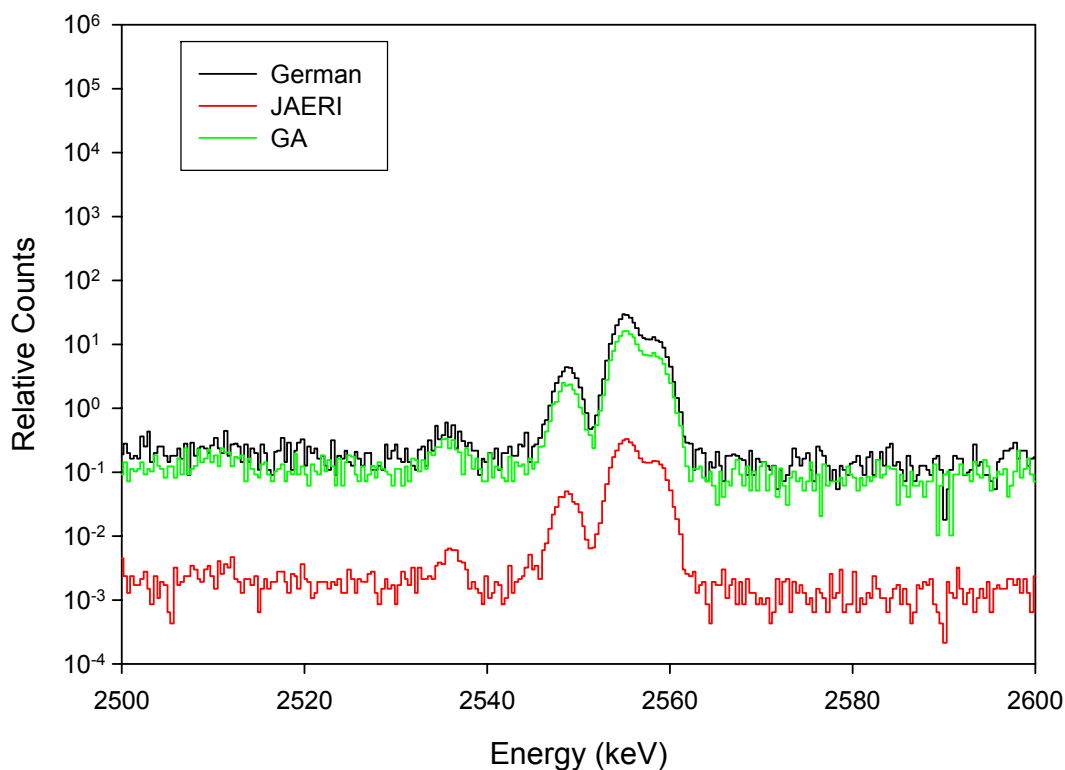


Fig. 3.3. Simulated spectra demonstrating the doublet formed by Kr-87 2554.8 keV and 2558.1 keV gammas along with the 2548.4 keV gamma from Kr-88

Direct inspection of the spectra reveals evidence of the same trends found in the previous section. The close proximity of the 151 keV Kr-85m line and 153.84 keV Xe-138 line permit a demonstration of the indicators being reflected in the spectrum. In Fig. 3.4 the spectra due to each failure model have been normalized to appear on the same scale. In the normalized spectra all the 151 keV Kr-85m peaks are approximately the same magnitude. However the three different 153.84 keV Xe-138 peaks are of varying heights. The varying heights are directly reflected in the failure indicators for Xe-138 referenced to Kr-85m shown in Table 3.1. The German indicator is 0.2319, the JAERI indicator is 0.1534, and the GA indicator is 0.1088.

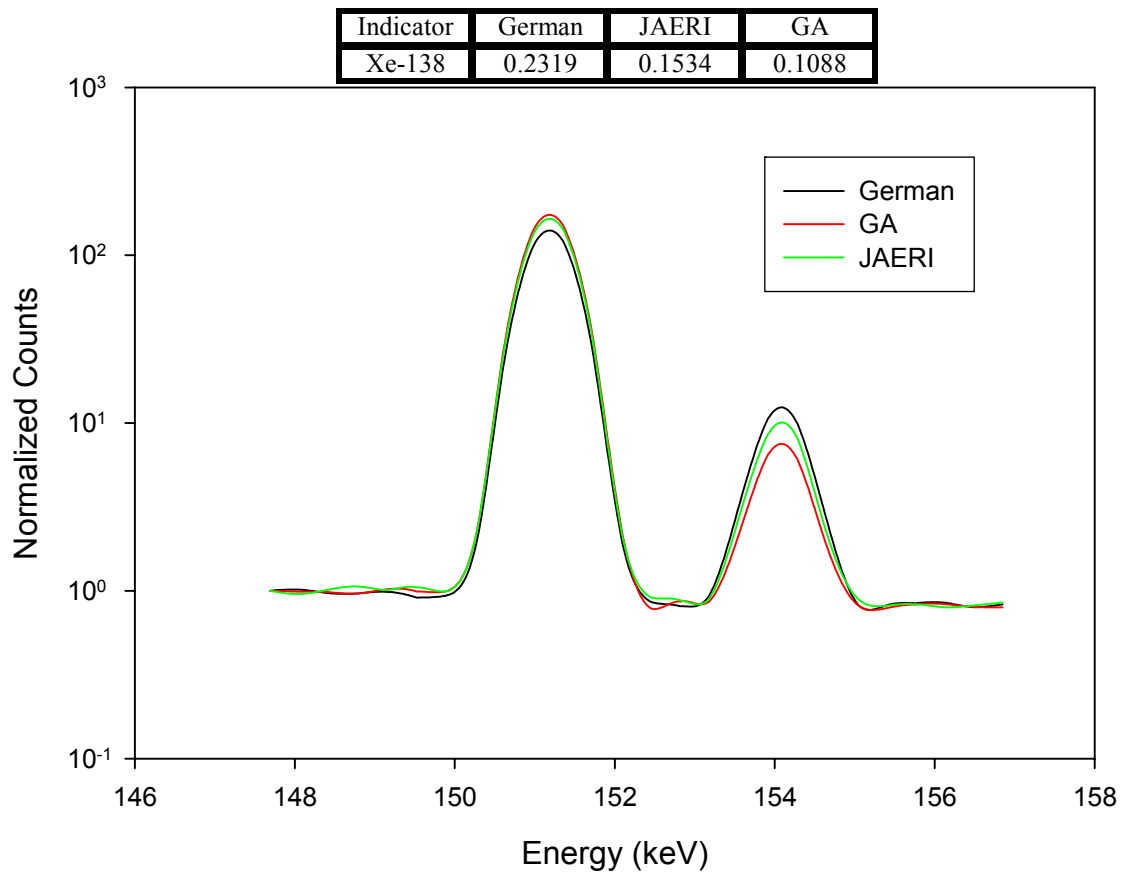


Fig. 3.4. Normalized plot of Kr-85m 151 keV line and Xe-138 153.86 keV line illustrating model differences

Chapter 4

Conclusions and Future Work

4.1 Conclusions

Validation of a Release to Birth model that accurately reflects the fission gas release of failed TRISO fuel is an important step in the continued design and certification of the Very High Temperature Reactor. Detecting the number of failed TRISO particles and their releases activity is critical to the development of fuel manufacturing techniques and quality assurance protocols for the VHTR fuel. Simulation of the AGR-1 experiment has shown that it is possible to use gamma ray spectrometry to benchmark the different R/B models that have been developed by various different groups.

Direct comparison of experimental and simulated release activities can be useful for some applications like calculation of the number of failed particles present in the experiment. However, the sensitivity of absolute release activity measurements to variations in experimental conditions makes them unsuitable for the validation of release to birth models. Many of the uncertainties prevalent in absolute measurements are eliminated through the use of relative indicators. Birth activity ratios in the relative indicators are relatively unchanged by variations in ATR power history that perturb the flux in the test capsules.

Relative indicators can be created by the ratio of the total R/B for an isotope to a reference total R/B given by the reference isotope. With proper understanding of the components of the different R/B models it is possible to observe trends in these indicators that are indicative of each model. The trends observed in the simulated ratio of total R/B

values can be seen in the experimental data. The experimental indicator trends will identify either the most correct model or help modify the current models to match reality. Many properties of R/B models can be observed by careful examination of the indicator trends which include effects related to half life, fission product recoil, nuclide precursor half life, and properties of the gas diffusion.

4.2 Future Work

There are several areas of this research which could merit further investigation. Even though a large fuel testing program (AGR) is currently underway to test TRISO fuel under in-core conditions, a smaller experiment could also be used to gather useful data on the fundamental nature of R/B models. All the R/B models are based on rate equations that differ little from the original idea set forth by Booth in 1957. With the advances in computing power over the last fifty years a more modern approach might be appropriate. Molecular Dynamics simulations have the potential to simulate the Uranium Oxycarbide system in order to better explain the fission gas release process. There may also be potential to use advanced spectral analysis techniques to help interpret simulated and experimental spectra. If low resolution detectors are used, the resulting Kr and Xe spectra are quite complex, and traditional spectral analysis techniques may fail in peak area determination. Modern techniques like genetic algorithms and neural nets may prevail. In this case modern room temperature detectors that have improved resolution may become useable as alternatives to HPGe detectors.

Furthermore, preliminary design work is underway at NCSU to investigate the feasibility of conducting an experiment similar in design to the AGR-1 experiment. The experiment would be placed in Beam Port 2 (BP2) of the NCSU PULSTAR reactor. The

AGR experiments place an emphasis on a pass fail evaluation of the newest TRISO fuel manufacturing processes. In the proposed experiment, conditions in the test capsule like temperature and gas flow rate can be more carefully controlled at NCSU than is practical at the ATR. In the ideal experiment a capsule would be placed at the core center line in BP2. The capsule could be loaded with either loose TRISO particles or a full TRISO compact. A heater would be used to regulate the temperature inside the capsule up to an ideal temperature of around 1500 K. Helium gas would be pumped in a loop through the capsule out of the core bio-shield and into a measurement chamber then back into the core. Fission products released from failed TRISO fuel would reach equilibrium activity inside the helium loop. A detector would look at the measurement chamber and record the gamma spectrum. The loop could also contain a device to preferentially separate either Krypton or Xenon fission products to send the selected element towards the detector [21]. The detectors used in this experiment would include a High Purity Germanium (HPGe) detector and lower resolution detectors like a $\text{LaBr}_3(\text{Ce})$ scintillator.

References

- [1] Goodjohn, A. J., “Summary of Gas-Cooled Reactor Programs,” Energy, Vol. 16, No. 1/2, pp. 79-106, 1991
- [2] LaBar, Malcolm P., “The Gas Turbine – Modular Helium Reactor: A Promising Option for Near Term Deployment,” GA-A23952, General Atomics, April 2002
- [3] Barnes, Charles M., “AGR-1 Fuel Product Specification and Characterization Guidance,” EDF-4380, Idaho National Laboratory, 4/21/2006
- [4] Hanson, D.L., Saurwein, J.J., “Development Plan for Advanced High Temperature Coated-Particle Fuels,” GA Document No. PC-000513, General Atomics
- [5] “Users Handbook for the Advanced Test Reactor,” INEEL/EXT-02-01064.
- [6] J.K. Hartwell, “Design and Expected Performance of the AGR-1 Fission Product Monitoring System,” INL/EXT-05-00073.
- [7] ORIGEN: Isotope Generation and Depletion Code System Matrix Exponential Method, Version 2.2, Oak Ridge National Laboratory, ORNL/TM-7175, 1980.
- [8] MCNP – A General Monte Carlo N-Particle Transport Code, Version 5, Vol. I, Los Alamos National Laboratory release 1.40, LA-UR-04-5921, 2004.
- [9] MacFarlane, R. E., Muir, D. W., “The NJOY Nuclear Data Processing System Version 91,” LA-12740-MS, Los Alamos National Laboratory, 1994.
- [10] Forrest R. A., Kopecky, J., Sublet, J-Ch, “The European Activation File: EAF-2003 cross section library”, UKAEA FUS 486, 2002.
<http://www.fusion.org.uk/easy2003/>
- [11] ENDF-201, ENDF/B-VI Summary Documentation,” BNL-NCS-17541,4th Edition, Brookhaven National Laboratory (October 1991).
- [12] Maki, J.T., “AGR-1 Irradiation Test Specification,” EDF-4731, Idaho National Laboratory, 1/30/2002
- [13] Chang, G. S., “Final Neutronics Evaluation for the AGR-1 Experiment in ATR East Position B-10,” Idaho National Lab, EDF-5683
- [14] Verfondern, K. (Ed.), “Fuel Performance and Fission Product Behaviour in Gas Cooled Reactors,” IAEA=TECDOC-978, International Atomic Energy Agency, (1997).
- [15] Booth, A. H., A Method for Calculating the Diffusion of Radioactive Rare Gas Fission Products from UO₂ Fuel Elements, DCI-27, Atomic Energy of Canada Limited, 1957.

- [16] Olander, D.R., "Fundamental Aspects of Nuclear Reactor Fuel Elements," TID-26711-P1, U.S. ERDA Technical Information Center, (1976).
- [17] R.M. Carroll, O. Sisman, "In-Pile Fission-Gas Release from Single-Crystal UO_2 ," Nuclear Science and Engineering, Vol 21, p 147-158 (1965)
- [18] "Development of Improved Models and Designs for Coated-Particle Gas Reactor Fuels," INEEL/EXT-05-02615, (2004).
- [19] Ueta S., Sumita J., et al, "Fuel and Fission Gas Behavior during Riste-to-Power Test of the High Temperature Engineering Test Reactor (HTTR)," Journal of Nuclear Science and Technology, Vol 40, No 9, p 679-686 (September 2003)
- [20] Richards, M.B., "Fission-Gas Release from UCO Microspheres: A Theoretical Model for Fractional Release from Non-hydrolyzed Fuel with Model Parameters Derived from Capsule HFR-B1 Data," General Atomics Report 818:MBR:001:94
- [21] Harp, J. M, Hawari, A.I., Bourham, M.A., "Simulation of gamma-ray spectrometry of failed TRISO fuel," Nuclear Instruments and Methods Section A, (2007), (In Press)
- [22] Harp, J. M., Martin, E.H., Hawari, A.I., Bourham, M.A., "Studying TRISO fuel failure using passive gamma-ray spectrometry," Transactions of the American Nuclear Society 2006 Annual Meeting and Embedded Topical Meeting - Nuclear Fuels and Structural Materials for the Next Generation Nuclear Reactors, 2006, p 672-673
- [23] McIsaac, C. V., Hartwell, J. K., et al., "Concentrations of Fission Product Noble Gases Released During the NP-MHTGR Fuel Compact Experiment-1A," INL report
- [24] Harp, J.M., Hawari, A.I., "Investigating TRISO Fuel Fission Gas Release Models Using Relative Release-To-Birth Indicators," Transactions of the American Nuclear Society, vol 96, 2007

APPENDICES

Appendix A Derivation of the Booth Equation

The derivation of the Booth equation for steady state fission gas release requires several steps. First the concentration of fission gas must be found by solving a form of the diffusion equation. The concentration must then be integrated to solve for the release of the fission product at the radius of the sphere. Once the activity of a given nuclide has reached the steady state, the concentration C of that nuclide as a function of radius r is given by the following differential equation and boundary conditions.

$$D \frac{d^2C}{dr^2} + \frac{2D}{r} \frac{dC}{dr} + B - \lambda C = 0 \quad (\text{A.1})$$

$$\left. \frac{dC}{dr} \right|_{r=0} = 0 \quad (\text{A.2})$$

$$C(r = a) = 0 \quad (\text{A.3})$$

Where D is the diffusion coefficient, B is the rate of production of the isotope, and λ is the decay constant. The solution to this equations is given by equation (A.4) where α and β are constants.

$$C(r) = \frac{\alpha \sinh(\beta r)}{r} + \frac{B}{\lambda} \quad (\text{A.4})$$

By using the initial conditions given in Equations (A.2) and (A.3) it is possible to solve for the constants to get the concentration equation (A.7).

$$\alpha = -\frac{Ba}{\lambda \sinh\left(\sqrt{\frac{\lambda}{D}}R\right)} \quad (\text{A.5})$$

$$\beta = \sqrt{\frac{\lambda}{D}} \quad (\text{A.6})$$

$$C(r) = \frac{B}{\lambda} - \frac{Ba \sinh\left(\sqrt{\frac{\lambda}{D}}r\right)}{\lambda r \sinh\left(\sqrt{\frac{\lambda}{D}}a\right)} \quad (\text{A.7})$$

The next step is to calculate the activity released over the spherical boundary. This is done by integrating current across the surface of a sphere of radius 'a', and Gauss' Theorem is applied to the surface integral.

$$R = \iint_A \mathbf{J}(r) \cdot d\mathbf{S} = \iiint_V (\nabla \cdot \mathbf{J}(r)) dV \quad (\text{A.8})$$

By applying Fick's second law to Equation (A.8), it is possible to integrate the concentration density to find the release. In gaseous diffusion current is defined as the opposite of the diffusion coefficient multiplied by the gradient of the concentration density of the gas. In this case the concentration density is the concentration divided by spherical volume at 'a'.

$$\mathbf{J}(r) = -D \nabla \frac{C(r)}{V} \quad (\text{A.9})$$

$$R = \frac{1}{V} \iiint_V -D \nabla^2 C(r) dV \quad (\text{A.10})$$

The Laplacian of the concentration is given by:

$$\nabla^2 C(r) = -\frac{Ba}{Dr} \frac{\sinh\left(\sqrt{\frac{\lambda}{D}}r\right)}{\sinh\left(\sqrt{\frac{\lambda}{D}}a\right)} \quad (\text{A.11})$$

Substitute the Laplacian back into Equation (A.10):

$$R = \frac{1}{V} \int +D \frac{Ba}{Dr} \frac{\sinh\left(\sqrt{\frac{\lambda}{D}}r\right)}{\sinh\left(\sqrt{\frac{\lambda}{D}}a\right)} 4\pi r^2 dr \quad (\text{A.12})$$

$$R = \frac{1}{V} \frac{4\pi Ba}{\sinh\left(\sqrt{\frac{\lambda}{D}}a\right)} \int r \sinh\left(\sqrt{\frac{\lambda}{D}}r\right) dr \quad (\text{A.13})$$

$$R = \frac{1}{V} \frac{4\pi Ba}{\sinh\left(\sqrt{\frac{\lambda}{D}}a\right)} \left[r \sqrt{\frac{D}{\lambda}} \cosh\left(\sqrt{\frac{\lambda}{D}}r\right) - \frac{D}{\lambda} \sinh\left(\sqrt{\frac{\lambda}{D}}r\right) \right]_a \quad (\text{A.14})$$

This equation can be simplified to:

$$R = \frac{1}{V} 4\pi Ba \left[a \sqrt{\frac{D}{\lambda}} \coth\left(\sqrt{\frac{\lambda}{D}}a\right) - \frac{D}{\lambda} \right] \quad (\text{A.15})$$

$$R = \frac{1}{V} 4\pi Da^2 \sqrt{\frac{D}{\lambda}} \left[\coth\left(\sqrt{\frac{\lambda a^2}{D}}\right) - \sqrt{\frac{D}{\lambda a^2}} \right] \quad (\text{A.16})$$

Now insert the sphere volume:

$$R = \frac{4\pi Ba^2}{\frac{4}{3}\pi a^3} \sqrt{\frac{D}{\lambda}} \left[\coth\left(\sqrt{\frac{\lambda a^2}{D}}\right) - \sqrt{\frac{D}{\lambda a^2}} \right] \quad (\text{A.17})$$

Divide by B and simplify to get the Steady State Booth Equation.

$$R/B = 3 \sqrt{\frac{D}{\lambda a^2}} \left[\coth\left(\sqrt{\frac{\lambda a^2}{D}}\right) - \sqrt{\frac{D}{\lambda a^2}} \right] \quad (\text{A.18})$$

Appendix B Simplification of JAERI Model to German Model

The goal of this appendix is to demonstrate how the JAERI model can be simplified to the German model. Each step will be explained in the equations and shown numerically in Table B.1. Table B.2 contains the German R/B ratio values divided by the values from Table B.1. First recall the German model for failure (Equation (B.1)) and the JAERI model for failure (Equation (B.2)).

$$\left(\frac{R}{B}\right)_{fail} = 3\sqrt{\frac{D'}{\lambda}} \left[\coth\left(\sqrt{\frac{\lambda a^2}{D}}\right) - \sqrt{\frac{D'}{\lambda}} \right] \quad (B.1)$$

$$\left(\frac{R}{B}\right)_{fail} = \left(\left(\frac{R}{B}\right)_{k,r} \times \left(\frac{R}{B}\right)_{m,d}\right) + \left(\left(\frac{R}{B}\right)_{k,d} \times \left(\frac{R}{B}\right)_{m,ad}\right) \quad (B.2)$$

Remember that the German model only accounts for fission gas release through diffusion, while the JAERI model accounts for diffusion $((R/B)_{k,d})$, recoil $((R/B)_{k,r})$ and matrix diffusion $((R/B)_{m,d})$. One approach to equilibrating the models without changing the structure of the JAERI model is the use equal reduced diffusion coefficients. The numerical results of this simplification are shown in the table, but it does not account for all or even most of the difference between the models with the German model values still 4 to 100 times larger than the JAERI model values. The first step in simplifying the JAERI model is to drop the recoil term. This leaves only the kernel diffusion term and the matrix diffusion term.

$$\left(\frac{R}{B}\right)_{fail} = \left(\left(\frac{R}{B}\right)_{k,d} \times \left(\frac{R}{B}\right)_{m,d}\right) \quad (B.3)$$

The next step is to remove matrix diffusion from the model. Notice the huge difference between the No Recoil Column and the No Matrix Diffusion Column. After matrix diffusion

is removed from the JAERI model, it is only 1.3 to 6.7 times smaller than the German model. Clearly, this is the largest single difference between the German and the JAERI models. Without matrix diffusion the JAERI model reduces to just $(R/B)_{k,d}$ or the kernel diffusion term.

$$\left(\frac{R}{B}\right)_{k,d} = 3 \left(\frac{1}{\Gamma_1} \left(\frac{\coth \sqrt{\mu_1}}{\sqrt{\mu_1}} - \frac{1}{\mu_1} \right) + \frac{1}{\Gamma_2} \left(\frac{\coth \sqrt{\mu_2}}{\sqrt{\mu_2}} - \frac{1}{\mu_2} \right) \right) f_{BU} \quad (\text{B.4})$$

The Γ terms in this equation give the JAERI model its dependency on precursor properties. The net effect of these terms is to increase the fractional release of an isotope if its precursor is long lived when compared to an isotope of similar half life but a short lived precursor. In the isotopes of interest a clear example is Xe-135m which has a higher R/B value when compared to Xe-138 which has and almost identical half-life. If these precursor terms are ignored ($(1/\Gamma_1)=0$ and $\Gamma_2=1$) and the μ terms are simplified the kernel diffusion term reduced to Equation (B.5). The resulting values after the removal of the precursor term are not as numerically close to the German model as the kernel diffusion term, but the resulting model is closer in form to the German model

$$\left(\frac{R}{B}\right)_{fail} = 3 \left(\frac{\coth \sqrt{\mu_2}}{\sqrt{\mu_2}} - \frac{1}{\mu_2} \right) f_{BU} = 3 \sqrt{\frac{D'}{\lambda}} \left(\coth \left(\sqrt{\frac{\lambda}{D'}} \right) - \sqrt{\frac{D'}{\lambda}} \right) f_{BU} \quad (\text{B.5})$$

The only other term that still remains that separates the German and JAERI models is the burn up correction factor. After the burn up term is removed, all the German over JAERI values are in near the range 6.90 to 7.00. This range corresponds to the square root of the ratio of the reduced diffusion coefficients for the two models at 1450 K which is 6.93. The tables plainly show that the precursor and burn up factor have little effect compared to the impact of the matrix diffusion term. All that remains is to replace the JAERI reduced

diffusion coefficients with the German values. The final factor that separated the two models is gone and the JAERI model has been simplified to the form of the German model.

The same logic can be applied to simplify the JAERI contamination term to the German contamination term. These two terms are much closer to each other in terms of formulation so the only term that needs to be removed is recoil. Table B.3 numerically demonstrates this process.

Table B.1. Reduction of the JAERI Failure Term to the German Failure Term

	JAERI Total	=D'	No Recoil	No Matrix Diffusion	No Precursor Term	No Burn-up	All Previous with =D'	German
Kr-85	6.67E-01	9.78E-01	6.47E-01	6.94E-01	6.94E-01	6.67E-01	9.88E-01	9.88E-01
Kr-85m	6.67E-04	2.15E-03	2.54E-04	1.32E-02	7.06E-03	6.78E-03	4.68E-02	4.68E-02
Kr-87	2.96E-04	7.43E-04	7.57E-05	7.35E-03	3.76E-03	3.61E-03	2.51E-02	2.51E-02
Kr-88	4.33E-04	1.05E-03	1.04E-04	6.77E-03	5.62E-03	5.40E-03	3.74E-02	3.74E-02
Kr-89	4.89E-05	7.27E-05	3.97E-06	1.89E-03	7.66E-04	7.35E-04	5.14E-03	5.14E-03
Kr-90	1.96E-05	2.56E-05	1.00E-06	1.16E-03	3.17E-04	3.04E-04	2.13E-03	2.13E-03
Kr-91	9.85E-06	1.15E-05	2.75E-07	6.15E-04	1.63E-04	1.57E-04	1.10E-03	1.10E-03
XE131M	1.43E-02	7.04E-02	1.11E-02	7.57E-02	5.55E-02	5.33E-02	3.32E-01	3.32E-01
XE133	6.24E-03	2.87E-02	4.11E-03	4.14E-02	3.70E-02	3.56E-02	2.31E-01	2.31E-01
XE135	9.69E-04	3.20E-03	3.82E-04	1.40E-02	1.01E-02	9.65E-03	6.62E-02	6.62E-02
XE135M	1.40E-04	3.80E-04	4.08E-05	8.82E-03	1.69E-03	1.62E-03	1.13E-02	1.13E-02
XE137	5.16E-05	6.42E-05	2.11E-06	9.11E-04	8.43E-04	8.10E-04	5.66E-03	5.66E-03
XE138	1.02E-04	1.46E-04	7.24E-06	1.63E-03	1.62E-03	1.56E-03	1.08E-02	1.08E-02
XE139	2.10E-05	2.31E-05	3.53E-07	3.67E-04	3.51E-04	3.37E-04	2.36E-03	2.36E-03

Table B.2. Table B.1 in Terms Relative to the German Values

German/ JAERI	JAERI Total	=D'	No Recoil	No Matrix Diffusion	No Precursor Term	No Burn-up	All Previous with =D'	German
Kr-85m	70.17	21.78	184.40	3.55	6.63	6.90	1	1
Kr-87	84.74	33.78	331.91	3.42	6.67	6.95	1	1
Kr-88	86.24	35.63	359.06	5.52	6.65	6.92	1	1
Kr-89	104.97	70.68	1292.40	2.71	6.71	6.99	1	1
Kr-90	108.46	83.01	2116.86	1.84	6.71	6.99	1	1
Kr-91	111.15	95.24	3985.63	1.78	6.72	7.00	1	1
XE131M	23.24	4.71	29.82	4.38	5.98	6.22	1	1
XE133	37.01	8.04	56.17	5.58	6.23	6.49	1	1
XE135	68.31	20.70	173.13	4.74	6.59	6.86	1	1
XE135M	80.83	29.77	277.17	1.28	6.70	6.97	1	1
XE137	109.57	88.07	2686.51	6.21	6.71	6.99	1	1
XE138	106.04	74.54	1499.19	6.65	6.70	6.98	1	1
XE139	112.38	102.07	6667.16	6.41	6.71	6.99	1	1

Table B.3. Reduction of the Contamination Component of the JAERI Model to the German Term

(R/B)	JAERI Total (f m,d + f m,r)	f m,d	f m,d = D'	German (R/B) Contamination
Kr-85m	2.02E-06	1.93E-02	3.04E-02	3.04E-02
Kr-87	1.12E-06	1.03E-02	1.63E-02	1.63E-02
Kr-88	1.63E-06	1.54E-02	2.42E-02	2.42E-02
Kr-89	2.92E-07	2.10E-03	3.32E-03	3.32E-03
Kr-90	1.68E-07	8.68E-04	1.37E-03	1.37E-03
Kr-91	1.26E-07	4.47E-04	7.07E-04	7.07E-04
XE131M	1.50E-05	1.47E-01	5.65E-02	5.65E-02
XE133	1.01E-05	9.93E-02	3.77E-02	3.77E-02
XE135	2.84E-06	2.74E-02	1.02E-02	1.02E-02
XE135M	5.46E-07	4.62E-03	1.72E-03	1.72E-03
XE137	3.13E-07	2.31E-03	8.59E-04	8.59E-04
XE138	5.27E-07	4.44E-03	1.65E-03	1.65E-03
XE139	1.78E-07	9.62E-04	3.58E-04	3.58E-04

German / JAERI	JAERI Total (f m,d + f m,r)	f m,d	f m,d = D'	German (R/B) Contamination
Kr-85m	15031.78	1.58	1.00	1.00
Kr-87	14566.05	1.58	1.00	1.00
Kr-88	14909.33	1.58	1.00	1.00
Kr-89	11377.32	1.58	1.00	1.00
Kr-90	8168.70	1.58	1.00	1.00
Kr-91	5621.20	1.58	1.00	1.00
XE131M	3752.70	0.38	1.00	1.00
XE133	3724.17	0.38	1.00	1.00
XE135	3607.46	0.37	1.00	1.00
XE135M	3150.37	0.37	1.00	1.00
XE137	2745.31	0.37	1.00	1.00
XE138	3134.61	0.37	1.00	1.00
XE139	2014.48	0.37	1.00	1.00

Appendix C Detector Catalog

This appendix contains a complete collection of the simulated spectra for different models and different detectors. It also contains data from the physical detectors that these simulations were based upon. The purpose of this appendix is to visually demonstrate the effect of different models and the effect of different detectors have on the resulting spectrum due to a release source.

C.1 Physical Measurements of Detector Properties

Spectra are shown for High Purity Germanium (HPGe), High Pressure Xenon (HPXe), Cadmium Zinc Telluride (CZT), and Lanthanum Bromide (LaBr or LaBr₃(Ce)) detectors. The HPGe detector is the nuclear industry standard for high resolution radiation detectors. The other detectors are considered mid resolution detectors since their resolutions fall between the fine resolution of the HPGe detector and the coarse resolution of NaI(Tl) detectors. The HPGe detector used in this work is a 40% Ortec Pop-Top Gamma-X detector. The HPXe detector is a Mirmar Sensor LLC small diameter (1.6 inch) model. The CZT detector contains a 10x10x15 mm crystal and is on loan from INL. The LaBr detector model is a Saint-Gobain BriLanCe 380 with a 1 inch crystal.

A Cs-137 spectrum has been collected on the different detector types to demonstrate their response to a mono-energetic source. Similar measurements were taken on each detector for different standard check sources which include Co-60, Ba-133, Eu-152, and Th-232 daughters. The full energy peaks from these sources were analyzed and used to create energy versus resolution plots. The data in these plots was then fit to the equation used in the MCNP GEB card. The results of this fit are also shown in Table 2.6 of the thesis.

C.1.1 Spectra Collected from Actual Detectors

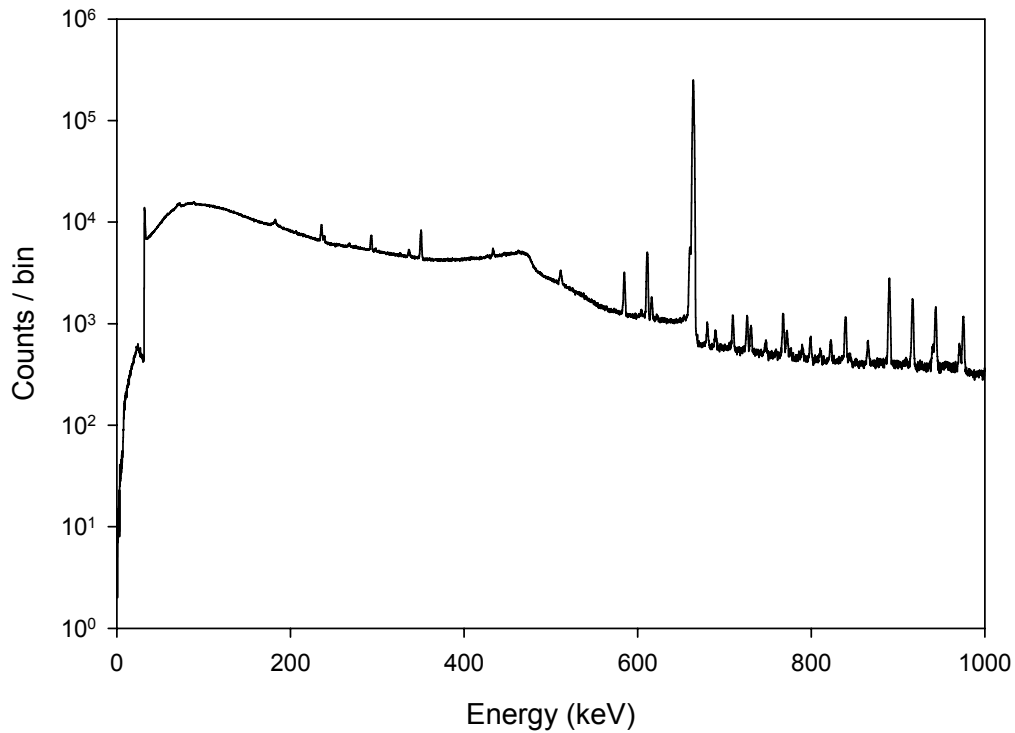


Fig. C. 1. Collected HPGe response to Cs-137 source (Background sources also contribute to this spectrum)

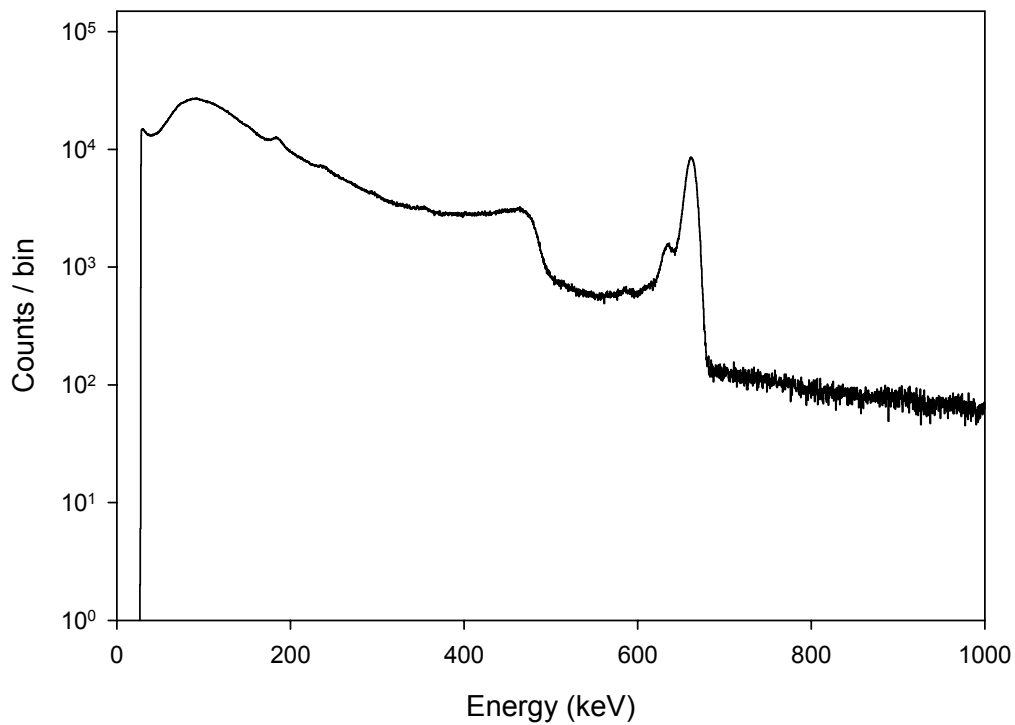


Fig. C. 2. Collected HPXe Response to Cs -137 source

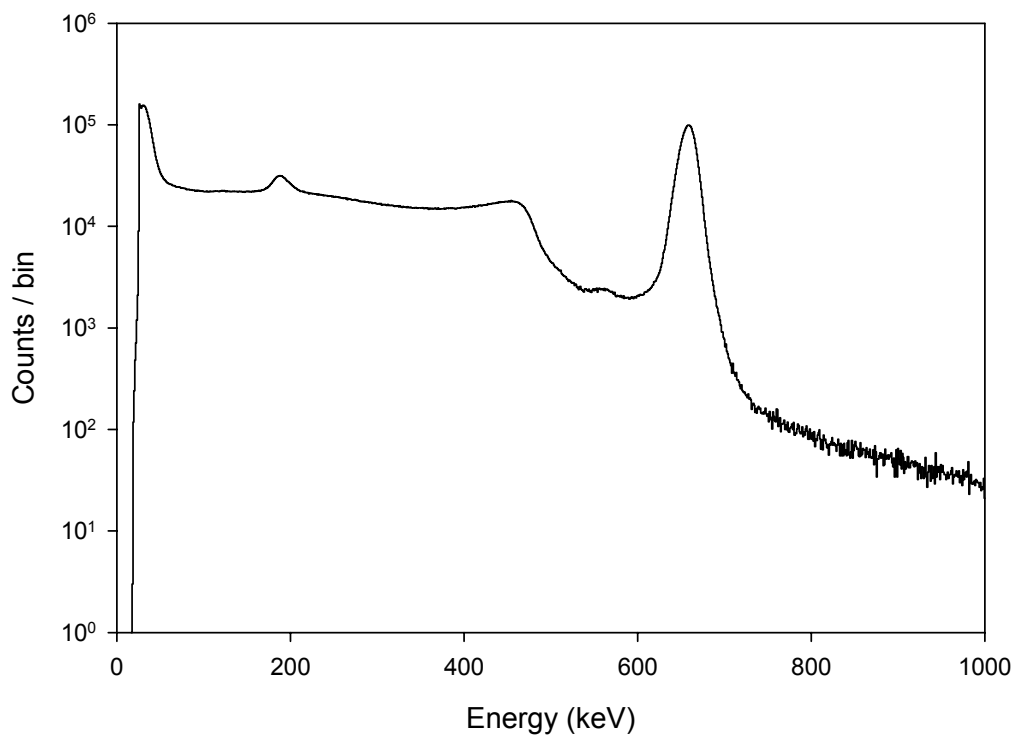


Fig. C. 3. Collected CZT Response to Cs-137 source

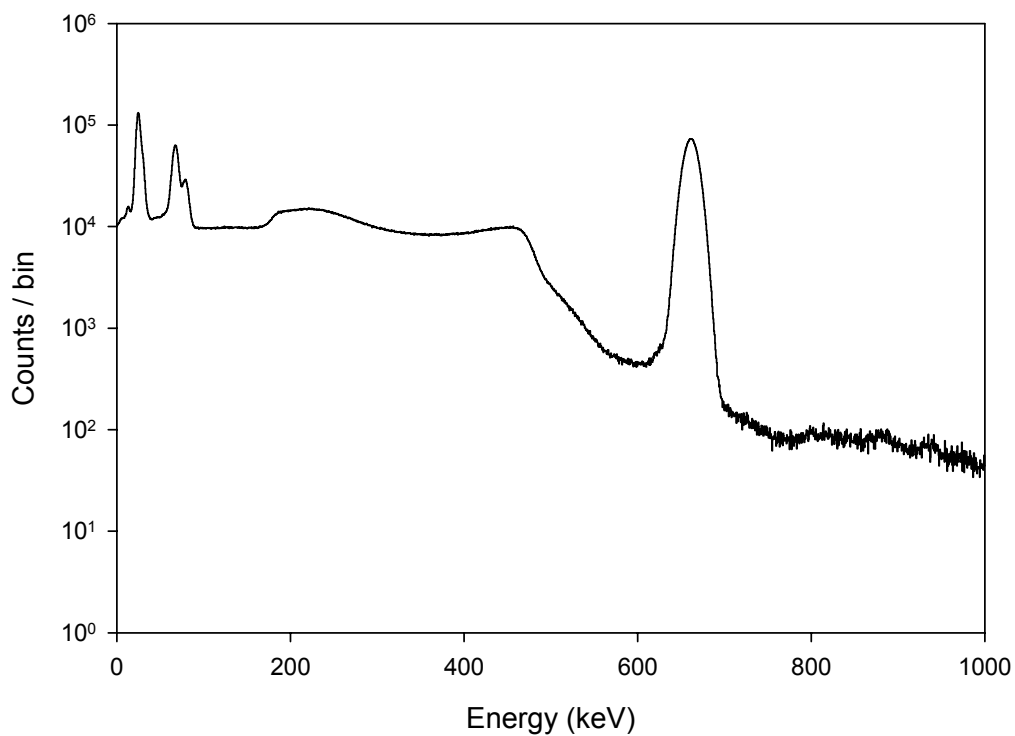


Fig. C. 4. Collected LaBr Response to Cs-137 source

C.1.2 Detector Properties

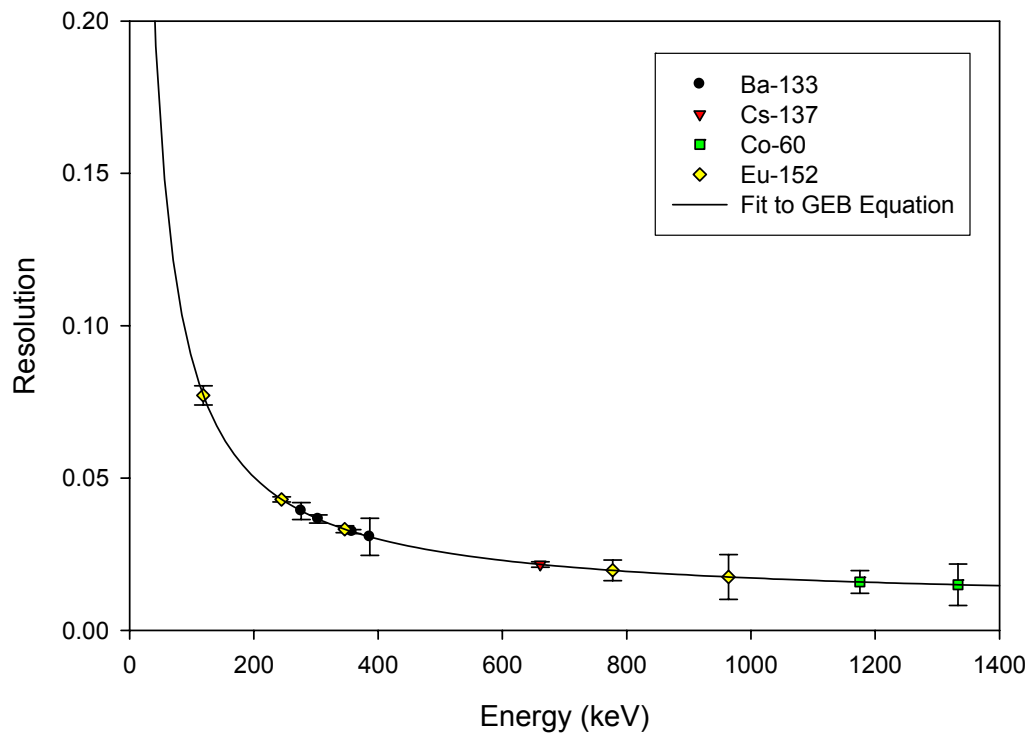


Fig. C. 5. Energy versus Resolution of Different Full Energy Peaks for the HPXe

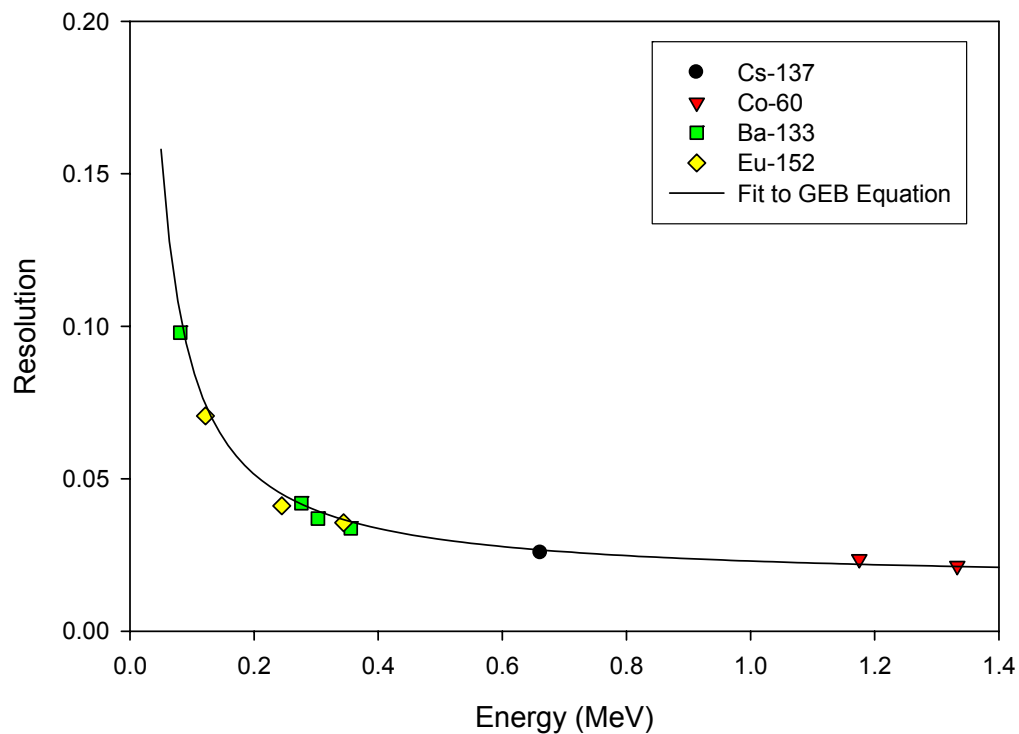


Fig. C. 6. Energy versus Resolution of Different Full Energy Peaks for the CZT

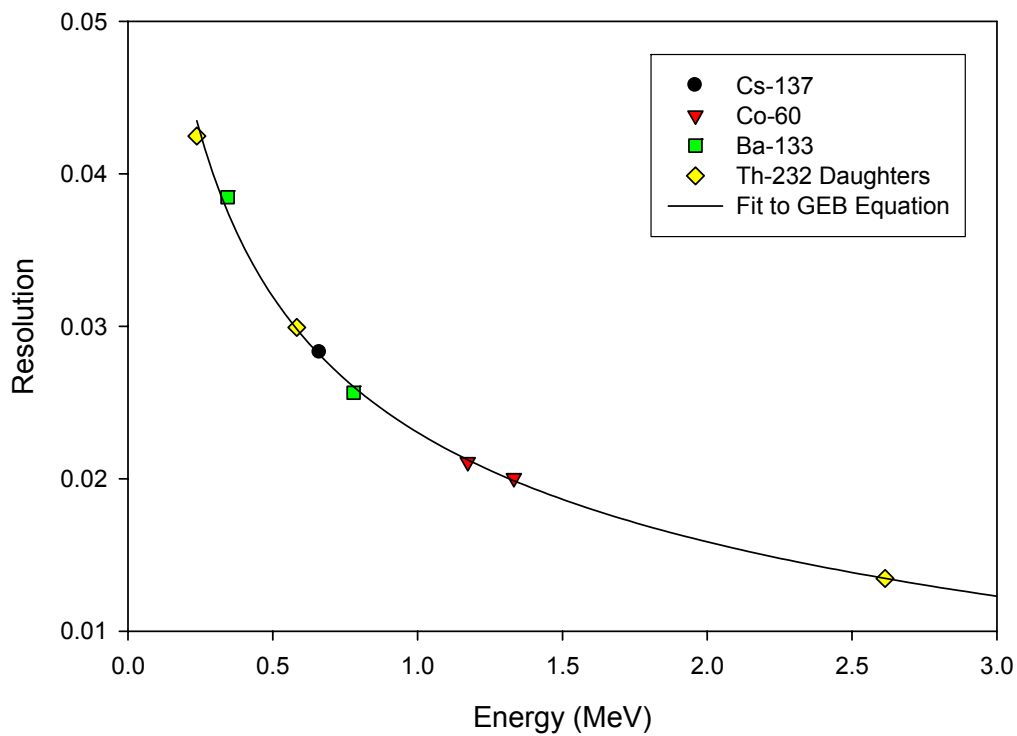


Fig. C. 7. Energy versus Resolution of Different Full Energy Peaks for the LaBr

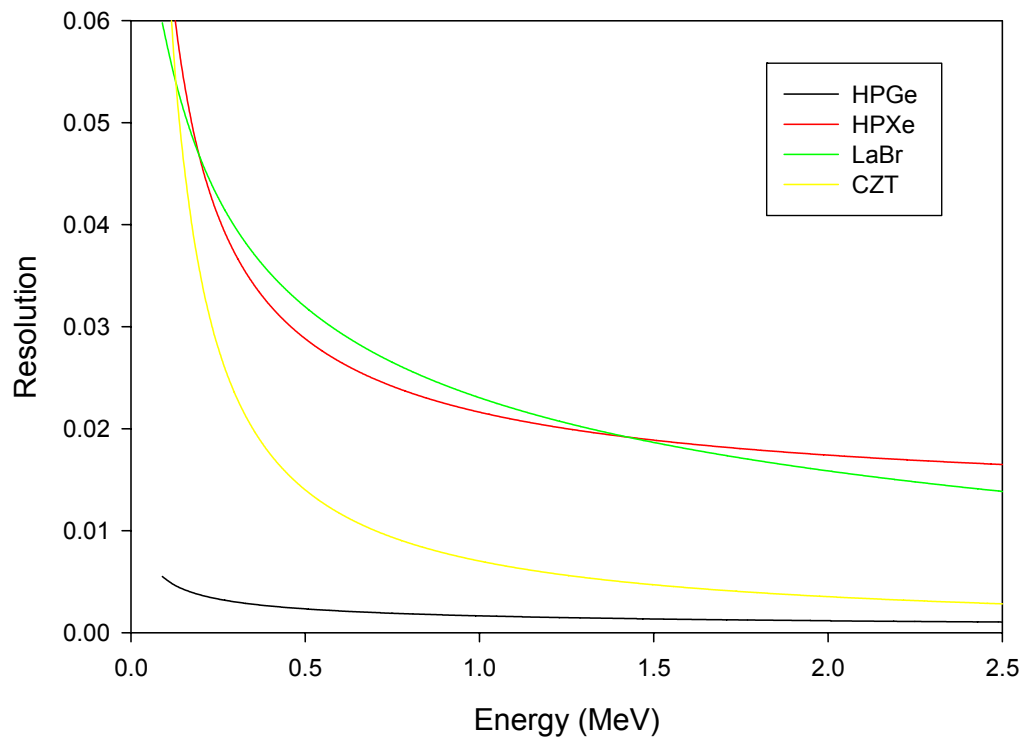


Fig. C. 8. Combined Energy vs. Resolution response of the 4 detectors

C.2 Simulated Detector Responses for Different Models

The following section contains the simulated spectra due to different models as they would appear in the response of different detectors. Only the German and the JAERI models have terms for matrix contamination. The contamination depicted roughly corresponds to the same birth activity as 5.14 TRISO particles. The failed particle spectra are graphed for a single failed TRISO. The primary failure modes are the German JAERI and GA models. These three models were simulated for each detector, and all the models were simulated for the HPGe detector. The contamination plus 1 failed TRISO spectra are also graphed to demonstrate the easy detectability of first failure in the German model as opposed to the JAERI model.

C.2.1 HPGe Detectors

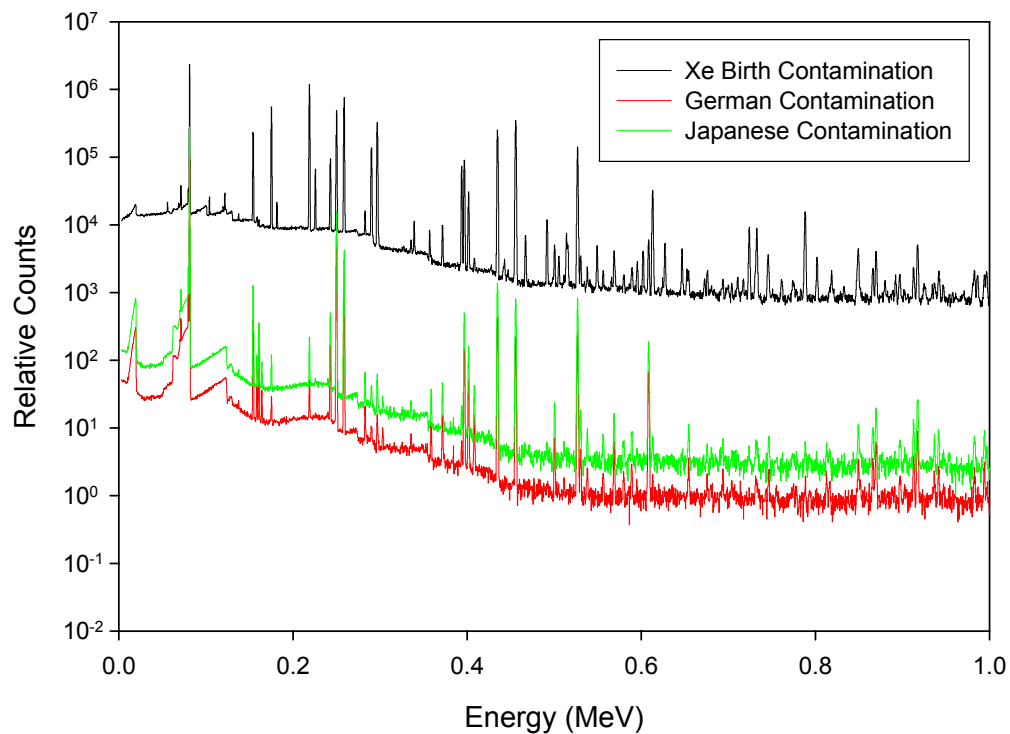


Fig. C. 9. Effect of applying the German and JAERI Models to Xe Birth Activity Due to Contamination

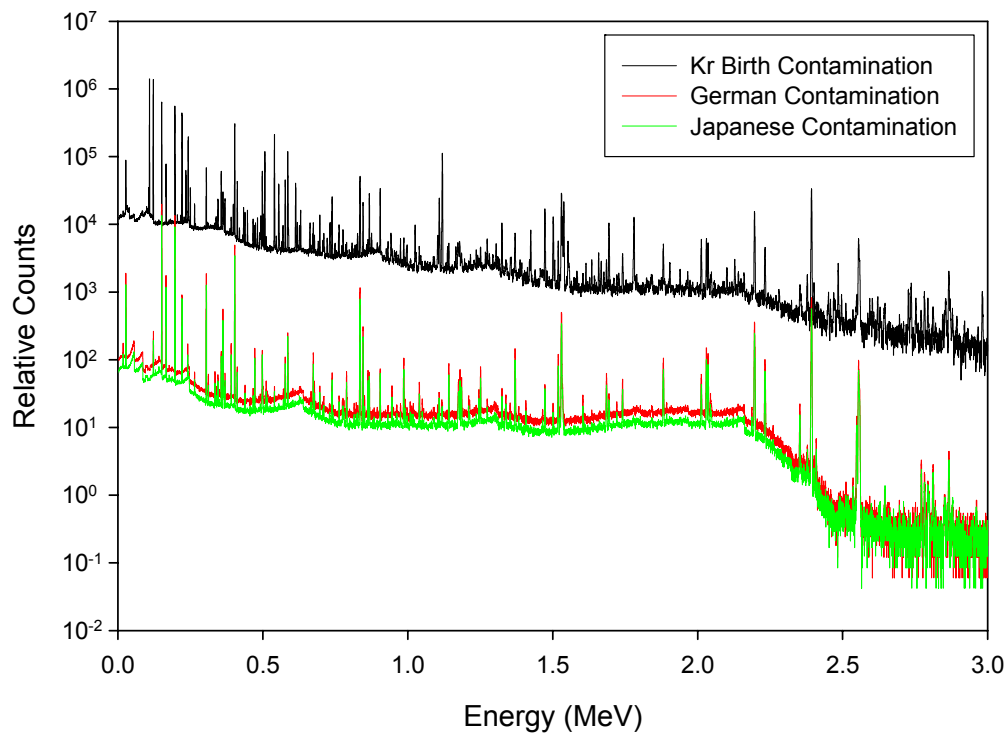


Fig. C. 10. Effect of applying the German and JAERI Models to Kr Birth Activity Due to Contamination

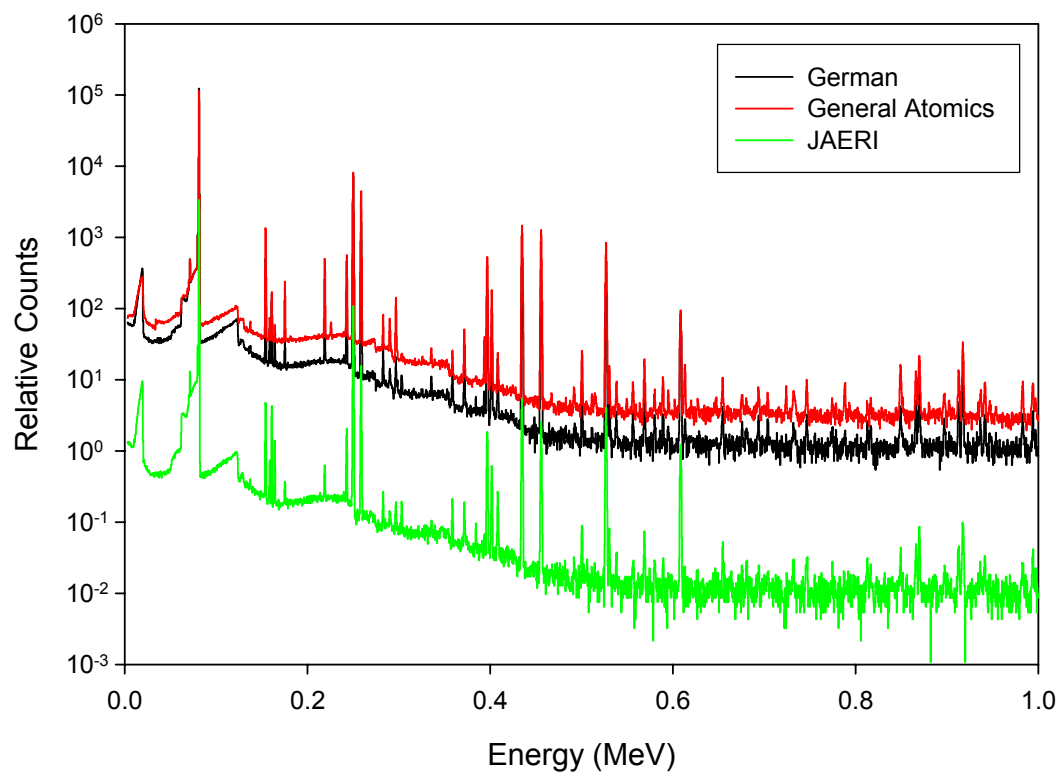


Fig. C. 11. HPGe Response for Different Models Due to the Xe from a Single Failed TRISO Particle

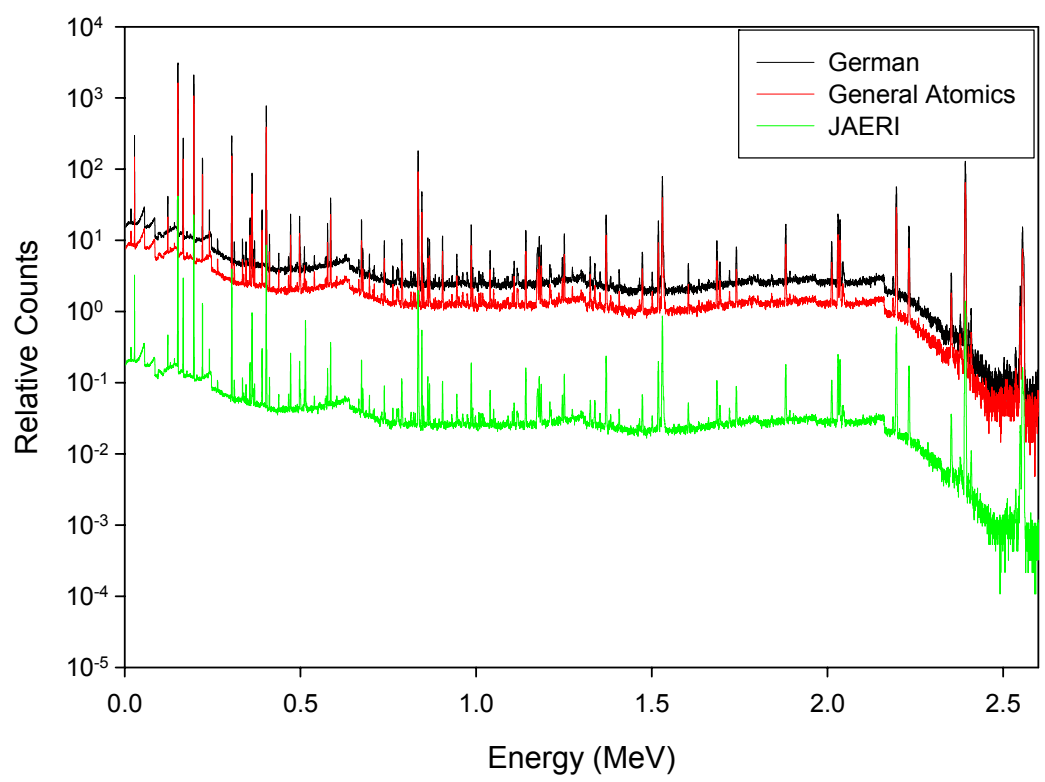


Fig. C. 12 HPGe Response from the Primary Models Due to the Kr from a Single Failed TRISO Particle

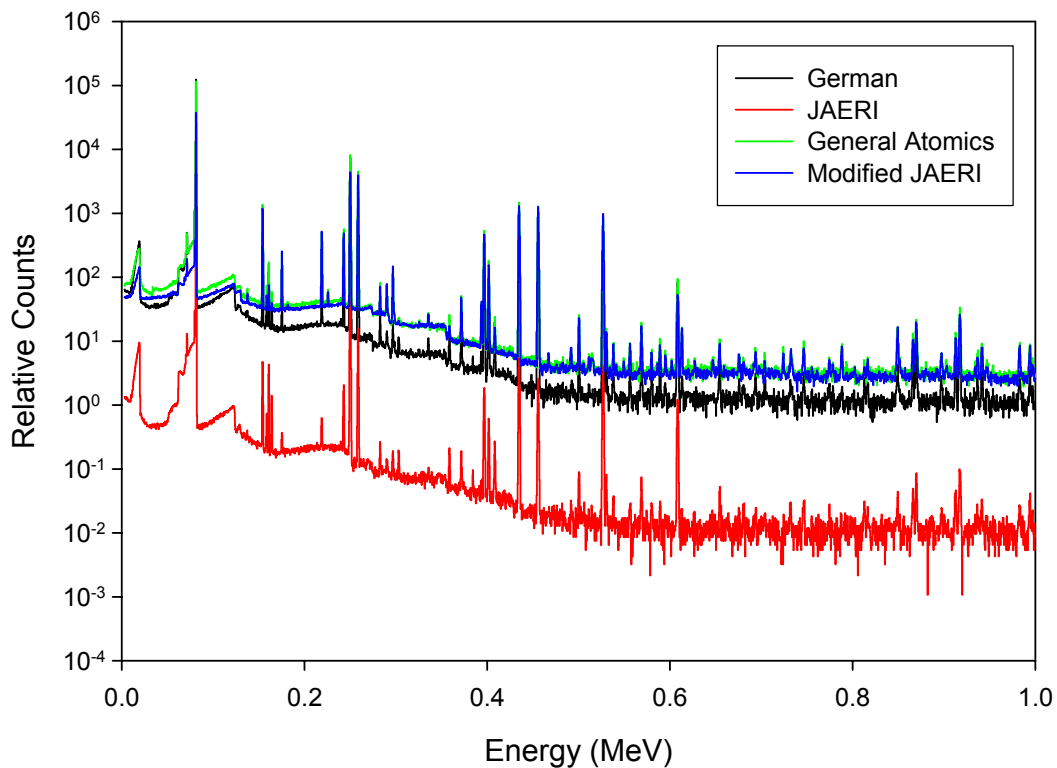


Fig. C. 13. HPG Response for all Models Due to Xe from a Single Failed Particle

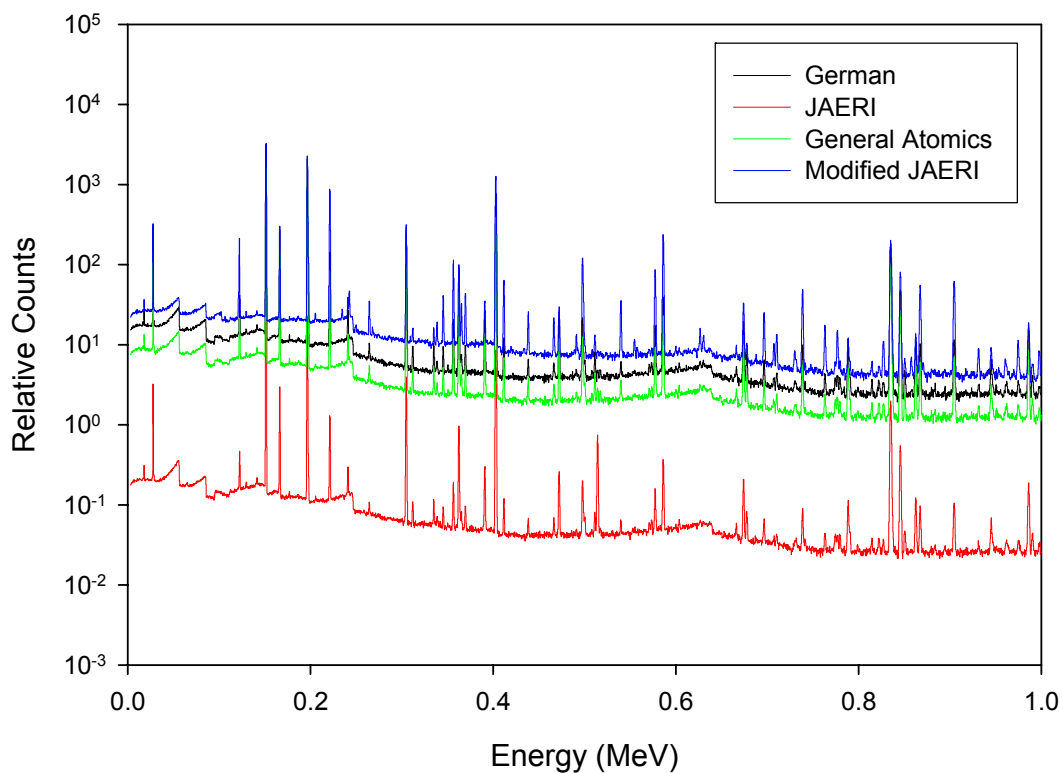


Fig. C. 14. HPG Response for all Models Due to Kr from a Single Failed Particle

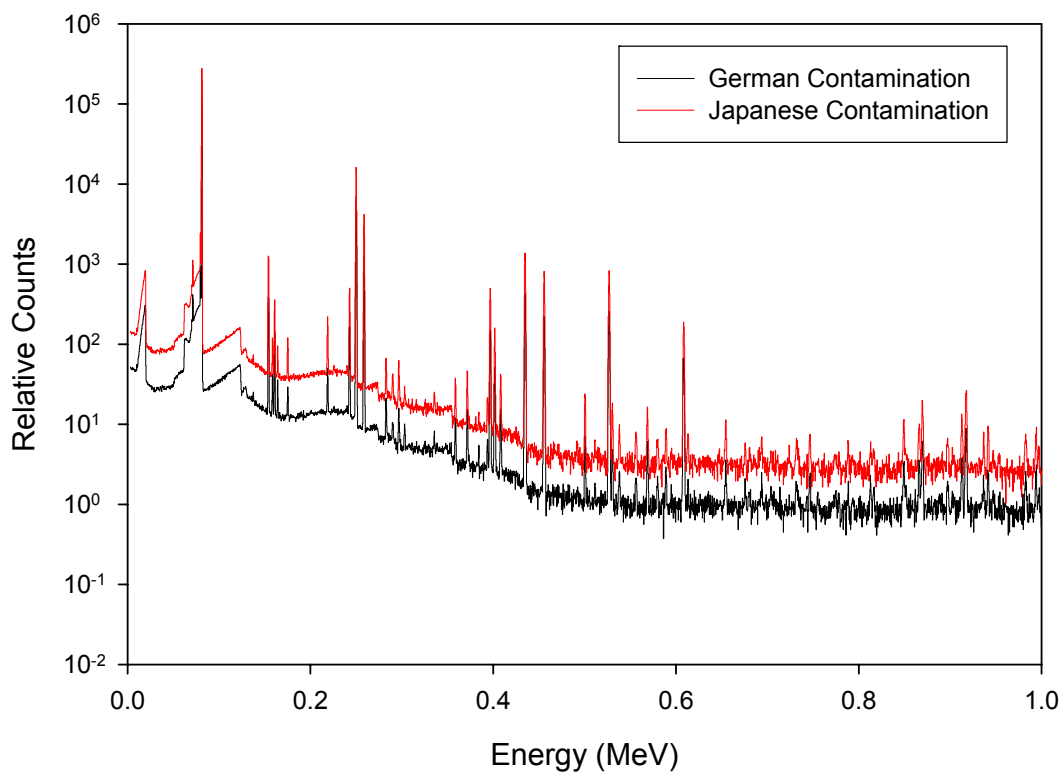


Fig. C. 15. HPGE response Due to Expected Compact Contamination from Xe

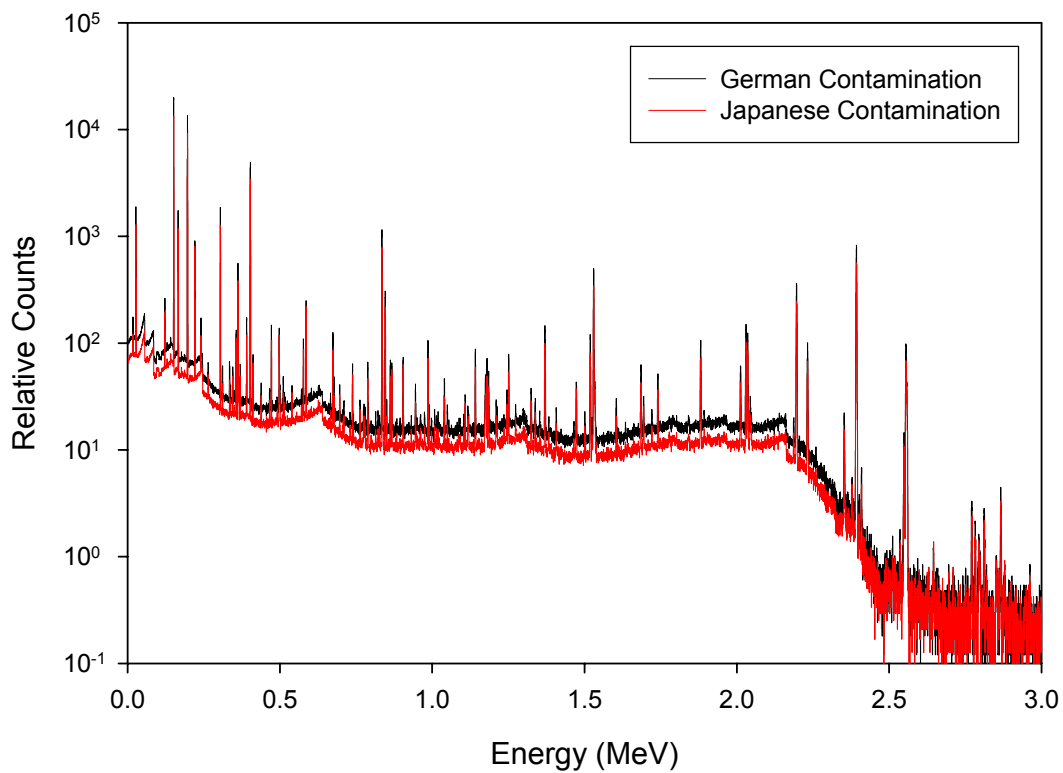


Fig. C. 16. HPGE response Due to Expected Compact Contamination from Kr

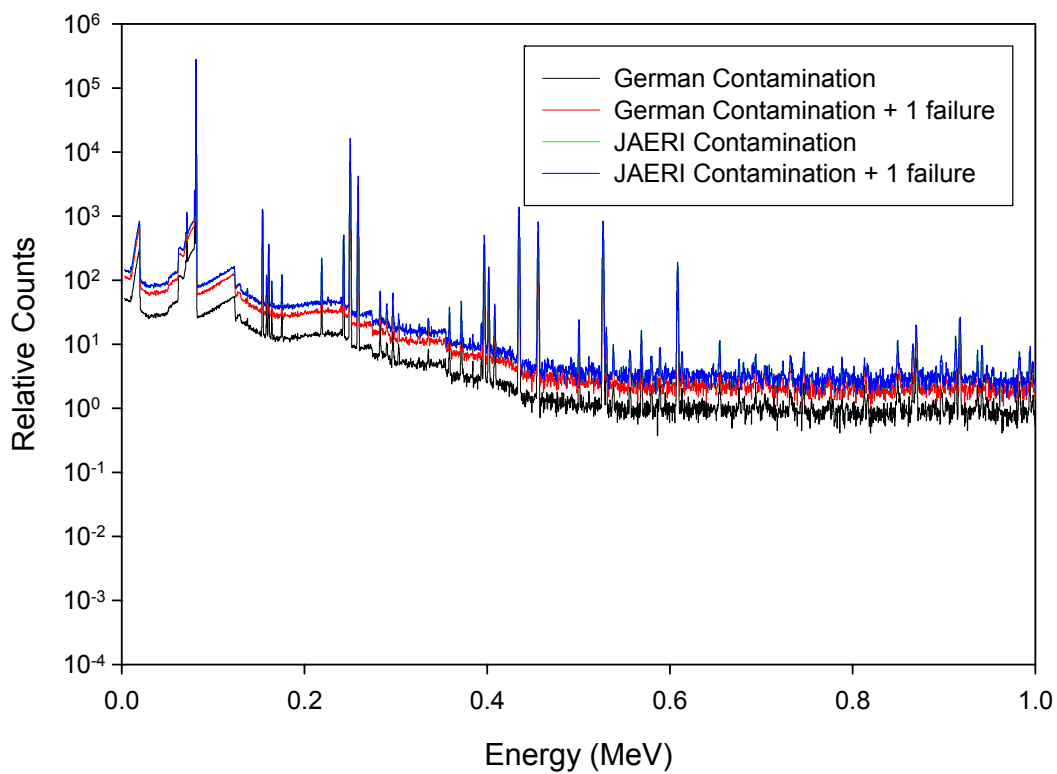


Fig. C. 17. Contamination and First Failure Spectra for Xe

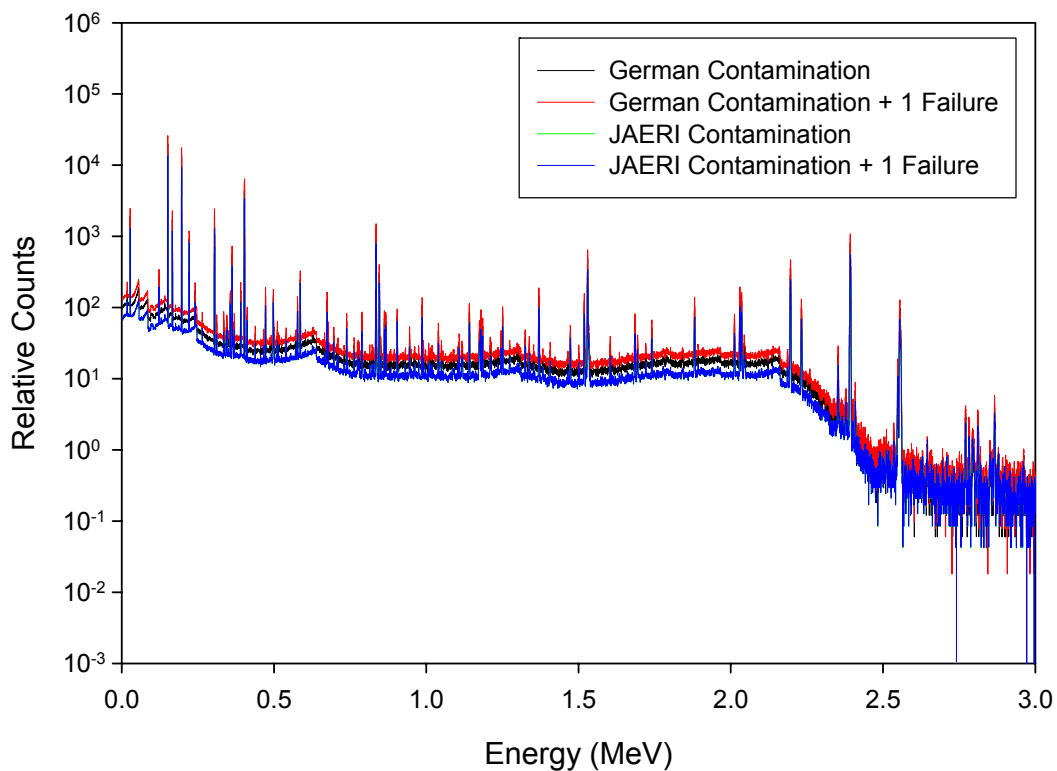


Fig. C. 18. Contamination and First Failure Spectra for Kr

C.2.2 High Pressure Xenon Detector

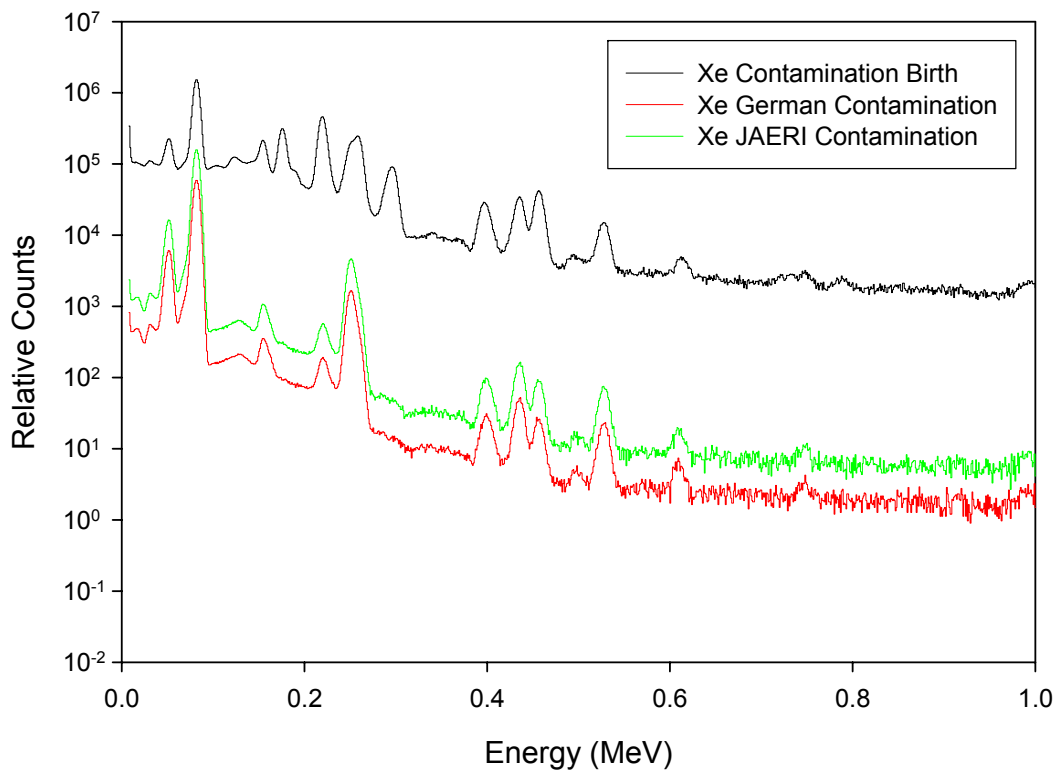


Fig. C. 19. HPXe Response for the Effect of Applying R/B Models to the Birth Activity for Xe

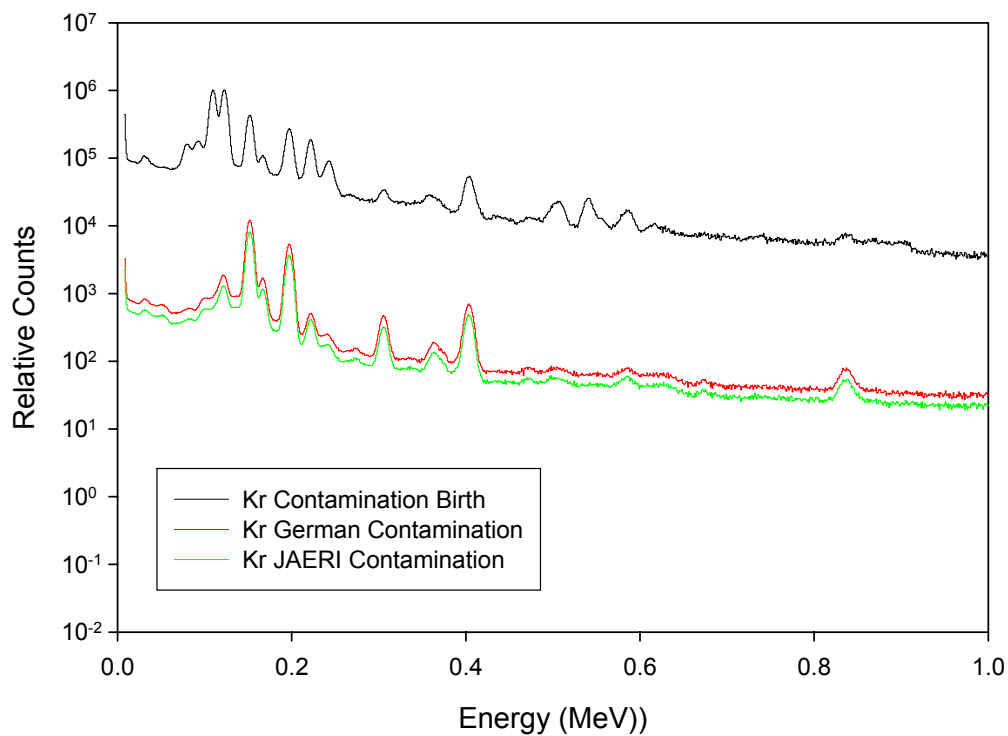


Fig. C. 20. HPXe Response for the Effect of Applying R/B Models to the Birth Activity for Xe

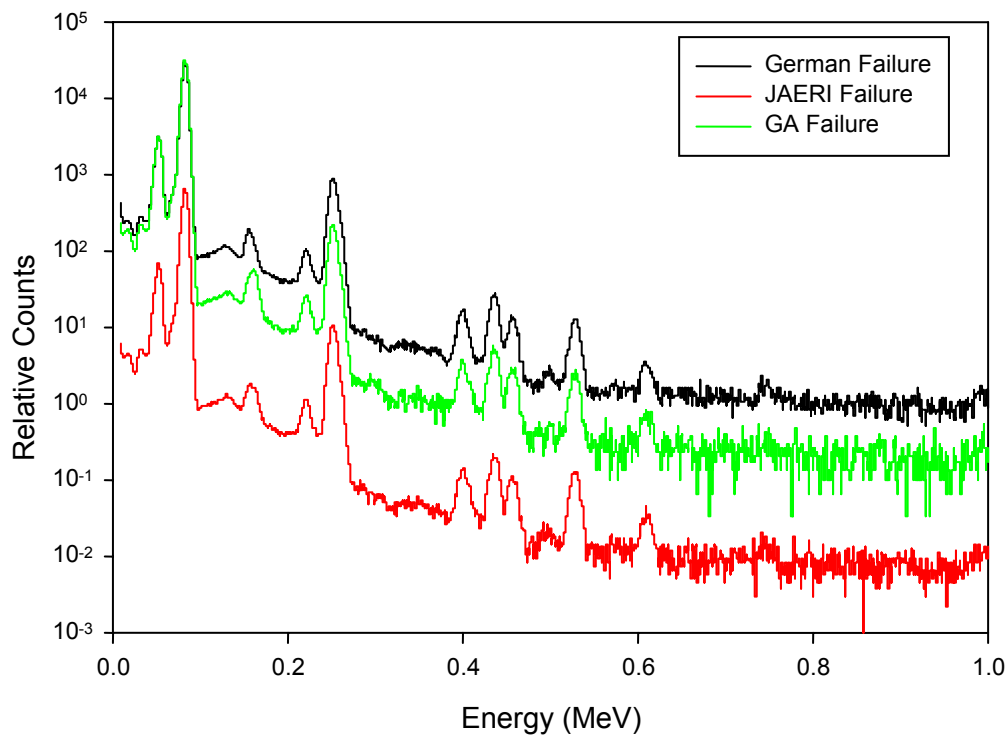


Fig. C. 21. HPXe Response Due to Xe for a Single Failed TRISO

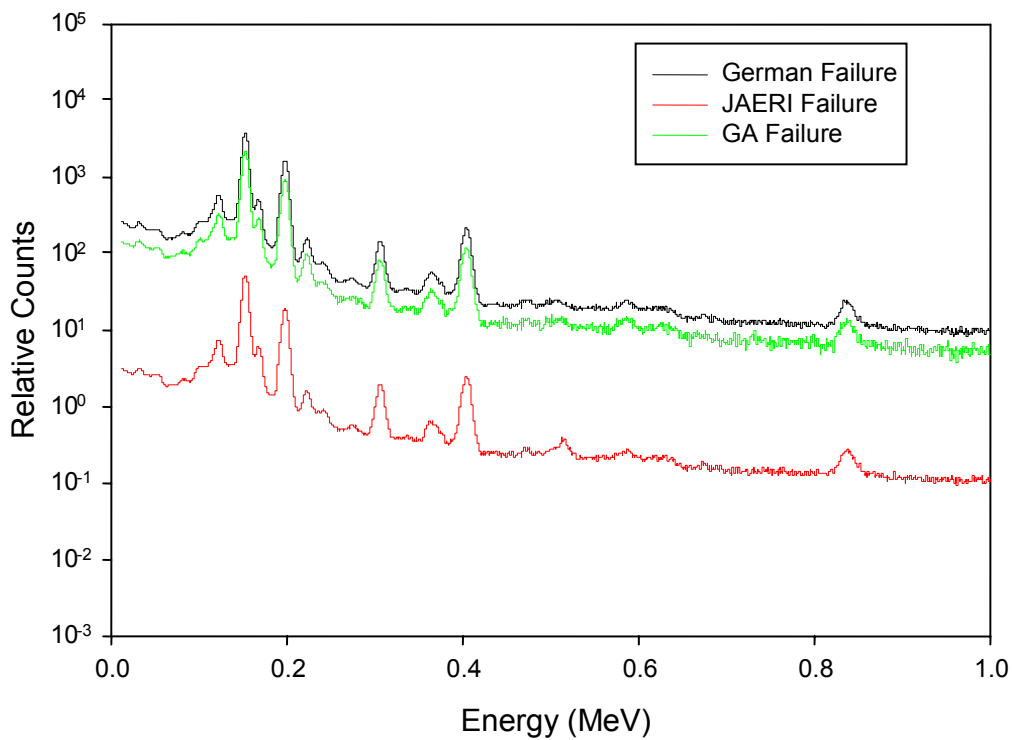


Fig. C. 22. HPXe Response Due to Kr for a Single Failed TRISO

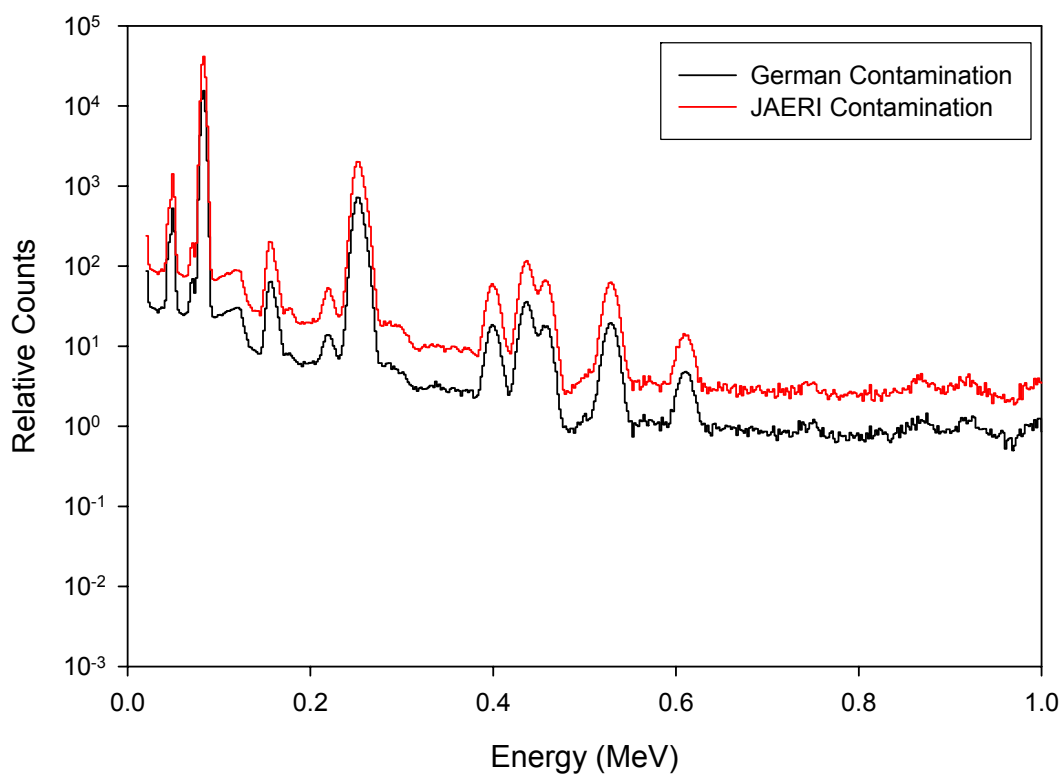


Fig. C. 23. HPXe Contamination Spectra Due to Xe

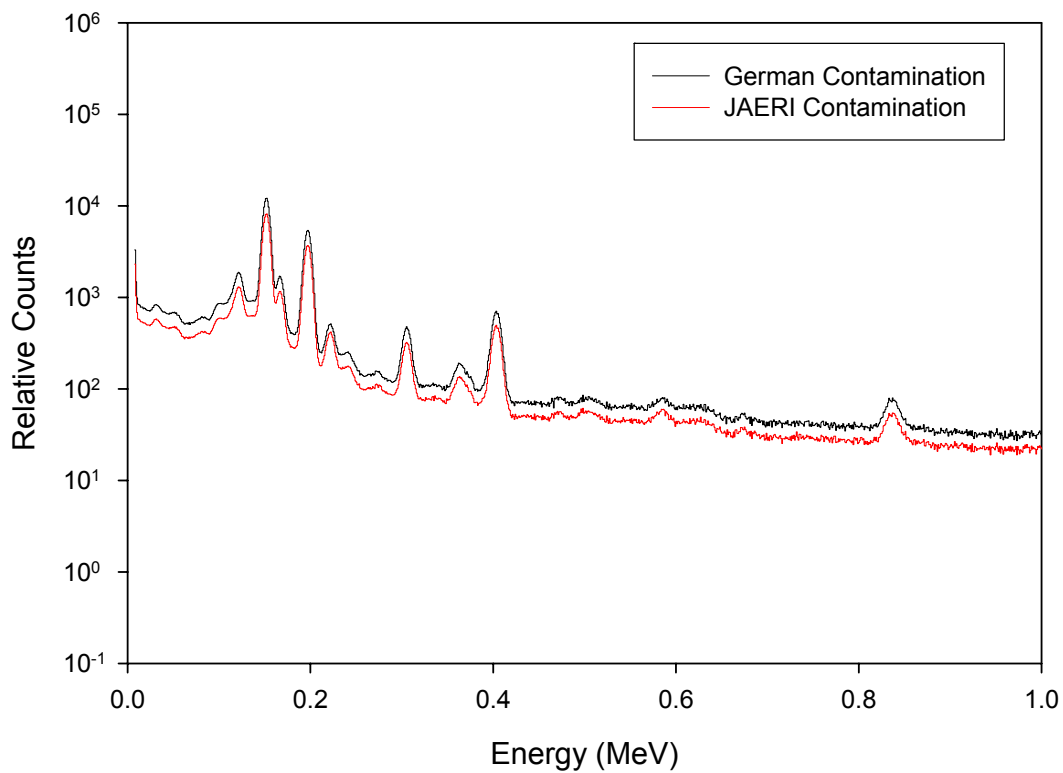


Fig. C. 24. HPXe Contamination Spectra Due to Xe

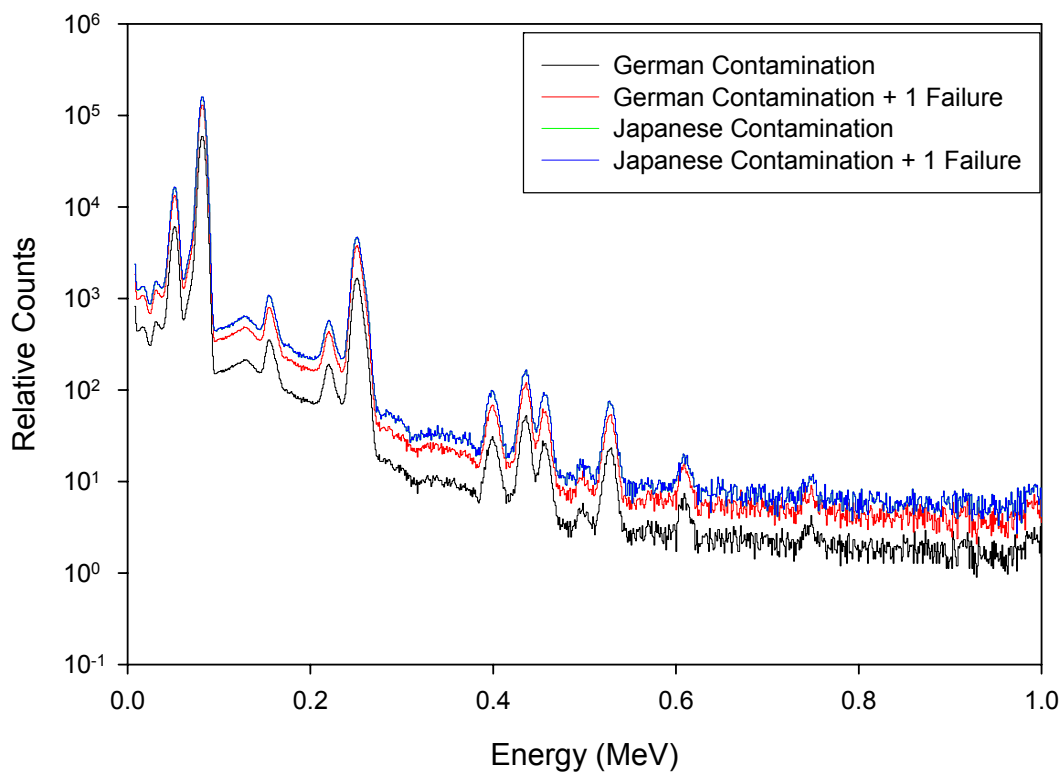


Fig. C. 25. HPXe Contamination and First Failure Spectra for Xe

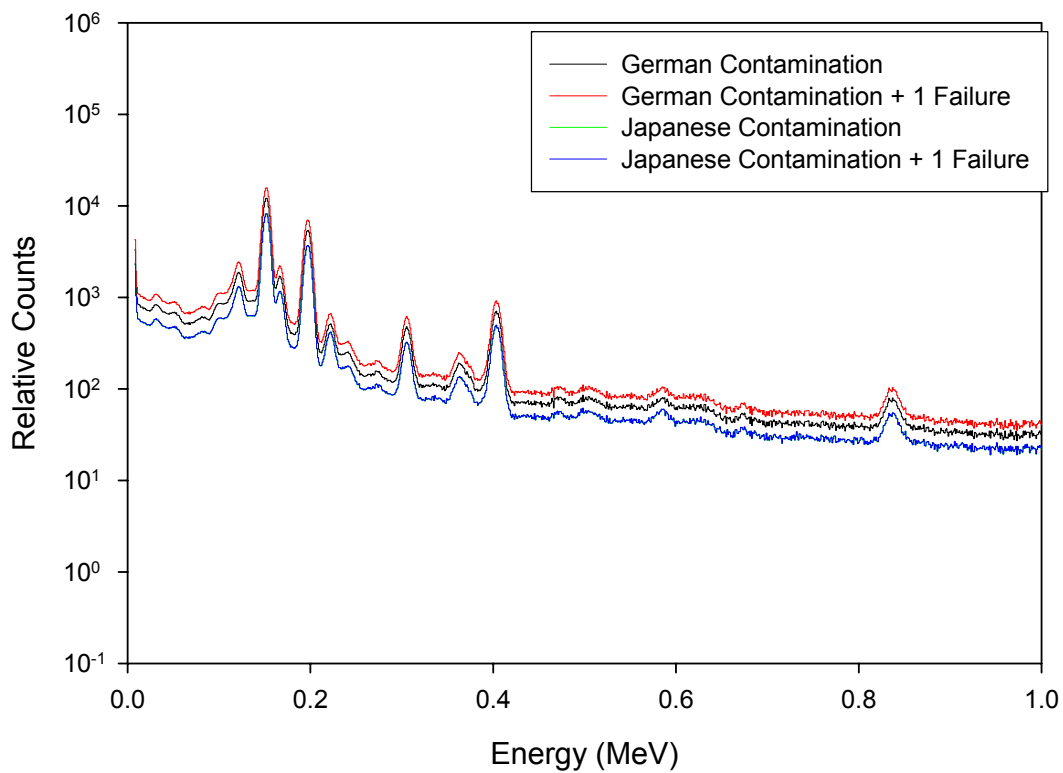


Fig. C. 26. HPXe Contamination and First Failure Spectra for Kr

C.2.3 CZT Detector

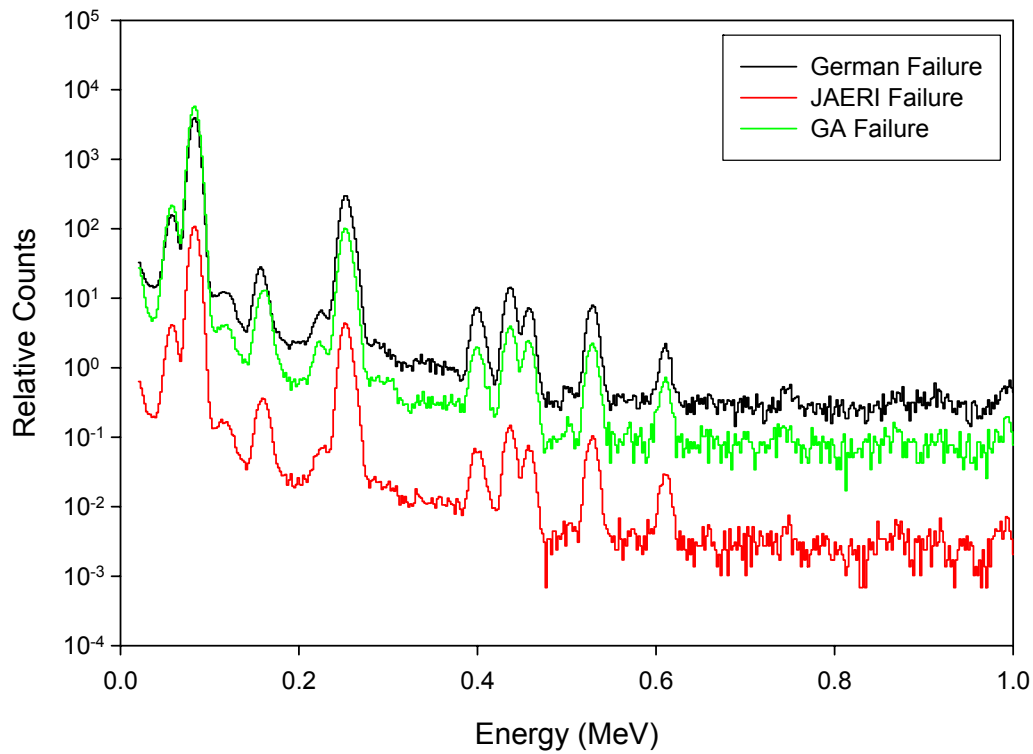


Fig. C. 27. CZT Response to Xe from a Single Failed Particle

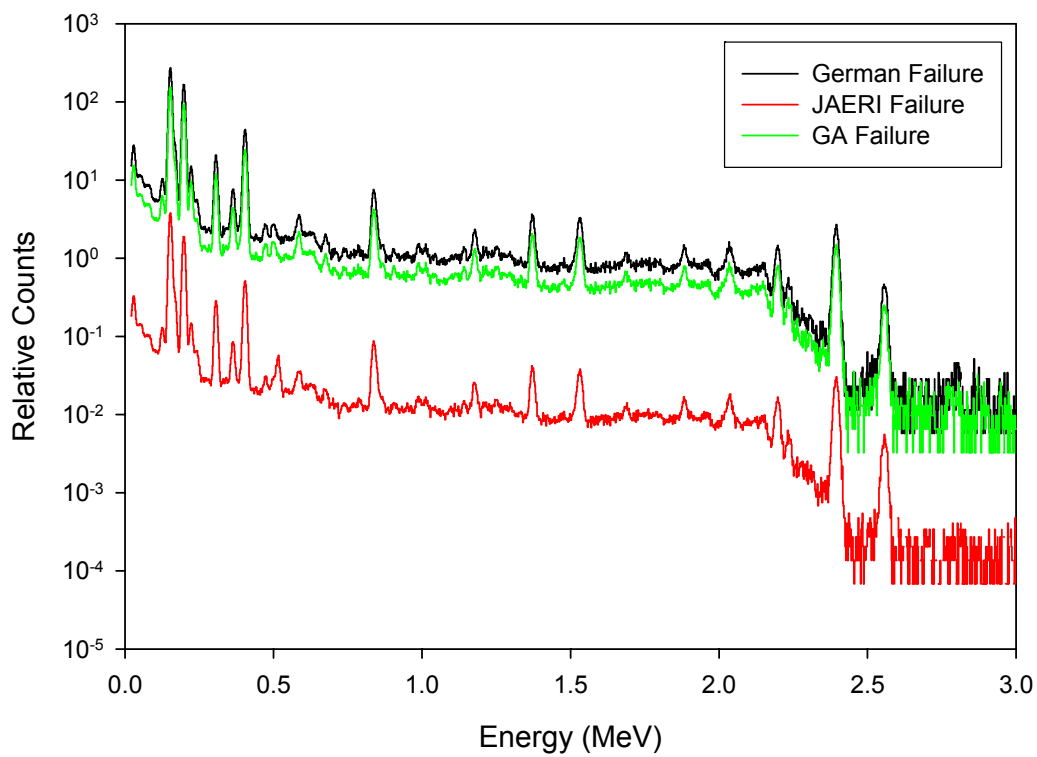


Fig. C. 28. CZT Response to Kr from a Single Failed Particle

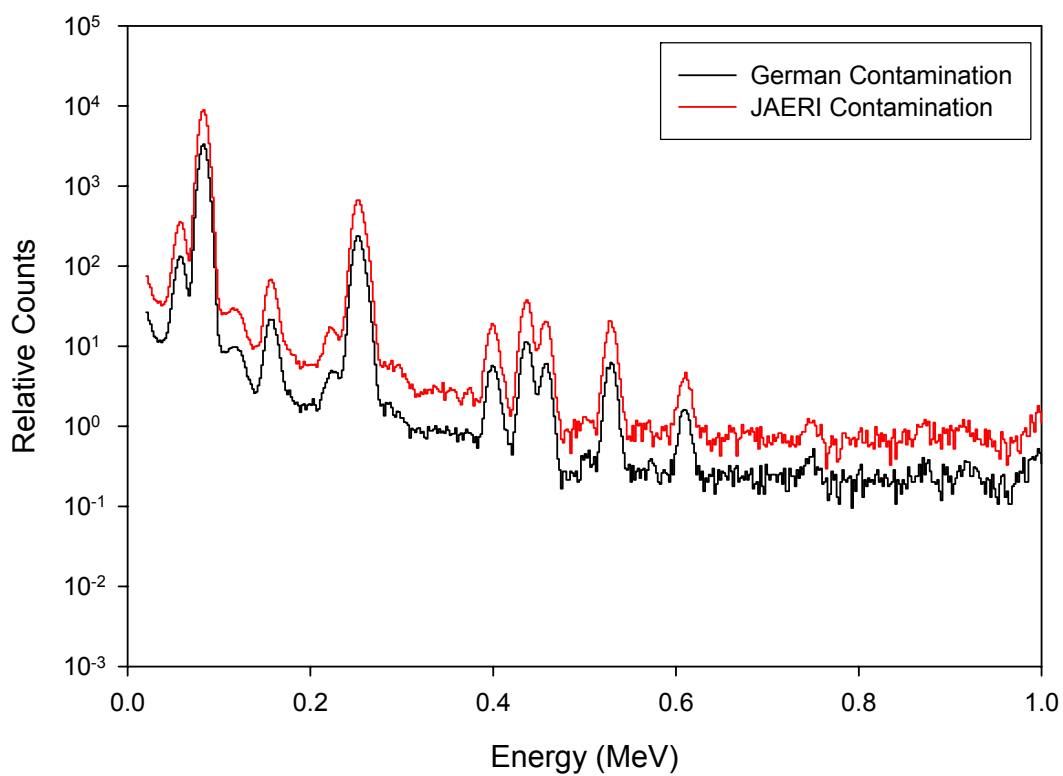


Fig. C. 29. CZT Response to Xe from Contamination

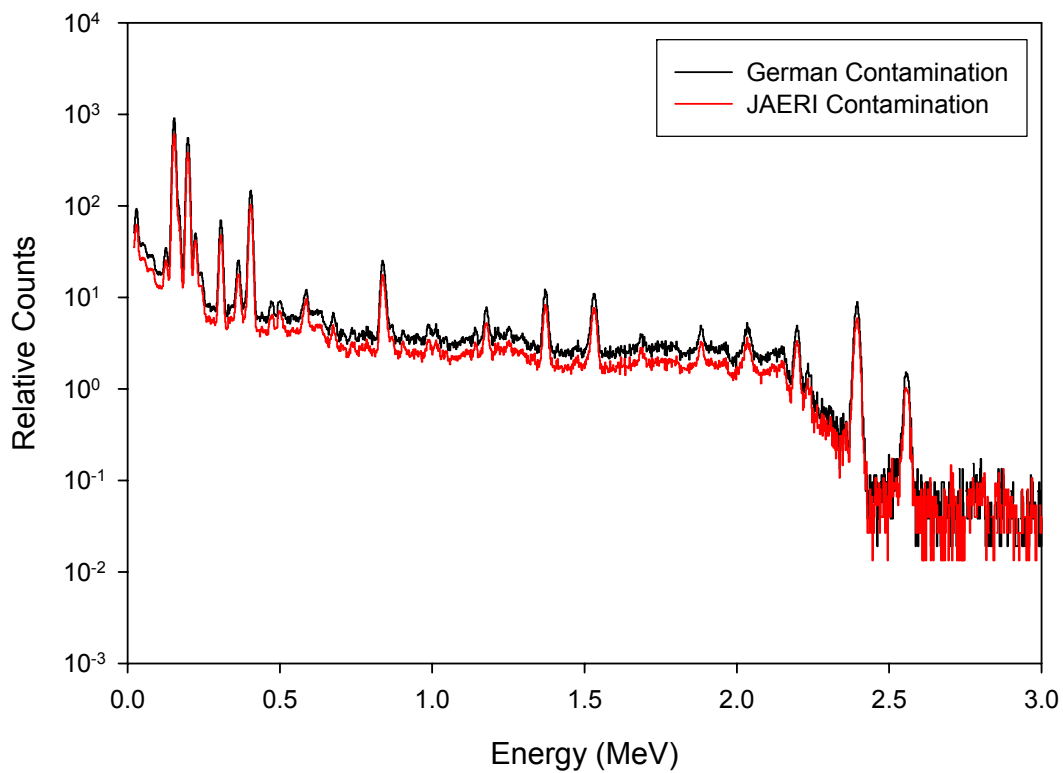


Fig. C. 30. CZT Response to Kr from Contamination

C.2.4 LaBr3(Ce) Detector

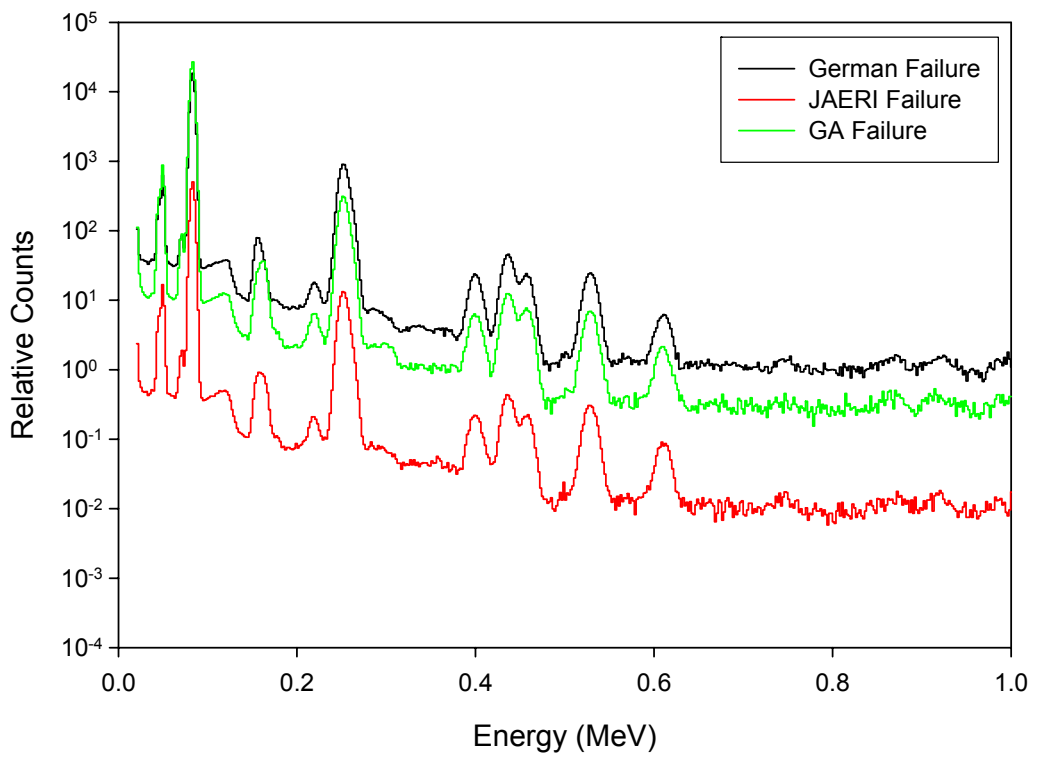


Fig. C. 31. LaBr Response to Xe from a Singe Failed Particle

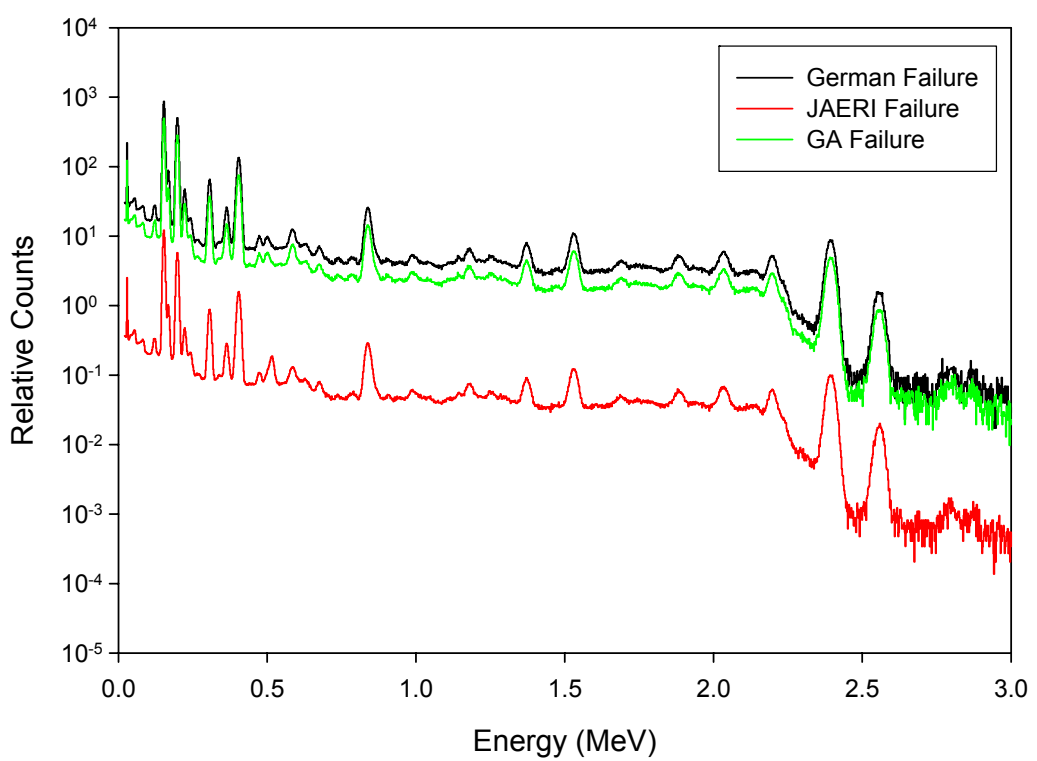


Fig. C. 32. LaBr Response to Kr from a Singe Failed Particle

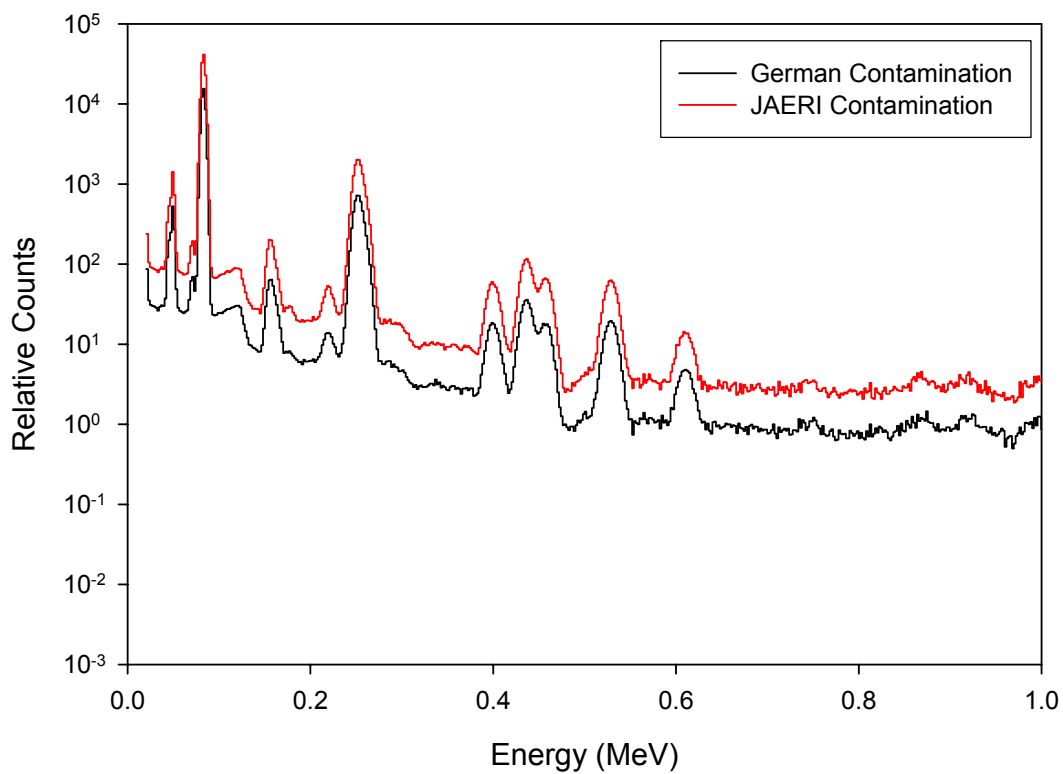


Fig. C. 33. LaBr Response to Xe from Contamination

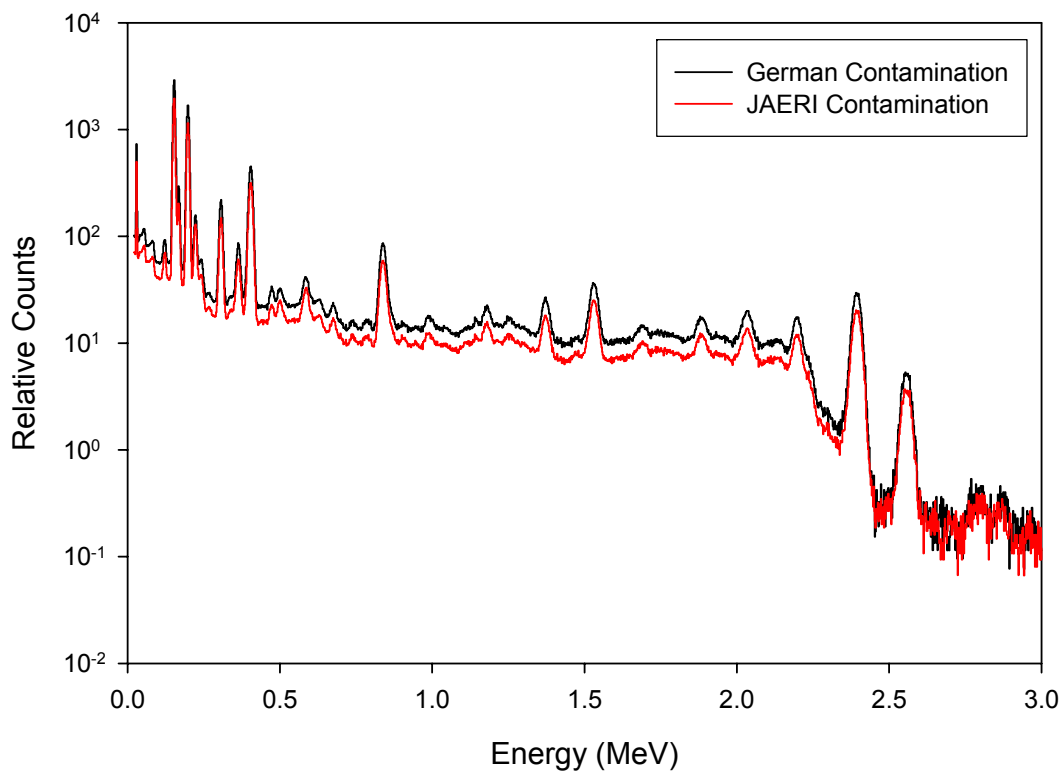


Fig. C. 34. LaBr Response to Kr from Contamination